FLEXURAL BEHAVIOR OF CONCRETE BEAMS REINFORCED WITH FRP

BARS UNDER LONG EXPOSURE TO UAE ENVIRONMENT

by

Hakem Mohammad Alkhraisha

A Thesis presented to the Faculty of the
American University of Sharjah
College of Engineering
In Partial Fulfillment
of the Requirements
for the Degree of

Master of Science in
Civil Engineering

Sharjah, United Arab Emirates

March 2021

Declaration of Authorship

I declare that this thesis is my own work and, to the best of my knowledge and belief, it does not contain material published or written by a third party, except where permission has been obtained and/or appropriately cited through full and accurate referencing.

Signed: Hakem Mohammad Alkhraisha

Date: 09/03/2021

Approval Signatures

We, the undersigned, approve the Master's Thesis of

Title:

Date of Defense:

Name, Title and Affiliation	Signature

Dr. Lotfi Romdhane
Associate Dean for Graduate Affairs and Research
College of Engineering

Dr. Sameer Al-Asheh
Interim Dean
College of Engineering

Dr. Mohamed El-Tarhuni
Vice Provost for Graduate Studies
Office of Graduate Studies

Dedication

To my family…

Abstract

Due to the large research pool of Fiber-reinforced Polymers (FRP) reinforcements, their utilization as main reinforcement in concrete structures has gained the trust of the engineering community. In fact, design codes such as the ACI 440.1R and the CSA S806 have been written due to the extensive research conducted in the realm of FRP reinforcement. The previously stated guidelines, however, do not include provisions for Basalt FRP reinforcements. In addition, research about the impact of harsh environments on the behavior of FRP reinforcement is scarce. In this study the flexural behavior and serviceability performance of Glass and Basalt FRP reinforcement exposed to a combination of ultraviolet rays, humidity, and rain for a period of 28 months were investigated. Specifically, the effects of the UAE climate on the flexural capacity of FRP Reinforced Concrete (RC) beams were examined. Additionally, bond-dependent coefficient (k_b) values were evaluated. The study also aims to evaluate the effects of reinforcement ratio, reinforcement surface texture, beam detailing, and reinforcement type on the flexural behavior and serviceability of FRP RC beams. In total, six sand coated GFRP RC beams, six ribbed GFRP RC beams, and nine sand coated BFRP beams were tested. In addition, one Carbon FRP RC beam and one steel RC beam were used as reference beams. It was concluded that exposure had a larger impact on the serviceability performance than it had on the flexural behavior of the beams. The k_b factor for all beams in this study was averaged to be 0.82 which is less than the 1.4 kb factor recommended by the ACI 440.1R code. The average k_b factor for beams reinforced with exposed ribbed GFRP bars was 7% higher than that of beams reinforced with the unexposed ribbed GFRP bars. However, the k_b factor was not affected by exposure variation in the BFRP RC beams. The study concluded that even with harsh exposure to the UAE climate, FRP bars are still resilient enough to be used in construction. Although FRP bars subjected to exposure showed inferior performance to their unexposed counterparts, they still showed superior performance when compared with steel reinforcement.

Keywords: *BFRP; GFRP; exposure; flexure; crack width; bond-dependant coefficient.*

Table of Contents

List of Figures

List of Tables

List of Abbreviations

ACI	American Concrete Institute
AFRP	Aramid Fiber-Reinforced Polymer
ASTM	American Society for Testing and Materials
AUS	American University of Sharjah
BFRP	Basalt Fiber-Reinforced Polymers
CFRP	Carbon Fiber-Reinforced Polymers
CSA	Canadian Standards Association
FRP	Fiber-Reinforced Polymers
GFRP	Glass Fiber-Reinforced Polymers
ISIS	Intelligent Sensing for Innovative Structures
LVDT	Linear Variable Differential Transformer
RC	Reinforced Concrete
OPC	Ordinary Portland Cement
UTM	Universal Testing Machine

Chapter 1. Introduction

This chapter provides a short introduction about the properties of Fiber-Reinforced Polymer (FRP) products. Then, the chapter discusses the problem investigated in this study as well as the objectives of the study. Finally, the chapter concludes with presenting the significance of the research and the general organization of the thesis.

1.1. Overview

Fiber-Reinforced polymer (FRP) reinforcement has been introduced in the past century as a potential alternative to the conventional steel reinforcement. Steel, in its nature, is susceptible to corrosion when exposed to the environment. In reinforced concrete structures, the steel reinforcement is encased by the concrete. This encasement combined with the alkalinity of concrete provides protection and reduces the chances of corrosive environment to ever affect the steel reinforcement [1-3]. The alkalinity of the concrete combined with the strength of the steel lead to an increase in the durability of structures [3]. However, If the support system between the concrete and steel is disturbed, the whole matrix is affected. Aggressive environments could cause great disturbance to the reinforcement system as it might diminish the alkalinity of concrete. When the alkalinity of concrete is neutralized, corrosion could wreak havoc on the steel reinforcement. Corrosion could diminish the strength of the steel reinforcement and, consequently, the whole concrete structure [2]. Corrosion is considered a major mode of deterioration of concrete structures. Specifically, corrosion is regarded as the main cause for deterioration of the reinforcement component of concrete bridges and the possibility of its occurrence increases in humid and saline environments. It is estimated that corrosion is responsible for up to 40% of damage of all engineering structures in the United States which results in a total loss of approximately $14 billion per year [4]. Aggressive environments, that could reduce the alkalinity of concrete, are characterized by a presence of chloride (i.e. marine structures) when if combined with moisture and high temperature produce a hospitable environment for corrosion [1, 3]. The high cost of maintenance of corroded structures pushed for new developments that could combat the short comes of the steel reinforcement. The focus of the developments was on the material aspect of the

reinforcement. It was in 1970 where a viable non-metallic material provided the needed resistance to corrosion; that material was FRP reinforcement [1].

From the dawn of their existence, FRP bars possessed very promising properties [5]. They can resist corrosion from sea-water in marine structures, de-icing salts in bridges, and any acidic environments present in concrete[3]. Furthermore, they have a better strength to weight ratio than steel [1, 3, 6, 7]. With only one-fourth of the density of steel, FRP reinforcement produce much higher tensile strength than steel reinforcement [1, 8]. Today, there are many types of FRP materials utilized as reinforcement in concrete structures. Up until recently, the most common types of used FRP reinforcement were: Carbon Fiber-Reinforced Polymer (CFRP), Glass Fiber-Reinforced Polymer (GFRP), and Aramid Fiber-Reinforced Polymer (AFRP) [2]. In the last few years, a new promising FRP material had surfaced in the market. The new material is composed of basalt fibers. Basalt Fiber-Reinforced Polymer (BFRP), as it became to be known, is one of the newest developments in the FRP realm. BFRP possesses the same properties as its FRP predecessors which is what makes it a very appealing to stakeholders who face problems with corrosion. Generally, FRP materials could be used as reinforcement bars or as composites that are prefabricated to perform a certain function. FRP fibers could, also, be of great use to strengthen the compressive and tensile properties of concrete [2].

Although FRP materials share an overarching matrix of advantages, some have unique attractive properties. GFRP, for example, is not effected by radio frequencies or magnetic fields and is thermally and electrically nonconductive [1]. The aforementioned properties can be very beneficial in places like Magnetic Resonance Imaging (MRI) rooms where the presence of magnetic fields is certain [1]. The overarching advantages of FRP reinforcement include: greater service life in corrosive environment, high strength to weight ratio, resistance to fatigue, resistance to chloride, and lower required protective concrete cover [1, 2]. These features slowly inch the FRP reinforcement toward full adoption as a viable alternative to the conventional steel reinforcement.

FRP reinforcement, however, are not perfect. One of the major short comes of FRP bars is their brittle nature [1-3, 9-11]. Unlike steel, FRP composites show a linear elastic behavior until failure when exposed to a tensile load. The lack of ductility in

the FRP reinforcement might lead to catastrophic failures without warning. However, what that lack of ductility certainly leads to is an extremely scrutinized design guideline. The guidelines for FRP Reinforced Concrete (RC) design impose a much higher reduction factor than required during the design of steel RC structures design. For example, in the tension-controlled zone, the capacity of the steel RC structures of is multiplied by a 0.9 reduction factor while the same capacity is multiplied by 0.65 reduction factor for FRP RC structures [1, 12].

Excluding BFRP composites, there have been many studies conducted on the behavior of FRP. The GFRP reinforcement, for example, has had extensive research done to verify its behavior and properties. These studies helped lay the foundations for the FRP design codes. Currently, design codes such as the ACI 440.1R [1], CAN/CSA S806[13], CAN/CSA S6 [14], and ISIS manual No. 3 [15] provide some guidelines for the design of FRP reinforced structures. The BFRP reinforcement, however, is not included in the previously stated design codes [16].

Studies conducted on FRP reinforcement ranged from testing mechanical properties such as the tensile strength and bond dependent coefficient (k_b) to testing FRP bars contribution as flexural and shear reinforcement. Some studies went as far as investigating the viability of combining steel and FRP bars as flexural reinforcement. A study conducted by El Refai et al., for example, investigated the viability of using a hybrid FRP-steel reinforcement [17]. The study found that the hybrid system was very effective. The FRP and steel reinforcement showed somewhat of a complementary relationship where the weakness of one reinforcement system was covered for by the strength of the other and vice versa. In other words, the strength of the system was magnified by the singular strength of the individual units.

1.2.   Problem Statement

The construction industry is not necessarily to most technologically advanced sector when compared with other industries. The industry is usually hesitant when it comes to implementing new technologies that might increase efficiency and sustainability, while reducing cost. Not only is there a pressing need to develop new construction materials, but those materials must be accepted alternatives to steer the reluctant construction industry toward utilizing such materials. There is a need to develop materials which can overcome the shortcomings of the conventional

materials. The new materials must also be tested and their capabilities are ought to be validated. After which, the engineering community will accept the new developments and employ them in the construction industry. Furthermore, structural and economic factors are to be pondered upon during the process of introducing new materials.

The steel reinforcing bar is the conventional construction material that has been used since the dawn of the modern construction era. The steel bar, although having some great features, is a metallic /conductive material that is vulnerable to various environmental conditions. The steel bar arch-nemesis is corrosion. Corrosion can degrade the steel bar and diminish its strength and nullify its other attractive features. To counter the corrosive environments, present almost everywhere, a non-metallic reinforcement bar has been developed. Fiber-Reinforced Polymer (FRP) bars are not affected by corrosion so it serves as great replacement to steel in that area. That being said, FRP bars are not without weaknesses. Unlike steel, FRP bars are brittle in nature where the yield linear elastic stress strain behavior until failure. The lack of ductility means sudden failure; if failure is to occur. Thus, the engineering community had to put more scrutiny on the application of FRP bars. This scrutiny is noticeable by observing the fact that the ACI 440.1R code is more stringent than the ACI 318 when applying reduction factors, for example.

The high level of scrutiny led to a pressing need for more research in the area of FRP reinforcement. Furthermore, some FRP reinforcement such as BFRP reinforcement are still relatively new and in need of much research. Although the area of GFRP reinforcement has a rich and extensive research foundation, studies such as the exposure effects on FRP reinforcement bars are still considered a frontier to explore and investigate. Real life exposures such as temperature and humidity exposure are more likely to occur than any other type of exposure. The temperature and humidity exposure could occur if the reinforcement bars are left exposed to the environment prior to being utilized in construction. Specifically, the practical impact of leaving FRP reinforcing bars in construction sites to be exposed to severe weather conditions, such as the one in the United Arab Emirates (UAE), for long periods of time has never been studied. The aforementioned exposure could cause reduction in the serviceability and flexural capacities of structures reinforced with FRP bars subjected to exposure.

1.3. Thesis Objectives

The main objective of this study is to investigate the impact that the weather condition in the UAE impose on FRP bars. Specifically, the impact of the aforementioned environment on FRP bars which are left unprotected in the vicinity of construction sites is to be investigated. The exposure program in this study simulates the process of leaving bars exposed to environmental parameters such as ultraviolet waves and heat from the sun and moisture from the air. The effect of such exposure has not been investigated under flexural tests such as the four-point loading test. Most of the tests conducted on exposed FRP bars are mechanical tests such as tensile strength test and the pullout test. A holistic flexural test has not been done for the type of exposure proposed in this research. The exposure program used in this study is discussed comprehensively in chapter 3 of this report. The sub-objectives of this research are stated below:

- Study the flexural behavior of concrete beams reinforced with BFRP and GFRP bars subjected to long term harsh exposure imposed by the UAE environment. The flexural response analysis includes analysis of moment capacity, strain behavior, and moment vs. deflection trends.

- Study the serviceability performance of concrete beams reinforced with GFRP and BFRP bars subjected to the same exposure as above. The serviceability analysis includes analysis of cracking moments and crack propagations as well as cracks width and spacing.

- Evaluate the bond-dependent coefficient (k_b) for the beams reinforced with exposed GFRP and BFRP bars.

- Compare the experimental results with the results predicted using the ACI 440.1R provisions.

The generalized objectives are going to be assessed using the following tangible and measurable criteria:

- Studying the effect of exposing GFRP and BFRP bars to high temperatures and moisture on the flexural and serviceability behavior of FRP RC beams.

- Examining the impact of different reinforcement ratios on the flexural behavior and serviceability criteria of FRP RC beams.

- Investigating the effect of variation in surface texture of GFRP bars on the flexural and serviceability limit states of FRP RC beams.

- Analyzing the impact of the number of GFRP and BFRP reinforcing bars on the flexural and serviceability behavior of FRP RC beams with similar axial stiffness.

- Assessing the influence of different reinforcement types (GFRP, BFRP, steel) on the overall flexural and serviceability behavior of the beam.

1.4. Research Significance

The area of BFRP reinforcement is still a pristine one, research wise. Research in the BFRP reinforced beams is much needed if the material is to be approved as a credible form of reinforcement. The ACI 440.1R code does not provide design criteria for BFRP reinforcement due to the lack of research. Studying the flexural behavior of BFRP composites may produce qualitative and quantitative results than can be implemented in the FRP design code. The bond-dependent coefficient (k_b) is going to be examined in this study and the results of the study will provide recommendation to ACI committee. The overall flexural behavior is also be studied and the conduct of the BFRP reinforced beams will provide beneficial data that will add to the pool of studies conducted beforehand.

Although GFRP reinforcement had existed for a longer time and has been extensively studied, the type of exposure explained herein combined with the holistic flexural test is a worthy addition to the literature. Many researchers had studied the effect of exposure on the material properties of FRP reinforcement by itself but very few studies have been done to evaluate the behavior of beams reinforced with exposed bars. Most of the studies evaluated the effect of exposure on FRP bars using tests such as the tensile strength test and pullout test. This study proposes a four-point bending flexural test to examine the effect of exposure. The exposure program of this study is also rarely studied. Most studies expose bars to alkaline compounds or seawater for instance. The Impact combination of ultra-violet waves/temperature, moisture/ rain, and humidity exposure is a commendable addition to the literature. More importantly, the results will prove the reliance of FRP bars, or its lack of, when exposed to the weather conditions present in the UAE. The results will provide recommendation to both the ACI committee and regional construction contractors.

1.5. Thesis Organization

The rest of the thesis is organized as follows: Chapter 2 provides background about FRP properties and recent studies about FRP reinforcement behavior in flexure and shear. Chapter 3 presents the experimental program followed in this report. The experimental program includes the material properties, design considerations and equations, test specimens and setup, as well as the exposure program studied herein. The results and analysis are presented in Chapter 4. Chapter 5 concludes the report with a summary of the findings and recommendations of the author. A detailed thesis organization is shown in Figure 1.
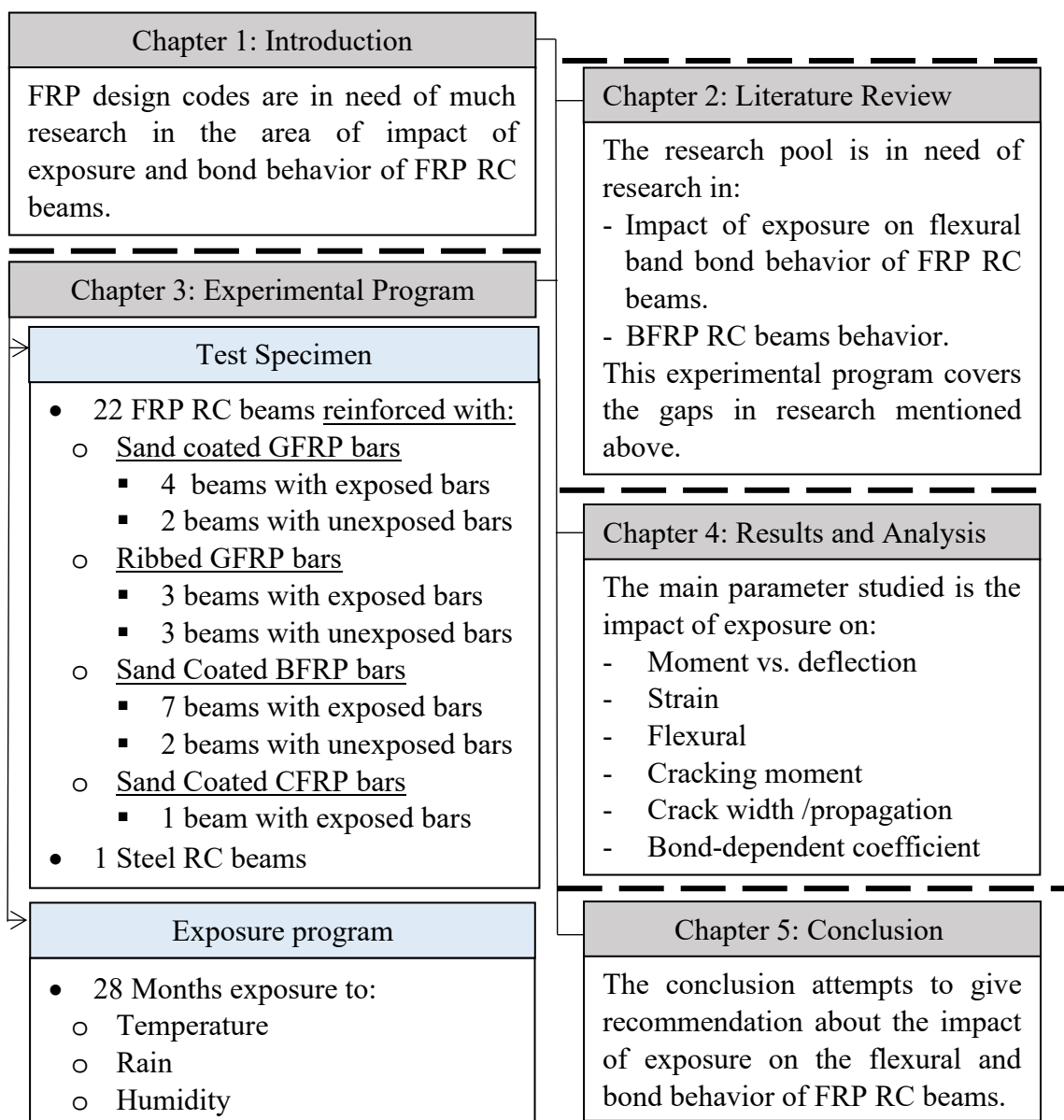
Figure 1: Thesis organization flowchart.

Chapter 2. Background and Literature Review

In this chapter, the properties of the FRP materials in general and FRP bars more specifically are presented. Then, the chapter summarizes the studies that were conducted to investigate the behavior GFRP and BFRP reinforced sections. Finally, the impact of exposure on the properties of FRP is discussed.

2.1.   Overview of Fiber-Reinforced Polymer (FRP) Properties

The overview of FRP properties focuses on the mechanical properties of the bars themselves as well as some design considerations. The mechanical properties discussed hereafter are the tensile and compressive strength of different FRP reinforcement along with the modulus of elasticity of said reinforcement. The discussed design considerations focus on the bond behavior. The cracking behavior of FRP reinforced beams is only briefly discussed in this subsection since it is examined more extensively later in the report. The section starts with a brief introduction about the fabrication of FRP material.

FRP composites are anisotropic material that are manufactured using techniques such as braiding, weaving, or pultrusion [1, 18]. The anisotropic nature of FRP bars is traced back to the different materials composition of the bar. The material makeup of FRP bars consists of the fibers themselves and the resin combing said fibers. Consequently, the axial strength is governed by the strength of the fiber while the transverse strength is governed by the strength of the resin [1]. The utilized fibers vary in type; as they can be glass, carbon, basalt, or aramid high strength fibers. Additionally, the resin can be vinyl ester, epoxy, or polyester [1, 19]. The resins vary in tensile strength and modulus of elasticity (as shown Table 1). FRP materials can serve different purposes; they are produced as bars, ropes, tendons, and grids[19].

Table 1: Resin Properties [20]

Criteria	Vinyl Ester	Epoxy	Polyester
Tensile Strength (MPa)	73 – 81	55 – 130	34.5 - 103.5
Tensile Modulus (GPa)	3 - 3.35	2.75 - 4.1	2.1 - 3.45

The properties of FRP bars are not universal as they vary depending on factors such as: the type of fiber used, the amount of used fiber, the orientation of the fiber,

and the type of the resin binding the fibers [1]. The variation in material properties prevented the adoption of universal unifying FRP material properties. However, consensus about material testing procedures can be found in codes such as the ACI 440.3R [21] and ASTM D7205 [22]. The aforementioned codes are used to determine material properties of FRP composites which are then utilized in the design phase of FRP reinforced structures. The material properties that are most important to investigate in the design phase are: the tensile strength, modulus of elasticity, and the bond dependent coefficient of FRP bars. The major tests used to determine the previously mentioned properties are the tensile test and the flexural loading test [21].

Despite the fluctuating behavior of FRP material properties, some statements can be made to describe FRP composites material properties in general. Unlike steel, FRP reinforcement are brittle as they portray a linear elastic behavior until rupture [1-3]. But what FRP reinforcement lacks in ductility, they make up in high tensile strength. On the contrary, FRP bars possess up to 25% lower modulus of elasticity than steel bars [2]. This relatively low modulus of elasticity of FRP bars makes serviceability limit (deflection and crack width), rather than strength limits, the governing limit state [23]. Table 2 shows the typical tensile properties of the common FRP reinforcement bars compared with the same properties of steel bars. The properties of FRP bars lay on a spectrum due to the variation in material properties as mentioned before. The strength values shown at the highest end of the spectrum reflect a higher fiber volume ratio and vice versa [1]. The strength of the resin, also, affects the strength values of the bars.

Table 2: Tensile properties of FRP reinforcing bars [1].

Criteria	CFRP	GFRP	AFRP	Steel
Yield stress (MPa)				276 to 517
Tensile strength (MPa)	600 to 3690	483 to 690	1720 to 2540	483 to 1600
Elastic modulus (GPa)	120 to 580	35 to 51	41 to 125	200
Yield strain (%)				0.14 to 0.25
Rupture strain (%)	0.5 to 1.7	1.2 to 3.1	1.9 to 4.4	6 to 12

BFRP tensile properties are not provided in the table above due to the fact that BFRP is still not considered a viable alternative to steel reinforcement yet. Basalt FRP composites are considered the most recent development in the FRP composites

industry. Studies, however, indicates that BFRP composites are more cost-effective than CFRPs, have greater strength and modulus of elasticity, and are more chemically stable than GFRP composites [19]. Furthermore, FRP bars have a lower carbon footprint than steel bars which makes them a good choice from an environmental standpoint [24]. The few studies conducted to investigate the material properties of BFRP bars reported that BFRP lays between the GFRP and CFRP, strength wise. The studies aimed to validate the merit of the BFRP properties and whether those properties are in line with guidelines provided by the available codes. Elgabbas et al. had conducted an investigation to examine the mechanical properties of the BFRP bars [19]. The study found that the physical and material properties of the newly developed BFRP bars meet the standards put forth by ACI 440.1R [1] and CAN/CSA S806 [13]. Studies conducted to investigate the flexure and shear behaviors of BFRP reinforced structures is going to be discussed in section 2.3 of this report.

As for the compressive behavior of the FRP bars, the codes are clear about their discouragement from utilizing FRP bars to resist compressive loads. Compressive strength of FRP bars is lower than their tensile strength; so is the case with the compressive modulus of elasticity [1]. The most common modes of failure for FRP bars loaded compressively are: fiber micro-buckling, shear failure, and transverse tensile failure [1]. Afifi et al. [25] studied the contribution that CFRP and GFRP bars have on the compressive strength of columns. The study concluded that the average load carried by the aforementioned FRP reinforcements concrete columns was just shy of 12 percent of the maximum load [25]. Another study conducted by Al Najmi and Abed, studied the mechanical properties of FRP reinforcement under compression [26]. The study concluded that, unlike tensile strength, compressive strength of FRP bars was proportional to the bar size. The study also reported that FRP reinforcement increased the compressive capacity of concrete columns by up to 35%. Despite the promising findings various studies about the behavior of FRP reinforcement in compression [27-32], the ACI 440.1R code neglects the contribution of FRP bars in columns, and in flexural member's compressive zone.

Higher strength and modulus of elasticity do not necessarily connote better performance for FRP reinforced concrete beams. As mentioned before, the serviceability limit state is the governing limit state in FRP reinforced structures. The

serviceability of a FRP reinforced structure is very dependent on the bond behavior between the FRP and concrete. The bond between FRP reinforcement and concrete differ from that of steel [33]. The bond behavior is affected by factors such as bar surface texture and concrete cover [34]. The bond behavior can be analyzed using the pullout test, splice test, and flexural test. The bond behavior is used to determine the embedment length required to prevent slippage [1]. The bond behavior is measured using the bond-dependent coefficient (k_b) which ranges from 0.6 to 1.72 according to the ACI 440.1R design guidelines [1]. Steel bars have a k_b equal to one; any value less than one indicates that the FRP bar have a superior bond behavior than the steel bars do and vice versa. The ACI 440.1R code recommends using a conservative k_b value of 1.4 in the design process.

Deflection of a FRP reinforced beam, also, differs from that of steel reinforced beams. The lack of ductility of FRP bars combined with the low modulus of elasticity cause the beam to experience larger deformation before failing [35]. The larger deformation leads to larger cracks which is why serviceability limit state requirements usually control the design of FRP reinforced beams [1].

2.2. Glass Fiber-Reinforced Polymer (GFRP)

Glass Fiber-Reinforced Polymer (GFRP) is one of the most commonly used FRP composites in structural elements. Extensive studies have been conducted to investigate the structural behavior of GFRP reinforced beams. Many studies were conducted to examine the flexural and shear behavior of concrete beams reinforced with GFRP bars. The investigation of flexural performance of GFRP reinforced beams has been conducted experimentally and numerically [9, 17, 36].

A study conducted by Habeeb et al. attempted to evaluate the flexural behavior of continuous GFRP RC beams [9]. In total, two simply supported and three continuously supported GFRP RC beams were tested. The main parameter of the experimental program of the study was the reinforcement ratio. Based on the reinforcement ratio, some of the specimens were over-reinforced, while others were under reinforced. The results showed that the load causing the first crack was much higher in the over-reinforced beams than it was in the under-reinforced ones. The study, also, indicated that continuously supported GFRP reinforced beams showed earlier and wider cracks than steel reinforced concrete beams [9].

El Refai et al. invistegated the structural performance of concrete beams reinforced with hybrid reinforcement [17]. Six concrete beams reinforced with a combanation of steel and GFRP bars and three other beams reinforced with only GFRP bars were tested to evaluate thier flexural behavior. The results showed that a combination of GFRP and steel rienforcment improved the behavior of the concrete beams as it enhnanced load carrying capacity, deformability, cracking stiffness[17]. Few of hybrid-reinforced beams failed in a ductile manner resulting from concrete crushing after the yielding point of steel reinforcement. The results indicated that the CAN/CSA S806 guildlines are conservitive for prediciting the delfection of hybrid reinforced concrete beams.

Saikia et al. studied the performance of beams reinforced with GFRP bars in flexure [36]. In total, ten beams with different reinforcement ratio were cast. The ten beams had various amounts of fibers added to the concrete mix. The beams had dimensions of (180 x 250 x 1340-mm) and were tested using four-point bending test to observe their flexural behavior. The results indicated that failure of the GFRP reinforced concrete beams resulted from the reduced post cracking stiffness and the slip between rebar and the concrete surface. The addition of fibers had negligible effect on the post cracking behavior of the GFRP reinforced beams because the strength of the GFRP was governing the behavior of the beam after the first crack appears [36].

2.3. Basalt Fiber-Reinforced Polymer (BFRP)

Basalt Fiber-Reinforced Polymer (BFRP) is the one of the most recent development in the fiber-reinforced polymer market. Basalt fiber is made from mined basalt rocks present near volcanic regions. The rocks are melted at a temperature of 1400° C and the molten basalt is extruded through special nozzles to produce the basalt fiber [19]. The chemical composition of BFRP is very close to the chemical makeup of the GFRP, except that basalt has a high ratio of iron which gives it its distinct dark color[19]. Limited number of studies have been conducted to investigate the behavior of BFRP reinforced structures [11, 16, 37-41].

Tomlinson et al. studied the performance of beams reinforced with BFRP in flexure and shear [11]. Nine beams with reinforcement ratios ranging from 0.28 to 1.60 were cast. The beams had dimensions of (150 x 300 x 3100-mm) and were tested

using four-point bending test to investigate the effect of BFRP flexural reinforcement ratio and the structural behavior of the beam. The beams were transversely reinforced by BFRP or steel stirrups while some beams had no shear reinforcement at all. The results indicated that the beams with no transverse reinforcement and the ones with BFRP stirrups failed in shear while the ones with steel stirrups failing in flexure [11]. Furthermore, it was concluded that, regardless of what stirrups were utilized, the ultimate capacities of the beams were disproportional to the BFRP flexural reinforcement ratio.

Elgabbas et al. (2016) studied the bond-dependent coefficient (k_b) and the structural performance of BFRP bars in concrete beams [16]. Six beams reinforced in the longitudinal flexural direction with 10 mm, 12 mm, and 16 mm sand coated BFRP bars were cast. The beams had dimensions of (200 x 300 x 3100-mm) and were tested using four-point bending test. The results yielded a k_b of 0.76 which is in agreement with the CSA S6 guidelines [14]. The study also indicated that the axial stiffness of the reinforcement considerably affected the flexural behavior of the beams. Beams with high axial stiffness showed lower deflection, strains, and number of cracks. The beams showed the same pre-cracking behavior due to the fact the behavior of the beam was governed by the concrete. After the first crack, beams with higher reinforcement ratios showed higher stiffness[16].

Elgabbas et al. (2017) aimed to investigate ribbed BFRP reinforced concrete beams flexural behavior and serviceability performance [37]. In total, eight beams were reinforced in the longitudinal flexural direction; six of which were reinforced with 8 mm, 12 mm, and 16 mm ribbed BFRP bars. The remaining two beams were reinforced with steel for reference purposes. The beams had dimensions of (200 x 300 x 3100-mm) and were tested using four-point bending test. The results yielded a k_b of 0.83 which is lower than the k_b=1 (for ribbed FRP bars) recommended by the CSA S6 [14]. The study also yielded that the axial stiffness of the reinforcement considerably influenced the flexural behavior of the beams [37].

Abed et al. studied effects of adding different types of fibers to the concrete mixes on the flexural behavior BFRP reinforced concrete beams [38]. Twelve beams were cast using plain, and basalt and synthetic fibers-reinforced concrete (FRC) with a 40 MPa compressive strength. The beams had dimensions of (180 x 230 x 2000-

mm) and were tested using four-point bending test. The BFRP reinforcement used are 8 mm, 10 mm, and 12 mm sand coated bars. The results indicated that increasing the BFRP flexural reinforcement ratio led to improving the flexural capacity of BFRP reinforced beams, regardless of the concrete type [38].

2.4. Exposure of Fiber-Reinforced Polymer (FRP)

Exposure to harsh environment can weaken the FRP bar strength. As previously mentioned, resin is a major component of FRP bars and it is impacted by exposure. Harsh environment can reduce the strength of the FRP bar by reducing the strength of the resin. Saline solutions, ultraviolet radiation, moisture, and alkaline solutions could substantially diminish the strength of the resin binding the fibers together [1]. There has been few studies investigating the effects of : Alkaline solutions [42-44], temperature [10, 45-47], and saline solutions [34, 48]. Some of the studies investigated the mechanical properties directly through tensile and pullout test while others studied the behavior of concrete beams reinforced with exposed FRP bars.

Wu et al. studied tensile properties of BFRP bars exposed to alkaline solution, salt solution, acid solution, and deionized water [42]. The study utilized scanning electronic microscopy (SEM) to monitor the degradation mechanism of BFRP bars in an alkaline environment. The results indicated that acid, salt, and deionized water had a lower impact on the durability of BFRP bars than the alkaline solution did [42].

Sim et al. examined the durability of basalt, glass, and carbon fiber exposed to alkali solution combined with high temperatures [43]. The results showed that after seven days exposure, basalt and glass FRPs lost 50% of their strength and volume. Carbon FRP, however, only lost 13% of its strength during the same exposure time. The resin and fiber type played a big role in degradation resistance and since GFRP and BFRP had almost the same chemical composition they degraded at similar rate. CFRP, however, did not face any, relatively, significant degradation. Wang et al. had also studied the durability of BFRP bars exposed to alkali solution [44]. The study concluded that after three months of exposure the strength of the bars decreased by 40% but the modulus of elasticity remained unaffected. The results also indicated that the BFRP bars had lower degradation than the basalt fiber with no resin protection [44].

Calvet et al. investigated the effect of the environmental conditions on the bond behavior of different CFRP bars [45]. The study indicated that at high temperatures, the textured part of the CFRP bar separated from the bar. CFRP bars had shown a better bond behavior than the reference steel bars did. The bond strength was 10% higher at the CFRP reinforcement system than at the steel [45]. Another study that investigated bond behavior was conducted by El Refai et al. in 2015 [34]. The study analyzed the impact of accelerated aging conditions on the bond degradation of BFRP bars. The bars were exposed to aggressive environment such as acid, saline, and alkaline. The results indicated that regardless of exposure, BFRP bars showed higher bond strengths than the ribbed GFRP did. The surface texture controlled the slippage resistance, as sand coated bars had better adhesion to concrete than ribbed bars regardless of the fiber type. Furthermore, the study indicated that GFRP bars exposed to acid solution suffered 25% loss in strength while the ones exposed to alkali and sea water lost 17% of its original strength.

Robert et al. invistigated the impact of high tempretures om GFRP bars [49]. The study found that tempretures from 40° to 50°C had no significant effect on the tensile strength and modulus of elasticity. Masmoudi et al. studied the effect of varation in temperature (20 °C to 80 °C) on the bond performance of GFRP bars in concrete [47]. In total, eighty pullout specimens were tested to determine the bond behavior of the GFRP bars. The exposure period reached up to eight months and the highest temperature reached 80 °C. the study found that the exposure cause a 14% reduction in bond strength of the tested GFRP speciemns [47].

Another study conducted to analyze the the impact of varation of temperture exposure on the bond performance of FRP bars was conducted by Alvarez et al. [50]. Speciafacly, the study invisitaged the impact of long term exposure to high tempretures and humadity on the pullout behavior of GFRP and CFRP bars [50]. The study concluded that the said exposure did not impact the bond strength in spciments reinforced with small diameter GFRP bars (9.5 and 12.7 mm). On the other hand, specimens reinforced with larger GFRP bars (15.9 and 19.1 mm) showed reduction equal to 26% in bond strength due to exposure. Another study to evalute the impact of thermal exposure on the bond between FRP bars and concrete was conducted by Galati et al. [51]. The FRP bars in the study were exposed to thermal cycles with

tempretures reaching up to 70° C and were tested through the direct pullout test. The study concluded that themal exposure had caused a significant degradation of the FRP bars. The bond strength in all of the afromentioned studies was determened using pullout test but no determination for impact of temperture and humidity on bond behavior. A previos study conducted by the author of this report aimed to study the impact of temperture and humadity specifically on the k_b factor of FRP reinforced beams [52]. A total of four beams reinforced with exposed BFRP bars were tested and the results indicated that no significant conclusion could be drawn to determine the impact of the temperature plus humidity combination on the k_b factor. To produce conclusive findings, the study conducted in this report expands the number of studied beams and FRP types; the exposure period is longer than the previous study as well.

The conclusion drawn by the literature is in agreements in some aspects but differs in other aspects. Generally, the literature shows that the design codes are conservative when predicting the bond-dependent coefficient. The literature also shows that the ACI 440.1R [1] code is conservative when predicting capacities and deflection values of FRP RC beams. Additionally, most of the studies were in agreements with regards to parameters such as impact of axial stiffness and reinforcement ratio on the behavior of FRP RC beams. The literature shows that an increase in reinforcement ratios leads to a disproportional increase the flexural capacity. With regards to the axial stiffness, the literature shows that increase in axial stiffness leads to lower deflection, strain, and number of cracks.

The literature, however, is not in agreements with regards to other parameters such as the impact of exposure and the impact of different surface texture on the behavior of FRP RC beams. For example, some studies concluded that ribbed FRP RC beams yielded better bond behavior than their sand coted counterparts; other studies showed the opposite to be true. With regards to the impact of exposure on the behavior of FRP RC beams, the literature is not conclusive about the extent of the damage exposure causes. Exposure to temperature, specifically, caused varying impact on the mechanical properties of FRP bars. Some studies concluded that moderate temperature caused minimal impact on the mechanical properties on FRP bra while other studies concluded that exposure to moderate temperature causes considerable impact on the mechanical properties of FRP bars.

This study attempts to confirm the common findings and conclusions such as the ability of the code to accurately predict the behavior differs from the literature. The study also attempts to confirm the superior bond behavior between FRP bars and concrete. The study differs from the temperature with respect to the exposure and conducted tests. The impact of exposing FRP bars to the environment on the flexural behavior and serviceability of FRP RC beams has not been studied in the literature. Specifically, the impact of exposing FRP bars to sunrays, rainfall, and humidity for a long period on the flexural capacity, crack behavior, and bond-dependent coefficient was not investigated in the literature. The current study attempts to study the aforementioned in order to add to the pool of research in the area of impact of exposure on factors such as flexural capacity, crack behavior, and bond-dependent coefficient.

Chapter 3. Experimental Setup

In this chapter, the experimental program followed in this study is discussed. The first section explains the exposure program studied herein. The second and third sections discuss the design considerations and equations. The fourth and fifth sections highlight the beam detailing and test matrix. The latter three sections discuss the material properties, sample preparation, and testing setup, respectively. A summary of the experimental program is shown in Figure 2.
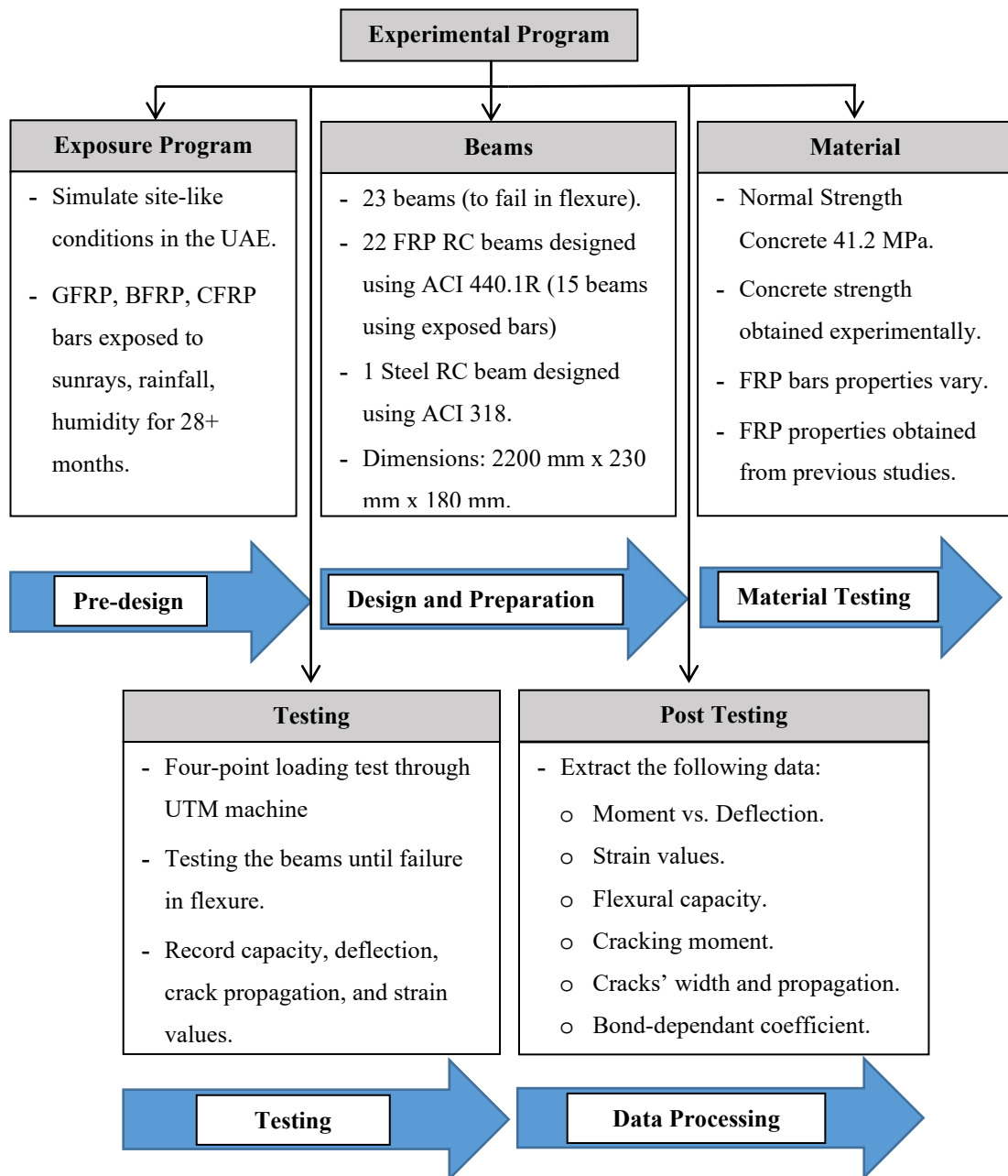
Figure 2: Experimental program flowchart.

3.1. Exposure Program

This section gives a general overview about the exposure program and its significance and practicality as well as data for the specific exposure parameters.

3.1.1. Exposure overview.
The exposure program presented herein seeks to simulate site conditions for FRP bars. In cases of lack of funding or even economic recession, construction project can be put on hold for a long period of time. During pauses in projects, materials are sometimes left outdoors exposed to the surrounding environment. The climate of such environments can range from very cold and rainy to very hot and dry including any mixture in between. The cold environment is accompanied by freeze and thaw cycles and the hot environment present heat, moisture, and ultra-violet waves. The exposure of concern in this study is based on the climate of the Arabian Gulf region, specifically the climate in UAE. To simulate the needed exposure, a group of BFRP (sand coated) bars and GFRP (sand coated and ribbed) bars were placed in an exposure tank in the vicinity of the American University of Sharjah (AUS). The bars were placed outdoors for a +28 mouths. The temperature, rain, and humidity records of the exposure period are presented in following sections. The tank used in this study is shown in Figure 3. The location and shape of the tank allowed for maximum sunrays, rain, and humidity exposure.
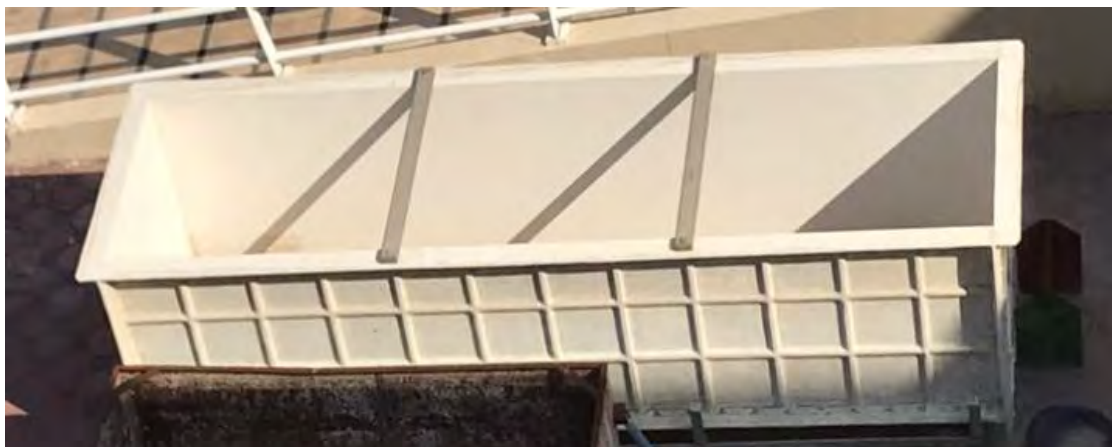
Figure 3: Exposure tank.

The Impact of exposure on the FRP bars is visibly evident as shown in Figure 4. Sand coated GFRP bars subjected to exposure are noticeably darker than their unexposed counterparts (as shown in Figure 4 (a)). As for ribbed GFRP bars, the

impact of exposure on the color of the bars is much clearer. As seen in Figure 4 (b), ribbed GFRP bars subjected to exposure showed darker dull color when compared with their unexposed counterparts. Lastly, exposure reduced the vibrant dark color of the BFRP bars as shown in Figure 4 (c).

(a)   (b)

(c)
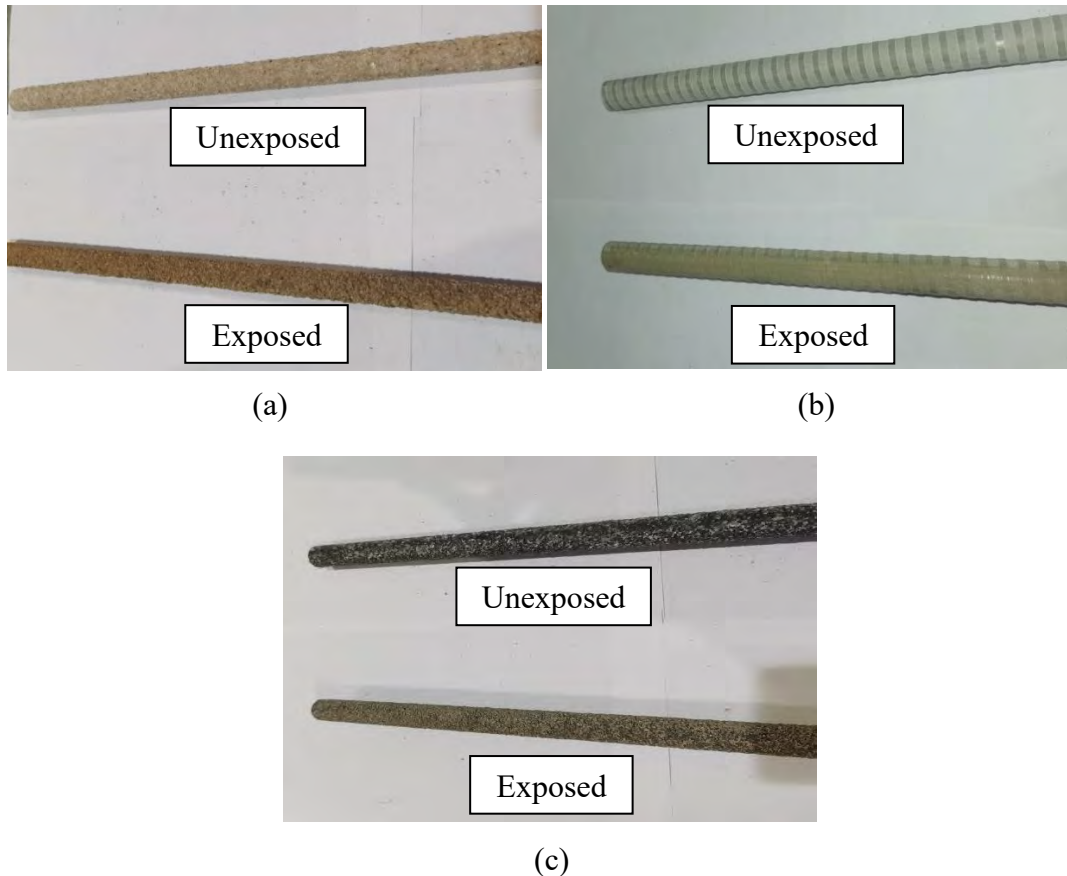
Figure 4: Visible impact of exposure.

3.1.2. Exposure parameters. The exposure parameters investigated in this report are temperature and ultra-violet waves, rainfall, and humidity. The records of the exposure period for the above stated parameters are shown in the following sections.

3.1.2.1. *Temperature and ultra-violet waves.* The recorded temperature for the duration of the exposure period is reported in Figure 5. Temperature fluctuated during the year but kept a constant trend across the years. The temperature peaks during the summer months reaching values of +40° Celsius and is at its lowest during the winter months where it reaches just below 20° Celsius. It shall be noted that the reported

temperatures are not the maximum daytime temperatures (reaching up to 50+ Celsius in some summer days) but rather an average of daytime and nighttime temperatures during the various seasons.

Figure 5: Temperature records in the city of Sharjah (SEP17-JAN20) [53].

3.1.2.2. *Rainfall.* The recorded rain for the duration of the exposure period is reported in Figure 6. Rain is scarce in Sharjah but nonetheless the rainfall records are reported since the FRP bars were exposed to rain. Throughout the first half of exposure duration, precipitation did not breach the 20mm average. The second half of the exposure period saw much higher precipitation levels. From January 2019 to January 2020, the city of Sharjah received a maximum level of rainfall higher than 110 mm. Rainfall records are included for reference despite the potential lack of impact on the properties of the FRP bars. Since the bars were, by default, exposed to rain, the rain records are reported even if rainfall was not an intended type of exposure.
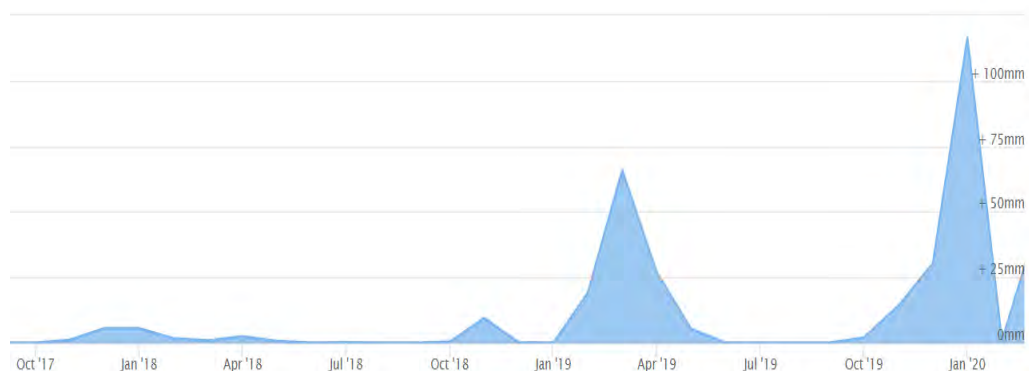
Figure 6: Rain records in the city of Sharjah (SEP17-JAN20) [53].

3.1.2.3. *Humidity*. The recorded Humidity for the duration of the exposure period is reported in Figure 7. Humidity fluctuated during the year but keeps a constant trend across the years. The humidity ranged from 50% to 60% during the exposure period. It shall be noted that the reported humidity are not the maximum daytime humidity values (reaching up to 80% on some occasions) but rather an average of daytime and night time temperatures.
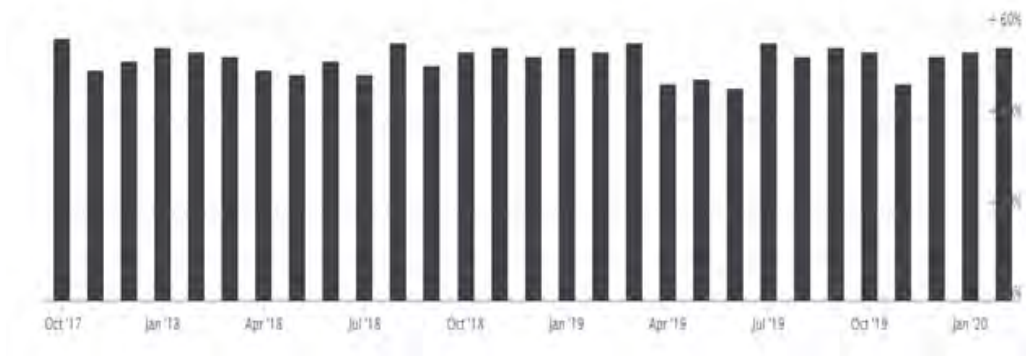
Figure 7: Humidity records in the city of Sharjah (SEP17-JAN20) [53].

3.2. Design Considerations

This section illuminates the important factors that should be taken into consideration while designing steel and FRP beams. The steel beam was designed in accordance with ACI 318 [12] for flexure failure. The FRP beams, on the other hand, were designed following the ACI 440.1R [1] for flexural failures as well.

3.2.1. Steel RC beams. The ACI 318 provides extensive details for flexural design beams reinforced with steel bars [12]. The code categorizes reinforced beam sections into tension-controlled and compression-controlled sections with a balanced section as a divider. In a balanced section, failure occurs due to concrete crushing and tensile yielding simultaneously. Preceding the balanced section, on the strain axis, is the compression-controlled section. Compression-controlled sections are overly reinforced which cause them to fail due to concrete crushing. The failure is sudden, and sometimes catastrophic, as crushing does not display warning signs. On the other hand, tensile-controlled sections are under reinforced which cause them to fail due to steel yielding. Due to the nature of failure for the tension and compression section, a lower reduction factor (ϕ) is used for compression-controlled sections than for

36

tension-controlled sections. Compression-controlled sections are more brittle and are affected by disparities in concrete properties and strength. Furthermore, they are designed to carry more load than tension-controlled sections which, for safety reasons, reduces the strength reduction factor for the compression-controlled sections. A schematic for the variation of the reduction factor based on the tensile strain level is shown in Figure 8.
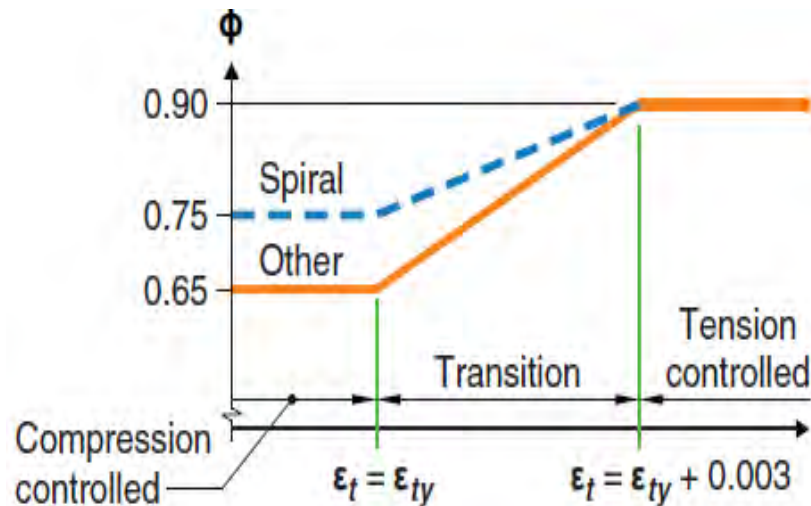
Figure 8: Variation of reduction factor with tensile strain, steel reinforcement [12].

The strength reduction factor of tension-controlled sections, as shown in Figure 8, is 0.9 compared with 0.65 for compression-controlled sections. The discrepancies in the reduction factors are due to the level of certainty about material properties and strength of beam sections. With a higher reduction factor, tension-controlled sections are more desirable in the design of concrete beams reinforced with steel bars. The ACI 318 does not allow the design of over-reinforced or balanced beams for flexural members. The tension-controlled section, or under reinforced sections, are more ductile because they are designed to utilize the yielding of the steel bars. The one steel beam used in this study carries a reinforcement over balanced ratio (pf/pfb) equal to 0.21 which is an indication that the beams would fail due to steel rupture (tension-controlled). As previously mentioned, the steel rupture mode of failure is the only permitted mode of failure in the ACI 318 code.

3.2.2. FRP RC beams. FRP reinforcement possess substantial tensile strength, large elongation, and show a linear stress- strain behavior. The former

reasons must be taken into consideration when designing FRP RC beams. However, the noncorrosive behavior of FRP bars must be put in mind when evaluating the merit of using FRP reinforcement [1]. To a much lower extent than the ACI 318 provides information about steel reinforcement, design codes such as the ACI 440.1R [1], CSA-806 [14], CSA-S6 [13], and ISIS Manual No. 3 [15] provide some guidelines that govern the design of FRP reinforcement. The focus of the study is based on provisions provided by the ACI 440.1R. The ACI 440.1R is still under development and many design criteria are still not provided. For example, the code does not recommend the use of FRP reinforcement where moment redistribution is required. The recommendation does not come from a certainty about the unsuitability of FRP bars in moment frames; on the other hand, it stems from an uncertainty about the behavior of the said reinforcement [1].

The ACI 440.1R covers flexural and shear design provisions of beams reinforced with FRP bars. Since FRP bars are anisotropic in nature, their properties differ in the longitudinal direction when compared with the properties in the transverse direction. The anisotropic nature of the bars must be taken into account when used as shear reinforcement. The code, also, neglects the contribution of FRP reinforcement in compression. Flexural design, provided by the code, has some similarities to the design process offered in the ACI 318 but they also differ in some cases. For example, unlike beams reinforced with steel bars, beams reinforced with FRP bars can be over reinforced or under reinforced. In fact, the practice of designing over reinforced FRP reinforced beams is encouraged. The similarity of the design process was done for consistency with the other ACI documents. Steel reinforced sections are deigned to be in the tension-controlled region to benefit from the ductility of the steel. The brittle nature of FRP bars, however, commended a change for the tension-controlled design approach. In fact, both tension-controlled and compression-controlled sections are satisfactory; on the condition that the design is in adherence with the strength and serviceability requirement. A schematic for the variation of the reduction factor based on the tensile strain level is shown in Figure 9. Furthermore, the figure shows the two zones of failure (FRP rupture and concrete crushing) as well as the transition zone. The 22 FRP reinforced concrete beams studied herein fall in all three zones of failure. 16 FRP RC beams fall in the compression-controlled zone, 4 FRP RC beams fall in the transition zone, and 2 beams fall in tension-controlled zone.
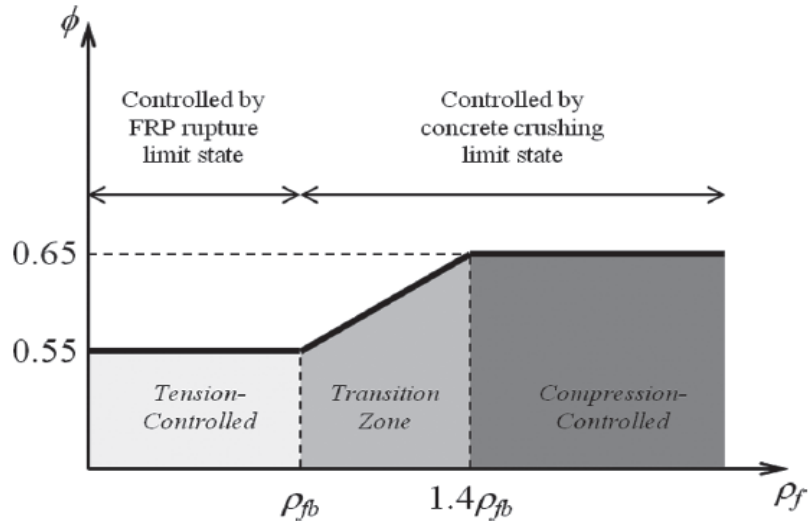
Figure 9: Variation of reduction factor with tensile strain, FRP reinforcement [1].

The ACI 440.1R takes into account the non-ductile behavior of FRP reinforcement as it reduces the design capacity through a reduction factor (ϕ). The reduction factors for FRP reinforcement, shown in Figure 9, are lower than their steel reinforcement structures counterparts. The reinforcement ratio is responsible for placing a section in the tension-controlled zone or the compression-controlled zone. The reinforcement ratio pf is compared to the balanced ratio pfb to show if the section is under reinforced or over reinforced. In the case of pf being less than pfb the section is considered under reinforced and the mode of failure would be due to FRP rupture. Subsequently, the FRP rupture limit state is assigned a 0.55 reduction factor. On the other hand, if pf is larger than 1.4 pfb, the section is considered over reinforced and the mode of failure would be due to concrete crushing. Consequently, the concrete crushing limit state is assigned a 0.65 reduction factor. In this study, all BFRP RC beams are over reinforced with pf higher than 1.4 pfb and, thus, fail in concrete crushing zone as per the ACI 440.1R code. Similarity, six GFRP RC beams are over reinforced with pf higher than 1.4 pfb and fail in concrete crushing as per the ACI 440.1R code. The remaining six GFRP RC beams diverge in failure mode. It is clear that two of the six remaining GFRP RC beams are under reinforced with pf lower than pf and thus fail in FRP rupture as per the code. The remaining four GFRP RC beams fall in the transition zone with pf higher than pfb but still lower than the 1.4 pfb compression-controlled zone cutoff. The exact failure mode of the four aforementioned GFRP RC beams is determined experimentally. The governing design

equations depend on the amount of beam reinforcement ratio. Tension-controlled and compression-controlled section, each, have distinct design equations corresponding to their mode of failure. The design equations for each mode of failure in section 3.3.

3.3. Design Equations

This section highlights the equations used to design the steel and FRP reinforced concrete beams.

3.3.1. Steel RC beams.
The code used for the design of steel RC beams is ACI 318 [12]. The steel reinforced concrete beam was designed to be under reinforced, tension-controlled, beam. The mode of failure for the steel reinforced concrete beam is steel yielding and the flexural capacity is computed using the following equation:

$$M_n = A_s f_y \left(d - \frac{a}{2}\right) \tag{1}$$

where:

M_n = moment capacity (kN.mm),

A_s = area of longitudinal reinforcement (mm^2),

f_y = yield strength of longitudinal reinforcement (MPa),

d = distance from extreme compression fiber to the centroid of the tension reinforcement (mm),

a = depth of the equivalent rectangular stress block which is calculated as using the following equation:

$$a = \frac{A_s f_y}{0.85 f'_c b} \tag{2}$$

The flexural capacity of the beams is adjusted using a reduction factor ϕ to account for uncertainty in the material. For the steel RC beam designed in this study, the reduction factor is 0.9 which corresponds to the tension-controlled failure for the under reinforced beam. The reduction factor is determined using the following equation:

$$\phi = \begin{cases} 0.65 & for\ (\varepsilon_t < (\varepsilon_y) \\ 0.65 + 0.25 \dfrac{(\varepsilon_t - \varepsilon_y)}{(0.005 - \varepsilon_y)} & for\ (\varepsilon_y < \varepsilon_t < 0.005) \\ 0.9 & for\ (\varepsilon_t > 0.005)) \end{cases} \tag{3}$$

3.3.2. FRP RC beams. The beam cross section and dimensions were designed according the ACI 440.1R code [1]. The following assumptions are used throughout the design process:

- Plane sections remain plane.
- Linear elastic tensile behavior of FRP reinforcement.
- The concrete section does not contribute to the tensile strength of the beam.
- The bond between the FRP reinforcement and concrete is perfect.
- The maximum concrete compressive strain is 0.003.

The aforementioned considerations are followed during the design process. The FRP design section is divided into flexural capacity provisions and serviceability provisions. The serviceability provisions discussed herein are restricted to the cracking behaviour provisions.

3.3.2.1 Flexural capacity. The design producers start with determining the reinforcement ratios, thus the type of failure, to utilize in this study. As mentioned in section 3.2.2, the ACI 440.1R code states that there are two types of flexural failures when designing FRP reinforced concrete beams [1]. The first mode of failure is FRP rupture which is similar to the tension-controlled failure cited by the ACI 318 code for steel reinforced beams [12]. The second failure mode is concrete crushing which is similar to the compression-controlled failure cited by the ACI 318 code for steel reinforced beams. The type of failure depends on the FRP RC beams reinforcement ratio as shown in section 3.2.2 of this report .

All BFRP RC beams and six GFRP RC beams and one CFRP RC beams, as subsequently shown in section 3.5, are designed to be over reinforced with a reinforcement ratio that exceeding the balanced reinforcement ratio ($\rho f > 1.4\ \rho fb$). The previous beams failed due to concrete crushing which allows for the study of such behavior in BFRP RC beams and GFRP RC beams. Four GFRP RC beams, with diameter of 10mm, fell in the transition zone between the tension-controlled and the compression-controlled zones. The reaming two GFRP beams, with diameter of 8mm, were designed to be under reinforced with a reinforcement ratio lower the balanced reinforcement ratio ($\rho f < \rho fb$). Balanced reinforcement ratio, ρfb, is defined as the amount of reinforcement needed to initiate the crushing of the concrete section at the

same time with the tensile rupture of the flexural reinforcement [1]. The balanced reinforcement ratio of FRP reinforced beams is determined through the following equation:

$$\rho_{fb} = 0.85\beta_1 \frac{f'_c}{f_u} \left(\frac{E_f \varepsilon_c}{E_{fu}\varepsilon_c + f_{fu}} \right)$$
(4)

where:

f'_c = concrete compressive strength (MPa),

f_{fu} = design tensile strength of FRP (MPa),

E_f = elastic modulus of FRP bar (GPa),

ε_c = ultimate concrete compressive strain,

β_1 = factor computed as follows:

$$\beta_1 = \begin{cases} 0.85 & for\ (f'c \le 28MPa) \\ 0.85 - 0.05 * \left(\frac{f'c - 28}{7}f \right) & for\ (28\ MPa < f'c < 56\ MPa \\ 0.65 & for\ (f'c \ge 56MPa) \end{cases}$$
(5)

The balanced ratio is compared with the reinforcement ratio to categorize the section; the reinforcement ratio is calculated as follow:

$$\rho_f = \frac{A_f}{bd}$$
(6)

where:

A_f = total area of the FRP reinforcement used in the section (mm^2),

b = width of the beam (mm),

d = effective depth (mm).

Using Equation (4) and (6), 16 FRP RC beams were designed to fail in concrete crushing where the reinforcement ratio of the beam is greater than the balanced reinforcement ratio ($\rho_f > 1.4\ \rho_{fb}$). Figure 10 shows the stress and strain distribution for the over reinforced concrete cross section. The neutral axis can be seen to be closer to the tension reinforcement than to the compression face. In this mode of failure, the properties of the concrete play a major role in determining the flexural capacity of the FRP RC beams. The concrete strain limit of 0.003 is surpassed in this mode of failure and the aforementioned limit is reached prior to the FRP rupture stain.
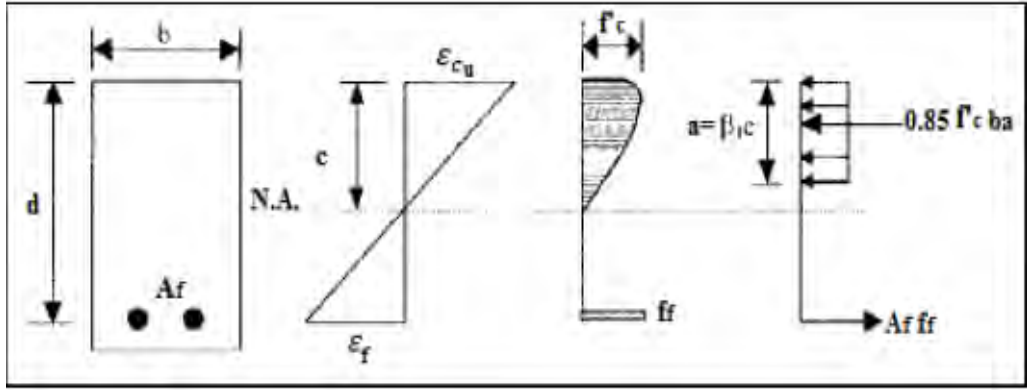
Figure 10: Failure governed by concrete crushing [1].

The nominal flexural strength for the over reinforced section shown in Figure 10 is computed using the following equation:

$$M_n = \rho_f\, f_f \left(1 - 0.59 \frac{\rho_f\, f_f}{f_c'}\right) bd^2 \tag{7}$$

where f_f stress in FRP reinforcement calculated using equation (8) below:

$$f_f = \left(\sqrt{\frac{(E_f \varepsilon_c)^2}{4} + \frac{0.85\beta_1 f_C'}{\rho_f} E_f \varepsilon_c} - 0.5 E_f \varepsilon_c\right) \le f_{fu} \tag{8}$$

Equation (4) and (6) yielded two beams that fail in FRP rupture. FRP rupture occurs when the reinforcement ratio of the beam is lower than the balanced reinforcement ratio ($\rho_f < \rho_{fb}$). Figure 11 shows the stress and strain distribution for the under reinforced concrete cross section.
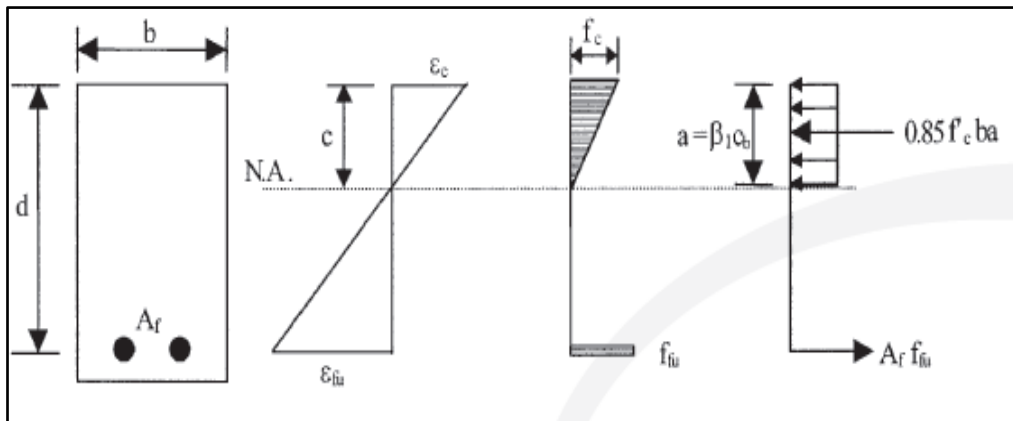
Figure 11: Failure governed by FRP rupture [1].

The nominal flexural strength for the under reinforced section shown, Figure 11, is computed using the following equation:

$$M_n = A_f \, f_{fu} \left(d - \frac{\beta_1 * c_b}{2} \right) \tag{9}$$

where c_b is the distance from the compression face to the neutral axis at balanced stain conditions and is computed as follows:

$$c_b = \left(\frac{\varepsilon_{cu}}{\varepsilon_{cu} + \varepsilon_{fu}} \right) * d \tag{10}$$

with ε_c being ultimate FRP rupture strain.

The remaining four GFRP zone fell in the transition zone between the tension-controlled and compression-controlled zones. The design equations were utilized based on the observed failure mode. It was concluded that out of the four aforementioned beams, three of which failed due to FRP rupture and one failed due to concrete crushing; the beams flexural capacities were calculated accordingly. However, it should be noted that for both over reinforced and under reinforced sections, the following provision must be satisfied:

$$M_u \leq \phi M_n \tag{11}$$

The equation above states that the applied moment should be less than the nominal flexural capacity of the beam. The flexural capacity is multiplied by a reduction factor to account for the lack of certainty in material properties and the lack of ductility of FRP and concrete. The reduction factor (ϕ) can be calculated as shown below:

$$\phi = \begin{cases} 0.55 \; for \; (\rho_f \leq \rho_{fb}) \\ 0.3 + 0.25 \dfrac{\rho_f}{\rho_{fb}} for \; (\rho_{fb} < \rho_f < 1.4\rho_{fb} \\ 0.65 \; for \; (\rho_f \geq 1.4\rho_{fb}) \end{cases} \tag{12}$$

3.3.2.2 Crack behavior. The two design provisions discussed hereafter are focussed on cracking moment and bond-dependant coefficient (k_b) calculations. Cracking moment is the moment at which the concrete section would start cracking. The cracking moment fully depends on the cross-sectional dimensions and concrete

strength. The cracking moment of all beams in this study is calculated using the following equation:

$$M_{cr} = \frac{2f_r I_g}{h}$$ (13)

where:

M_{cr} = cracking moment (kN.mm),

I_g = gross moment of inertia for the section (mm^4),

h = depth of beam (mm),

f_r = modulus of rupture calculated as follows:

$$f_r = 0.62\sqrt{f'_c}$$ (14)

The bond-dependent coefficient (k_b) is the factor that determines the strength of the bond between FRP reinforcement and concrete as previously mentioned. The k_b factor is closely tied to the crack width of FRP RC beams. The first attempt to calculate the k_b factor was developed by Gergely and Lutz in 1968 [54]. The equation is presented below:

$$w = 2.2\frac{f_f}{E_f}k_b\frac{h_1}{h_2}\sqrt[3]{d_c A}$$ (15)

where:

w = crack width (mm),

h_1 = distance between neutral axis and tension face,

h_2 = distance between neutral axis to centroid of reinforcement,

d_c = concrete cover from tension face to the center of closest bar (mm),

A = average effective area of concrete (mm^2).

The equation developed by [54] was utilized in the first ACI 440.1R code [55] and is still used in the ISIS manual No. 3 [15]. The ACI 440.1R committee replaced the Gergely-Lutz equation with an equation developed by Robert Frosch in 1999 [56]. The ACI 440.1R-6 [57] and CSA-S6 [14] both use the Modified Frosch Eqauition to calculte the k_b factor as shown in the following equation:

$$w = 2\frac{f_f}{E_f}k_b\frac{h_1}{h_2}\sqrt[2]{d_c^2 + (\frac{s}{2})^2}$$ (16)

where:

s = spacing between bars (mm).

The Modified Frosch Eqauition adds the spacing between bars to the crack width eqaution. A study conducted by Bakis et al. concluded that the k_b values calculated using the Modified Frosch Equation were 19% greater than the k_b values calculated from the Gergely–Lutz equation [58]. In other words, the Modified Frosch Equation is more conservative when compared to the Gergely–Lutz equation. The Modified Frosch Equation is rearranged to measure the k_b values in this study.

3.4.   Beam Detailing

In the design process for the cross section, the width of the beam is determined while taking into account all the recommendations of the ACI codes related to the number of bars, size of the bars, spacing between the bars and concrete cover. A minimum concrete cover of 40 mm is adopted by ACI 318-19 code [12] when using 12 mm bar to ensure an adequate protection for bars from the external exposure conditions. The FRP bars are not as sensitive to external conditions as steel bars are; the cover was chosen as 40 mm for uniformity purposes. For spacing between the bars, The ACI 318-19 code [12] has recommended a face-to-face spacing to be the greater of rebar diameter (db) or 25 mm (1 in). The bar diameters in this study as flexural reinforcement are: 8, 10, 12, 16, 20, and 26 mm. Therefore, it is ensured that face-to-face spacing is more than 25mm or 26 mm (Φ 26 RC beams).

To ensure flexural failure, the shear reinforcement ratio was provided in the shear span by two legs stirrups of 10 mm diameter spaced at 100 mm. After considering of all of previous requirements; the width of the beam was found to be 180 mm. As for the beam depth, the ACI 440.1R code has recommended a minimum thickness for the simply supported FRP beam to be one tenth of the span length ($L/10$). The depth of the beam is also governed by (a/d) ratio, the shear span to effective depth ratio. In this study, to ensure a pure flexural behavior, (a/d) ratio is taken to be more than 3.

Development length plays a role in determining the length of the beam. The minimum development length of glass FRP bars required to avoid failure by pullout is in the range of 26-37 times the bar diameter [1]. The largest diameter used is 26 mm

which mandates a development length of 962mm.

After considering all the requirements, the beam detailing became as follows: the width of the beam, already stated above, was picked to be 180 mm while the depth of beam was determined to be 230 mm. The resulting beam cross section is shown in Figure 12.
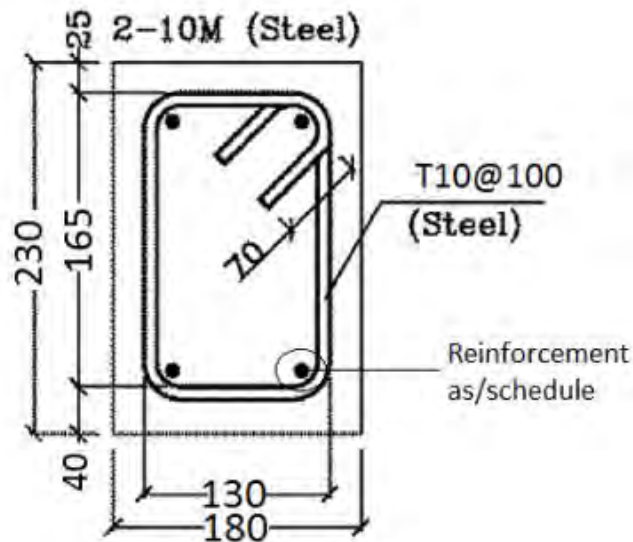
Figure 12: Beam cross section [52].

The clear span of the beam is 1900 mm. However, an extension of 150 mm from each side over the support must be added to ensure enough development length during the flexure test, resulting in a total length of 2.2 m (2200mm) for the beam specimens. The middle section of 400 mm was designed with no shear reinforcement to stimulate a flexural failure. The beam elevation is shown in Figure 13.
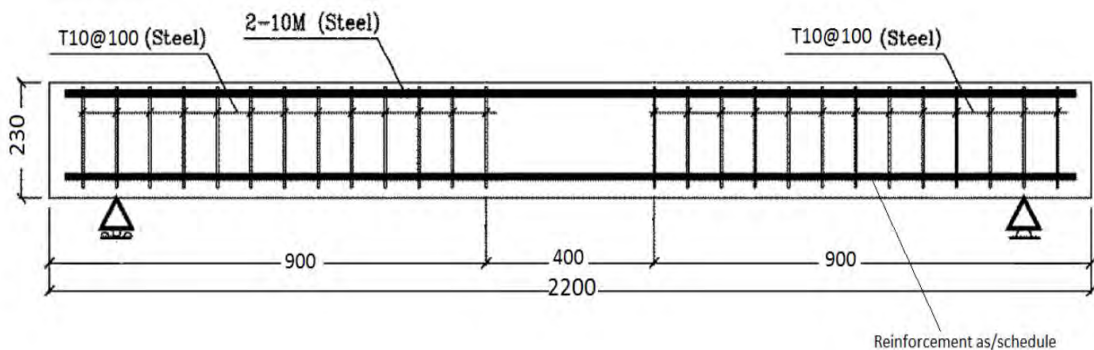
Figure 13: Beam elevation [52].

3.5. Test Matrix

A total of 23 beams were designed and cast and tested to study their flexural and serviceability behaviors. The beams were identified and named systematically based on the number of reinforcement bars, the type of reinforcement bars, the diameter of the bars, the surface texture of the bars, and the exposure of the bars or its lack of. The first part indicates the number of the flexural reinforcement bars used in the beams. The second part indicates the type of reinforcement. The third part provides information about the diameter of the bar in mm. The fourth part deals with exposure (E for exposed bars and U for unexposed bars). The last part, scripted in all but the steel beam, specifies the surface texture of the FRP bars (C for sand coated bars and R for ribbed bars). For example, 3G16EC means that three bars are used as reinforcement, the bars have a diameter of 16 mm, and are sand coated GFRP bars subjected to exposure. The test matrix of this study is shown in Table 3.

Table 3: Test matrix.

#	Beam ID	Reinforcement	A_f (mm^2)	ρf	$\rho f / \rho fb$	Axial Stiffness (MN)
1	2G8EC	GFRP	100.5	0.0030	0.93	4.51
2	2G10EC	GFRP	157.0	0.0047	1.39	7.05
3	3G16EC	GFRP	603.0	0.0184	4.55	27.07
4	2G20EC	GFRP	628.0	0.0194	3.87	28.20
5	2G8UC	GFRP	100.5	0.0030	0.93	4.51
6	2G10UC	GFRP	157.0	0.0047	1.39	7.05
7	2G10ER	GFRP	157.0	0.0047	1.36	7.05
8	2G20ER	GFRP	628.0	0.0194	4.19	28.20
9	2G26ER	GFRP	982.0	0.0308	5.54	44.09
10	2G10UR	GFRP	157.0	0.0047	1.36	7.05
11	2G20UR	GFRP	628.0	0.0194	4.19	28.20
12	2G26UR	GFRP	982.0	0.0308	5.54	44.09
13	2B8EC	BFRP	100.5	0.0030	1.40	4.95
14	2B10EC	BFRP	157.0	0.0047	2.16	7.74
15	3B10EC	BFRP	236.0	0.0071	3.25	11.63
16	2B12EC	BFRP	226.0	0.0068	2.47	11.14
17	2B16EC	BFRP	402.0	0.0123	4.37	19.82
18	3B16EC	BFRP	603.0	0.0184	6.55	29.73
19	2B20EC	BFRP	628.0	0.0194	4.76	30.96
20	2B10UC	BFRP	157.0	0.0047	2.16	7.74
21	2B12UC	BFRP	226.0	0.0068	2.47	11.14
22	2C12EC	CFRP	226.0	0.0068	2.36	25.54
23	2S12	Steel	226.0	0.0068	0.21	45.20

The flexural and serviceability behaviors of the beams shown in Table 3 were evaluated using a four-point bending test. The study examines the effect of few variables on the bond behavior and flexural capacity of the beams. The tested variables include exposure, reinforcement ratio, reinforcement surface texture, number of reinforcing bars, and type of reinforcement.

The experimental program consists of: analysis of the exposure influence on the flexural behavior and bond behavior, analysis of the influence of the reinforcement ratio on the flexural behavior and bond behavior, analysis of the effect different reinforcement surface texture on the flexural behavior and bond behavior, analysis of the impact of number of reinforcing bars on the flexural behavior and bond behavior, and analysis of the impact of the different types of reinforcing bars on the flexural behavior and bond behavior of concrete beams. The results are analyzed to obtain parameters such as: moment vs. displacement curves, moment vs. strain curves, flexural capacity, cracking moments, cracks width, and k_b values. The results are also compared to the predicted values calculated through the code provided equations presented beforehand in section 3.3.

The analysis of the influence of exposure on the flexural behavior and bond behavior of RC beams is conducted according to the schematic presented in Figure 14. The 14 beams used to analyze the impact of exposure are referred to as group 1. Group 1 is broken down into three subgroups (sand coated GFRP RC beams, ribbed GFRP RC beams, and BFRP RC beams) as shown in Figure 14. Each subgroup contains beams reinforced with exposed and unexposed bars of the same diameter.
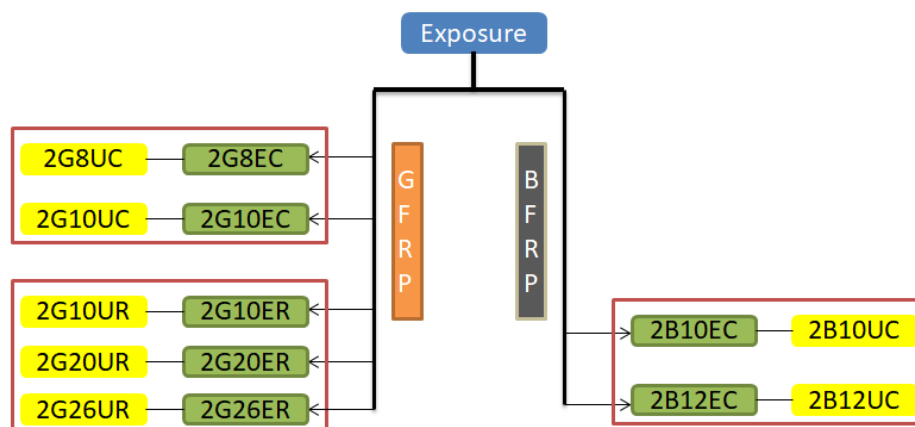
Figure 14: Exposure analysis group (group 1).

The analysis of the impact of reinforcement ratio on the flexural behavior and bond behavior is conducted according to the schematic presented in Figure 15. The 11 beams used to analyze the impact of reinforcement ratio are referred to as group 2. Group 2 is broken down into three subgroups (sand coated GFRP RC beams, ribbed GFRP RC beams, and BFRP RC beams) as shown in Figure 15. Each subgroup contains beams with reinforced ratios ranging from 0.0030 to 0.0194 for sand coated GFRP and BFRP RC beams and from 0.0047 to 0.0308 for ribbed GFRP RC beams.
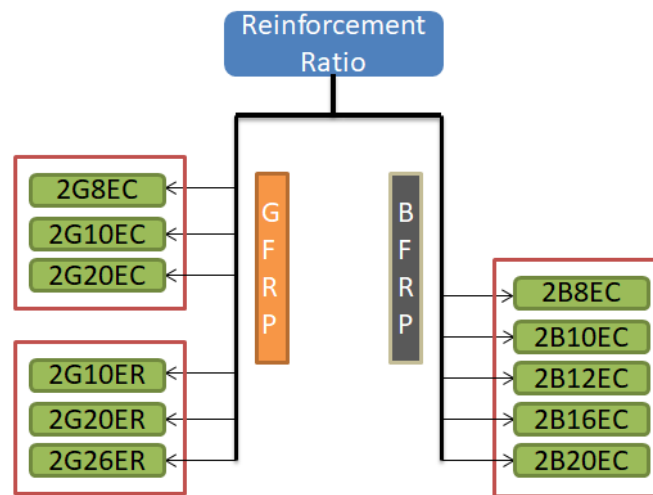
Figure 15: Reinforcement ratio analysis group (group 2).

The analysis of the influence of surface texture on the flexural behavior and bond behavior is conducted according to the schematic presented in Figure 16. The 4 beams used to analyze the impact of surface texture are referred to as group 3. The group contains beams reinforced with Φ 10 and Φ 20 ribbed and sand coated GFRP bars.
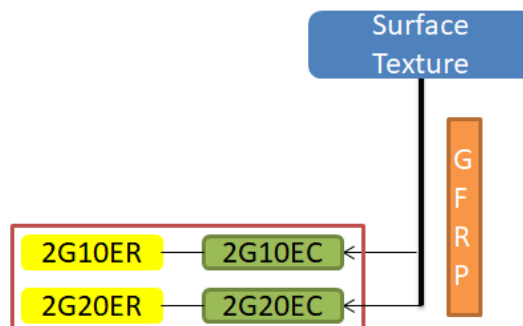
Figure 16: Surface texture analysis group (group 3).

The analysis of the impact of beam detailing (number of bars) on the flexural behavior and bond behavior is conducted according to the schematic presented in Figure 17. The 6 beams used to analyze the impact of number of bars are referred to as group 4. Group 4 is broken down into two subgroups (sand coated GFRP RC beams, and BFRP RC beams) as shown in Figure 17. Each subgroup contains beams similar axial stiffness but with different number of reinforcing FRP bars (2 vs. 3 reinforcing bars).
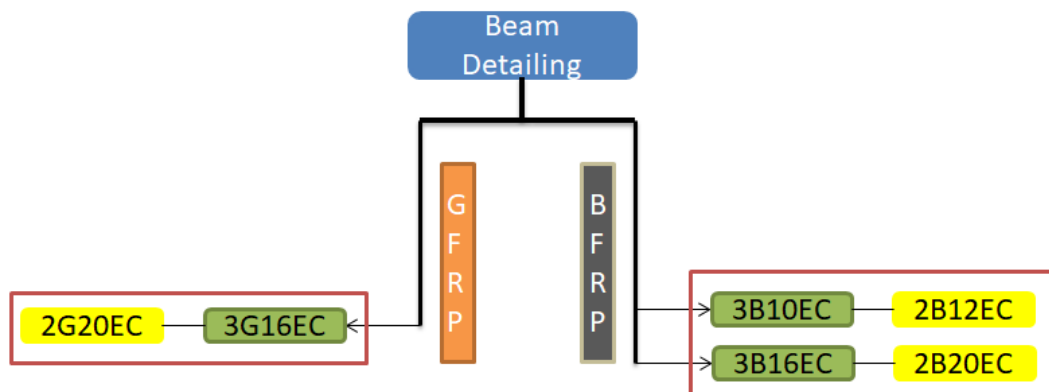
Figure 17: Number of bars analysis group (group 4).

The analysis of the impact of reinforcing bar type on the flexural behavior and bond behavior is conducted according to the schematic presented in Figure 18. The 3 beams used to analyze the impact of number of bars are referred to as group 5. The group contains a beam reinforced with two exposed BFRP bars, a beam reinforced with two exposed sand coated CFRP bars, and a beam reinforced with unexposed steel bars.
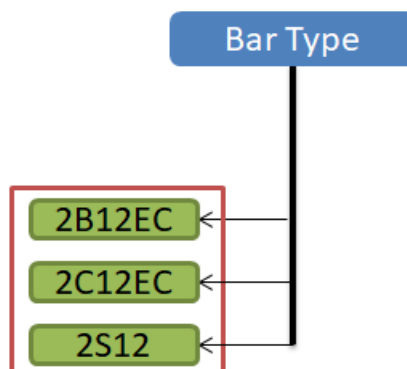
Figure 18: Bar type analysis group (group 5).

3.6. Material Properties

This section explicates the properties of the materials used in the experimental program. The values provided herein are obtained from experimental testing, previous studies, manufacturer specifications, and design codes. The materials discussed in this section are: concrete, steel, GFRP, BFRP, and CFRP.

3.6.1. Concrete. Normal strength concrete was used to cast the beams in this study. More specifically, 40 MPa Ordinary Portland Cement (OPC) provided by JAMIX Readymix was used. Cubes and cylinders were cast and tested to verify the properties of the concrete. The actual compressive strength of concrete was obtained through compression test conducted by crushing machine (shown in Figure 19).

Figure 19: Crushing machine (AUS lab).

In total, six cube and three cylinder specimens were tested to determine the compressive strength of concrete utilized in this study. The results of the compressive tests conducted by the crushing machine are presented in Table 4. The six tested cubes yielded compressive strength values ranging from 39.3 MPa to 42.9 MPa. The compressive strength of the cube specimens yielded a 41.2 MPa average compressive strength with 2.0 standard deviation. The three cylinder specimens yielded compressive strength values ranging from 31.3 MPa to 34.1 MPa. Average cylinder compressive strength was 32.6 MPa with a standard deviation of 1.3. The ratio of cylinder to cube compressive strength is 0.79 which falls in the range of 0.65 to 0.90 ratios reported in the literature [59].

Table 4: Concrete properties.

Cubes		Cylinders	
Specimen	f'c (MPa)	Specimen	f'c (MPa)
Cube # 1	39.5	Cylinder #1	32.5
Cube # 2	42.0		
Cube # 3	40.8	Cylinder #2	34.1
Cube # 4	42.6		
Cube # 5	42.9	Cylinder #3	31.3
Cube # 6	39.3		
Average (MPa)	41.2	Average (MPa)	32.6
SD	2.0	SD	1.3
Cylinder strength / Cube Strength			0.79

The failure of the cube and cylinder specimens can be seen in Figure 20. The cube specimens had a satisfactory type of failure as shown in Figure 20 (a) while the cylinder specimens yielded a cone and split type of failure as shown in Figure 20 (b).
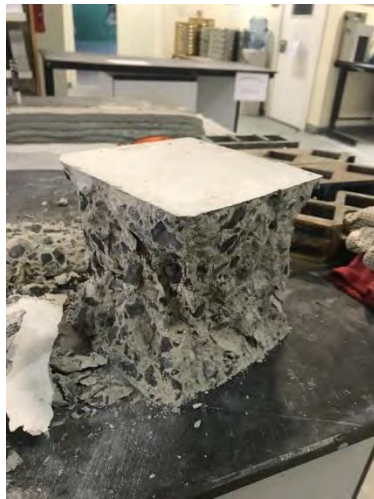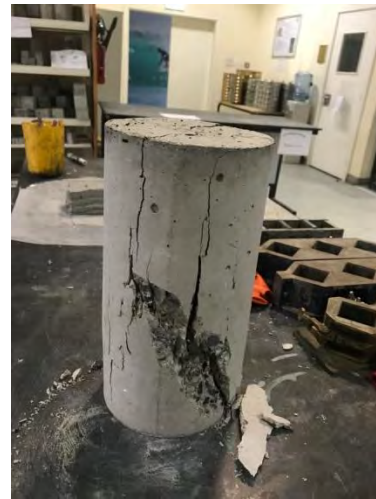
(a)   (b)

Figure 20: Cubes and cylinders failure.

3.6.2. Reinforcement. The properties of the reinforcement are reported as per previous studies, manufacturers' specifications, and design codes and as shown below:

3.6.2.1. *Steel.* Steel bars were used as the main flexural reinforcement for one beam as well as shear reinforcement for all beams in this study. In addition, all beams contained two #10 steel bars in the compressive zone of the cross-section. Furthermore, shear reinforcement in all beams were comprised of #10 stirrups. The

steel used was Grade 460 with an expected ultimate strength of 550 MPa and yield strength of 460 MPa; as per the ACI 318 [12].

3.6.2.2. *Glass Fiber-Reinforced Polymer (GFRP) bars.* GFRP bars were used as the flexural reinforcement for 12 of the beams in this study. Six of the GFRP Reinforced Concrete (RC) beams were reinforced with ribbed GFRP bars. The remaining six GFRP RC beams were reinforced with sand coated GFRP bars. The diameter of the GFRP bars ranges from 8mm up to 26mm. Two or three bars were used in each of the twelve beams as subsequently shown in section 3.5. Theoretically, GFRP bars have a 552 MPa tensile strength and 41.3 GPa modulus of elasticity [1]. The actual properties of the GFRP bars were, subsequently, obtained from previous studies on the same bars.

The sand coated GFRP bars were provided by Galen, a Russian manufacturing company based in the city of Cheboksary. The properties of the sand coated bars were reported in previous studies on similar bars [26, 32]. The tensile strength and elastic modulus for the sand coated GFRP bars are shown in Table 5.

Table 5: Sand coated GFRP bars properties [26, 32].

Bar type	Diameter (mm)	Tensile strength (MPa)	Elastic modulus (GPa)
GFRP (Sand Coated)	8	983	44.9
	10	960	44.9
	16	874	44.9
	20	779	44.9

The ribbed GFRP bars were provided by Pultron Composites Middle East, a GFRP manufacturing company based in Dubai. The properties of the ribbed bars were tested and reported in previous studies on similar bars [32, 60] The tensile strength and elastic modulus for the sand coated GFRP bars are shown in Table 6.

Table 6: Ribbed GFRP bars properties [32, 60].

Bar type	Diameter (mm)	Tensile strength (MPa)	Elastic modulus (GPa)
GFRP (Ribbed)	10	950	44.9
	20	813	44.9
	26	736	44.9

3.6.2.3. *Basalt Fiber-Reinforced Polymer (BFRP) bar.* BFRP bars were used as the flexural reinforcement for nine of the beams in this study. The diameter of the BFRP bars used ranged from 8mm to 20mm. Two or three bars were used in each of the nine beams as subsequently shown in section 3.5. The properties of the sand coated BFRP bars were reported in previous studies on similar bars [26, 32, 61]. The tensile strength and elastic modulus for the sand coated GFRP bars are shown in Table 7.

Table 7: Sand coated BFRP bars properties [26, 32, 61].

Bar type	Diameter (mm)	Tensile strength (MPa)	Elastic modulus (GPa)
BFRP (Sand Coated)	8	1268	49.3
	10	1268	49.3
	12	1118	49.3
	16	1109	49.3
	20	909	49.3

3.7. Sample Preparations

The 23 beams were prepared using 4 major steps shown in Figure 21. First, the FRP bars, provided by Galen and Pultron, were grouped into 23 separate clusters as shown in Figure 21 (a). Each separate cluster was, then, used to construct the 23 reinforcement cages as shown in Figure 21 (b). The strain gauges where, then, placed on the cages at Emirate Stone which is a Sharjah-based precast concrete company. The cages were, subsequently, placed in formworks and the 23 beams were cast in using concrete provided by JAMIX Readymix as shown in Figure 21 (d).

| (a) | (b) |

(c)   (d)
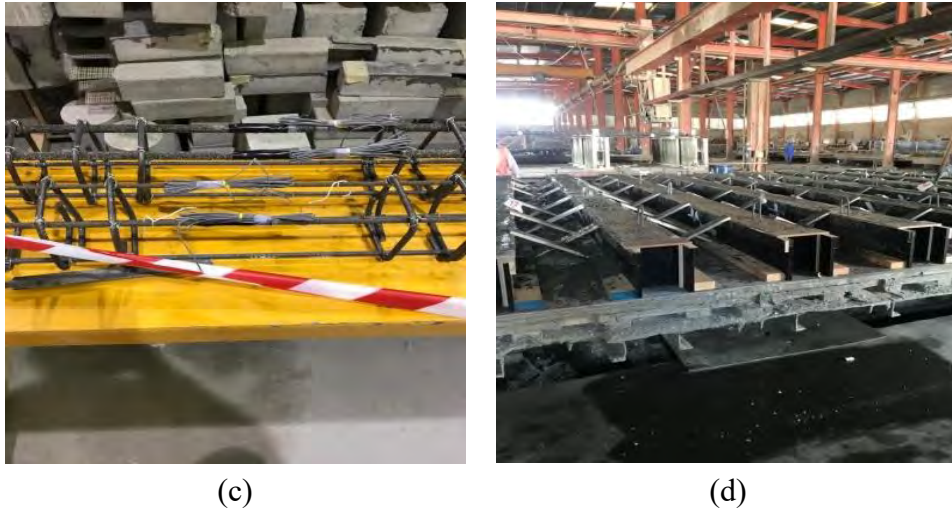
Figure 21: Preparation process.

3.8. Test Setup

The material properties are obtained using testes mentioned in section 3.1. The main test in this study is the four-point loading test. The four-point loading setup, shown in Figure 22, is used in this study to analyze the flexural response of all beams. The testing is conducted using a Universal Testing Machine (UTM) where jacks are used to apply the load directly on a spreader beam. The spreader beam divides the load equally on two points that are 400 mm apart. The area between the two load points becomes a constant maximum moment region as shown Figure 23.
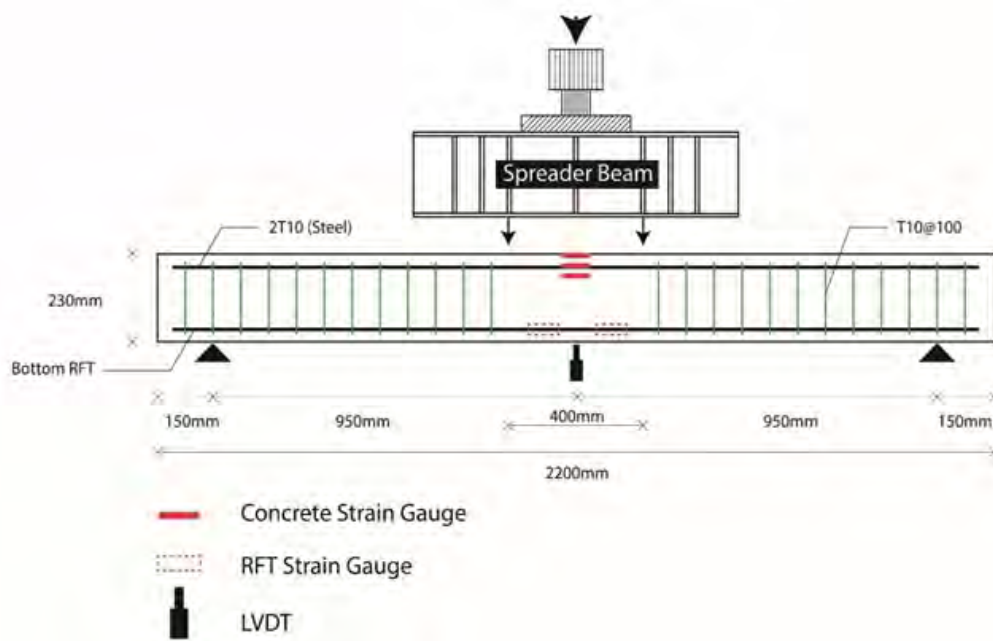
Figure 22: Test setup [52].
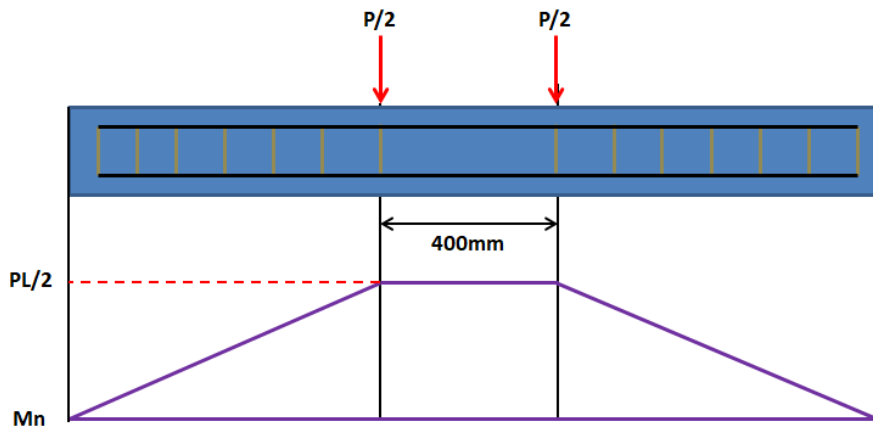
Figure 23: Constant moment zone.

Strain gauges were fitted on the surface of the concrete beams and on the flexural reinforcing bars to record the strain values throughout the test. A Linear Variable Differential Transformer (LVDT) was utilized to measure deflection. Lastly, crack transducers were utilized to measure the cracks width during the tests; the crack width was later used to calculate the k_b factors for the tested beams. The aforementioned testing instruments are shown in Figure 24. The UTM, LVDT, and crack transducer are shown in Figure 24 (a), (b), (c), respectively.

(a)

(b)

(c)

Figure 24: Testing instruments.

Chapter 4. Results and Analysis

In this chapter, the experimental results are presented in five sections as follows: Impact of variation in exposure, impact of variation in reinforcement ratio, impact of variation in surface texture, impact of variation in number of bars, and impact of variation in bar type on the flexural behavior and serviceability of FRP RC beams.

4.1. Impact of Exposure

This section highlights the impact of exposure on the strain values, flexural capacity, moment-deflection behavior, cracking moment, cracks width propagation, and bond-dependent coefficient.

4.1.1. Reinforcement and concrete strain. The effects of exposure on the longitudinal reinforcement and concrete strains of the 14 beams discussed hereafter are presented in Table 8, Figure 25, Figure 26, and Figure 27. The first set of beams presented includes sand coated GFRP RC beams. The set contains four beams reinforced with Φ 8 and Φ 10 sand coated GFRP bars as shown in Figure 25. The second set of beams includes ribbed GFRP RC beams. The set contains six beams reinforced with Φ 10, Φ 20, and Φ 26 ribbed GFRP bars as shown in Figure 26. The last set of beams studied in this section includes sand coated BFRP RC beams. The set includes four beams reinforced with Φ 10 and Φ 12 sand coated BFRP bars as shown in Figure 27.

Table 8: Reinforcement and concrete strain values (Group 1).

Beam	Moment (kN·m)	Longitudinal Reinforcement Strain	Concrete Strain
2G8EC	15.33	0.020	0.0011
2G8UC	17.11	0.020	0.0020
2G10EC	21.04	0.014	0.0030
2G10UC	25.28	0.019	0.0024
2G10ER	26.05	0.015	0.0016
2G10UR	26.43	0.018	0.0025
2G20ER	42.00	0.008	0.0026
2G20UR	42.62	0.009	0.0030
2G26ER	49.56	0.007	0.0033
2G26UR	44.65	0.006	0.0025
2B10EC	22.90	0.017	0.0022
2B10UC	24.76	0.019	0.0018
2B12EC	27.09	0.018	0.0028
2B12UC	26.96	0.015	0.0026

4.1.1.1. *Sand coated GFRP RC beams.* Sand coated GFRP RC beams show varying failure modes. Beams 2G8EC and 2G8UC were designed to fail by FRP rupture ($pf/pfb < 1$) so it was expected that the FRP bars would reach their rupture strain. Both of the aforementioned beams reached their maximum FRP rupture strain of 0.02 as shown in Table 8 and Figure 25 (b). The concrete strain of beams 2G8EC and 2G8UC was 0.0011 and 0.0020, respectively, which is below the maximum concrete strain of 0.003 and as depicted in Figure 25 (a). 2G10EC and 2G10UC, as previously stated, fall in the transition zone of failure ($1 < pf/pfb < 1.4$). Due to the fact that both Φ 10 reinforced GFRP beams fall in the transition zone, no clear determination about the mode of failure would have been possible prior to observing the strain behavior of the reinforcement and concrete. After analyzing the strain values, it is concluded that beam 2G10EC failed by concrete crushing while beam 2G10EC failed by FRP rupture. The strain in FRP reinforcement in beam 2G10EC is just shy of 0.014 which is lower that the rupture strain of sand coated GFRP bars. The concrete strain of beam 2G10EC, on the other hand, breached the 0.003 limit of max concrete strain as shown in Figure 25 (a). On the contrary, the concrete strain of beam 2G10UC is found to be 0.0024 which is less than the maximum concrete strain of 0.003. The FRP reinforcement of the aforementioned beam reached the rupture strain which is shown in Figure 25 (b). With regards the impact of exposure on FRP strain, it can be concluded the exposed bars and non-exposed bars showed quiet similar curve steepness. Concrete strain wise, no conclusion could be drawn to evaluate the impact of exposure on the concrete strain which can be attributed to the variation in the failure modes of the beams shown in Figure 25.

(a)   (b)
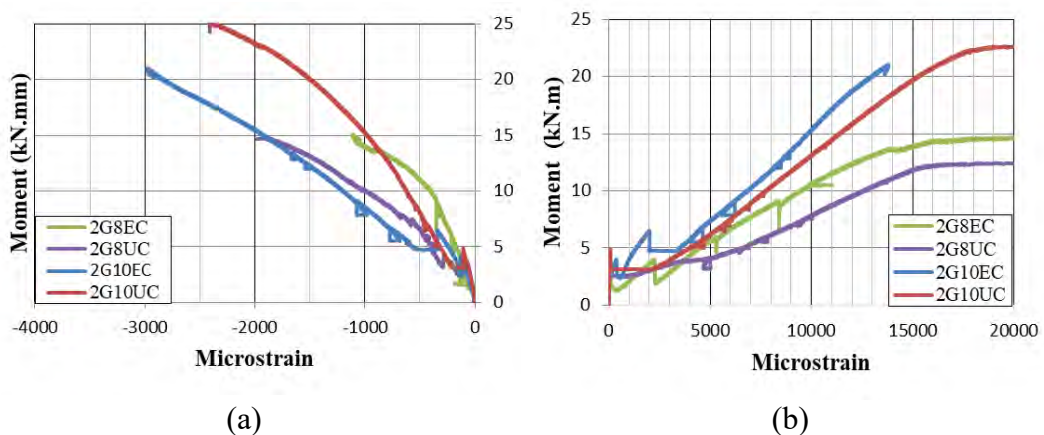
Figure 25: Moment vs. strain of sand coated GFRP RC beams (Group 1).

4.1.1.2. *Ribbed GFRP RC beams.* Ribbed GFRP RC beams were to fail due to concrete crushing, in theory. With complete certainty, beams reinforced with Φ 20 and Φ 26 GFRP bars were predicted to fail by concrete crushing since they possess pf/pfb values much higher than 1.4. On the other hand, beams reinforced with Φ 10 GFRP bars in the transition zone of failure where $1 < pf/pfb < 1.4$. Thus, the strain values were utilized to determine the mode of failure for beams reinforced with Φ 10 GFRP bars. The strain values of the Φ 10 ribbed GFRP reinforced beams presents FRP rupture as the mode of failure. As can be observed in Figure 26 (b), it is seen that GFRP bars in beams 2G10ER and 2G10UR reached their max strain values of 0.015 and 0.018, respectively. The concrete strain of the aforementioned beams did not reach the max 0.003 strain limits. The exposed bars show maximum FRP rupture strain that is 17% lower than the maximum FRP strain of the unexposed bars.

For the over reinforced Φ 20 and Φ 26 beams, the strain values confirm the predicted concrete crushing mode of failure. It is seen in Figure 26 (a) that the concrete strain for all beams reinforced Φ 20 and Φ 26 was in the vicinity of the 0.003 limiting strain. The fact that some beams are not shown to breach the 0,003 limit is due to the fact that the concrete cover carrying the concrete strain gauges might have fallen off due to the crushing forces present in the compression face. Beams 2G20ER, 2G20UR, 2G26ER, and 2G26UR yielded a maximum FRP strains equal to 0.008, 0.009, 0.007, and 0.006, respectively. No conclusion could be drawn about the impact of exposure on the FRP strain values for the aforementioned over reinforced beams since the FRP bars were not tested to their rupture limit.
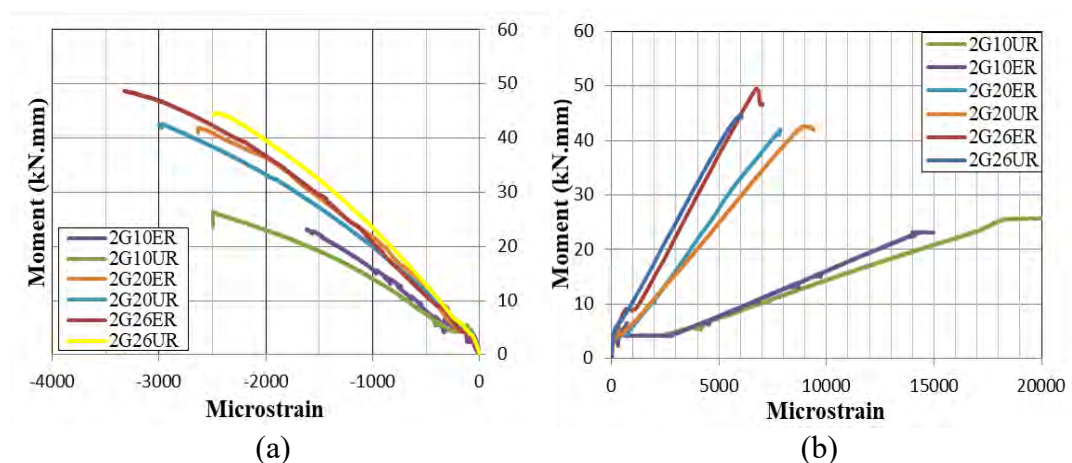
Figure 26: Moment vs. strain of ribbed GFRP RC beams (Group 1).

4.1.1.3. *BFRP RC beams.* BFRP RC beams are predicted to fail by concrete crushing. The FRP strain values as seen in Figure 27 (b) show that all beams had max reinforcement strain values less than the rupture strain provided by the ACI 440.1R code. The BFRP RC beams' reinforcement strain values ranged from 0.015 to 0.019. While all BFRP RC beams in group do fail in in crushing, Figure 27 (a) does not show any beam reaching the 0.003 concrete strain limits. The low reported concrete strain limits are due to detachment of the concrete cover carrying the strain gauges. However, the crushing failure was visually observed when testing the beams. Section 4.1.2 of this report provides images of the beams after failure and the concrete crushing failure is seen more clearly in the images of the beams. Strain wise, beams reinforced with exposed bars do not yield variations in the concrete strain (see Figure 27 (a)) but did yield variations in the strain of the FRP reinforcement (see Figure 27 (b)) . It is observed that strain values of unexposed bars were more resistant to change in loading when compared with exposed bars as can be seen in Figure 27 (b). In other words, Beam 2B10UC and beam 2B12UC yielded steeper moment vs. strain curves than beam 2B10EC and beam 2B12EC. Steeper moment vs. strain curves ultimately indicates better bond between reinforcement and concrete.

(a)   (b)
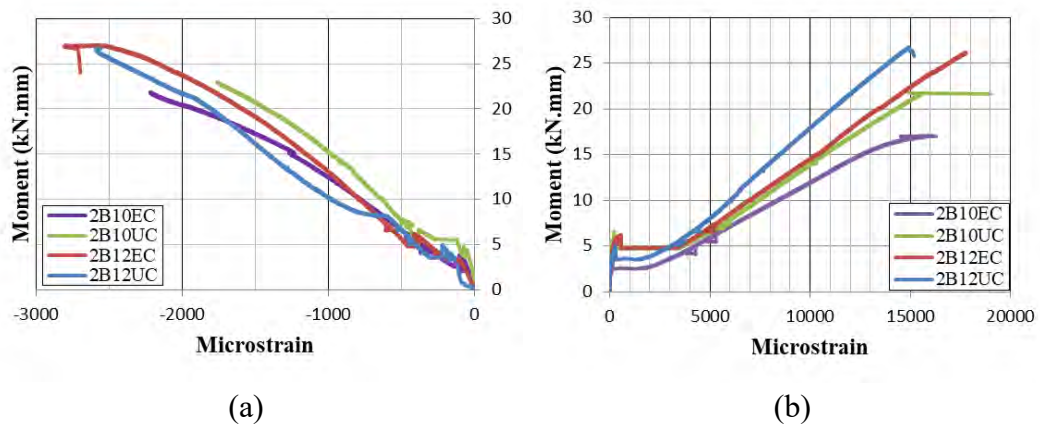
Figure 27*:* Moment vs. strain of sand coated BFRP RC beams (Group 1).

4.1.2. Flexural capacity and mode of failure. This section presents the failure modes for the beams reinforced with exposed vs. unexposed FRP bars. The section also discusses the accuracy of the ACI codes [1, 12] in predicting ultimate moment capacities of beams reinforced with FRP bars subjected to exposure. The section begins with presenting the tabulated experimental vs. predicted moment

capacities as well as the failure modes for the 14 beams used to study the impact of exposure. Successively, the section presents the experimental vs. predicted moment capacities schematically. After which, Images of beams at failure are presented.

Table 9 presents the experimental vs. analytical moment capacities of the 14 beams used to study the accuracy of the ACI 440.1R code in predicting capacities of beams reinforced with bars subjected to exposure. Five beams in this group failed in FRP rupture while the remaining 9 failed in concrete crushing. Subsequently, the appropriate design equations were utilized.

Table 9: Experimental vs. analytical moment capacities (Group 1).

Beam	Experimental		Predicted	Exp./Pred. ACI [1]	Failure
	M_n (kN.mm)	δ (mm)	M_n (kN.mm)	M_n (kN.mm)	Mode
2G8EC	15.33	53.66	17.28	0.88	TC[1]
2G8UC	17.11	46.12	17.28	0.99	TC
2G10EC	21.04	36.54	22.11	0.95	CC[2]
2G10UC	25.28	43.21	26.13	0.97	TC
2G10ER	26.05	36.83	25.86	1.01	TC
2G10UR	26.43	42.00	25.86	1.02	TC
2G20ER	42.00	28.81	37.24	1.13	CC
2G20UR	42.62	33.42	37.24	1.14	CC
2G26ER	49.56	23.14	42.57	1.16	CC
2G26UR	44.65	23.34	42.57	1.05	CC
2B10EC	22.90	41.22	23.02	0.99	CC
2B10UC	24.76	38.91	23.02	1.08	CC
2B12EC	27.09	36.60	26.65	1.02	CC
2B12UC	26.96	35.46	26.65	1.01	CC

[1]TC: Tension-controlled (FRP Rupture). [2]Compression-controlled (Concrete Crushing).

4.1.2.1. *Tension-controlled failure.* The code slightly underestimated the moment capacities for the sand coated GFRP bars. Within the subgroup of sand coated GFRP RC beams, 3 beams fail in rupture and 1 beam fail in concrete crushing as shown in Table 9. The three beams that fail in FRP rupture are used to validate the codes provisions to calculate the ultimate capacities according to such failure mode. Figure 28 shows the experimental moments for the sand coated GFRP RC beams that failed in FRP rupture vs. the limit as predicted by the ACI 440.1R code. It is seen in Figure 28, as is observed Table 9, that the experimental capacities of the tension-controlled sand coated GFRP RC beams are slightly lower than the predicted capacities. The code, on the other hand, accurately predicted the capacities of the 2 ribbed GFRP beams that fail in rupture.
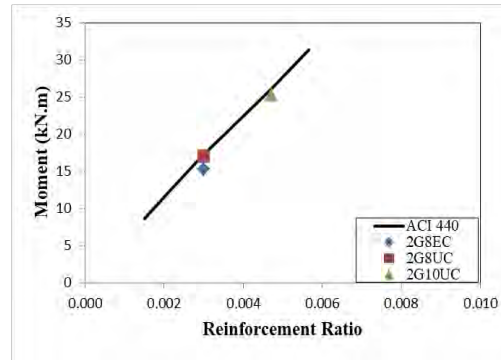
Figure 28: Experimental vs. predicted moment capacities (TC).

4.1.2.2. *Compression-controlled failure.* As for the 4 remaining ribbed GFRP RC beams and the 4 BFRP RC beams in group 1, concrete crushing is the mode of failure. As show in Table 9, the code was, for the most part, conservative when predicating the ultimate capacities of the beams that failed due to concrete crushing. Figure 29 shows the experimental capacities compared with the lower limit of ultimate capacities as predicted by the ACI 440.1R code.

(a)   (b)
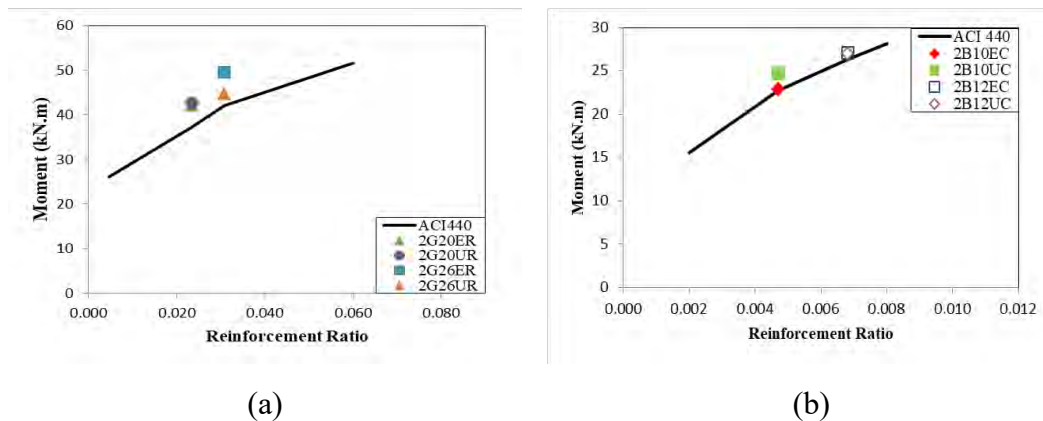
Figure 29: Experimental vs. predicated moment capacities (CC).

The two modes of failure observed in this study are shown in Figure 30. As previously discussed beam 2G8EC failed in FRP rupture which is, previously, observed through observing the strain behavior. Figure 30 (a) gives a visual representation of failure of beam 2G8EC. The figure shows the beam at the ultimate capacity and as observed, there are no signs of concrete crushing in beam 2G8EC. On the other hand, beams such as 3B10EC, for example, fail in concrete crushing which is visually clear as seen in Figure 30 (b). Figure 30 serves as a representative for the

63

remaining beams as all beams showed one mode of failure or the other. The remaining images for all the beams at failure are presented in the Appendix A.

(a)

(b)

Figure 30: Failure modes: (a) 2G8EC rupture failure; (b) 3B10EC crushing failure.

4.1.3. Moment-deflection behavior. One of the major areas of analysis that this study aims to highlight is the impact that exposure has on the flexural behavior of beams. Figure 31 sheds light on the flexural response of the 14 beams that are used throughout the study to examine the impact of exposure. More specifically, Figure 31 (a) and Figure 31 (b) illuminate the impact of exposure on the flexural response of the beams reinforced with sand coated and ribbed GFRP bars, respectively. Subsequently, Figure 31 (c) highlights the same response for beams reinforced with sand coated BFRP bars.

(a)

(b)

(c)
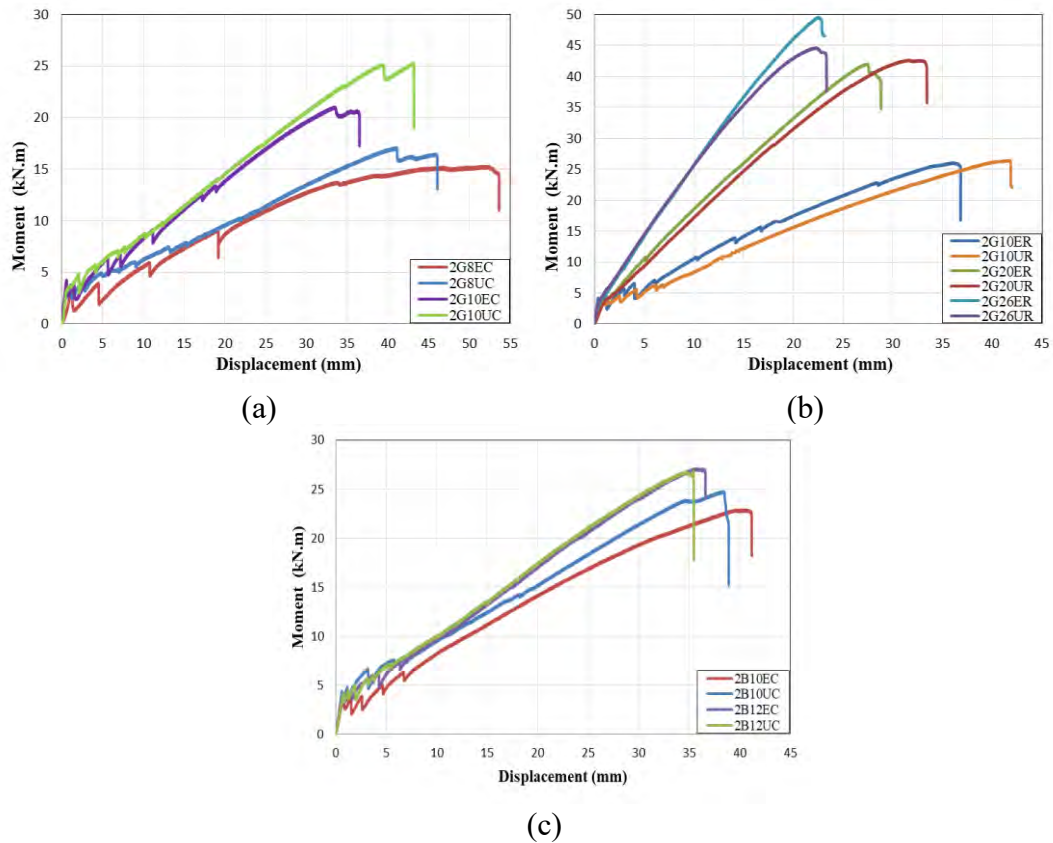
Figure 31: Moment vs. defelction (Group 1).

The moment vs. deflection of the four beams used to study the impact of exposure on sand coated GFRP RC beams is shown in Figure 31 (a). In the clearly under-reinforced beams where Φ 8 sand coated GFRP bars were used as main longitudinal reinforcement, the ultimate moment was reduced by almost 11 % due to exposure. Beam 2G8UC showed an ultimate moment of 17.11 kN.mm while beam 2G8EC yielded a 15.33 kN.mm ultimate moment. In under-reinforced beams, as discussed previously, the strength of reinforcement dictates the flexural behavior of the beam; thus, variation of exposure on the bars would translate onto the moment capacity of the beams. The same trend was observed in beams reinforced with Φ 10 sand coated GFRP bars. Beam 2G10UC showed a maximum moment of 25.28 kN.mm while beam 2G10EC showed a 21.04 kN.mm maximum moment; a reduction of almost 17 %. Although beams reinforced with Φ 10 sand coated GFRP bars are not under-reinforced, their pf/pfb of 1.39 puts them in the transition zone between concrete crushing and FRP rupture failures as previously shown in Figure 9. This mixed mode of failure, not exposure, impacted the capacity of BFRP RC beams.

No clear conclusion could be drawn regarding the impact of exposure on the deflection of beams reinforced with sand coated GFRP bars. In the under-reinforced 2G8 beams, the beam reinforced with the exposed GFRP bars (2G8EC) shows higher deflection value when compared with the beam reinforced unexposed GFRP bars (2G8UC). The aforementioned could be attributed to a possible reduction in the modulus of elasticity of the exposed GFRP bars. On the contrary, an opposite behavior can be observed in beams reinforced with Φ 10 sand coated GFRP bars. Unlike what is observed in the 2G8 beams, the beam reinforced with the unexposed Φ 10 GFRP bars (2G10UC) shows higher deflection when compared with the beam reinforced with exposed Φ 10 GFRP bars (2G10EC). The aforementioned behavior could possibly be attributed to the fact that, as previously mentioned, beams reinforced with Φ 10 GFRP bars fall in the transition zone of failure types; thus, the deflection may be affected by the concrete properties rather than the FRP properties in one beam and vice versa in the other beam.

Figure 31 (b) shows the moment vs. deflection behavior of the beams reinforced with exposed and unexposed ribbed GFRP bars. No clear impact of exposure can be observed from analyzing the clearly over reinforced beams (2G20 and 2G26). In beam 2G26UR, the ultimate moment is 10% less than that of beam 2G26ER while deflection of both beams is almost identical. For the Φ 20 beams, the beam reinforced with the unexposed bars showed a slightly higher value for maximum moment. Deflection, however, is higher in the beam reinforced with unexposed Φ 20 ribbed GFRP bars (2G20UR) when compared with the beam reinforced with exposed bars (2G20ER). The lack of clear impact of exposure is due to the fact that concrete crushes before the GFRP bars reach the failure threshold. The impact of exposure can be observed in the beams reinforced with Φ 10 ribbed GFRP bars since such beams fall in the transition zone of failure and therefore, the impact of exposure on bars can translate onto the flexural behavior of the beam. Beam 2G10UR shows an ultimate moment equal to 26.43 kN.mm while beam 2G10ER shows an ultimate moment equal to 26.05 kN.mm. This subtle difference can be due to variation in concrete rather than variation in FRP strength. Due to the fact that no under-reinforced ribbed GFRP beams are tested, no clear conclusion about the impact of exposure on the flexural response of ribbed GFRP RC beams can be drawn.

Lastly, Figure 31 (c) shows the moment-deflection behavior of the beams reinforced with exposed and unexposed sand coated BFRP bars. It is observed in that beams reinforced with exposed BFRP bars and beams reinforced with unexposed BFRP bars showed almost identical behavior, defection wise. The difference in the ultimate deflection is very subtle when comparing beams reinforced with exposed BFRP bars and beams reinforced with exposed BFRP bars. When observing the ultimate moment response to variation in exposure, on the other hand, the difference is less subtle. The impact of exposure on the ultimate moment of beams differed based on the size of the bars and as follows. Beams where the prominent mode of failure is concrete crushing (2B12UC and 2B12EC) showed indifference to variation in exposure. Both the aforementioned beams yielded an ultimate moment of approximately 27 kN.mm. The lack of response toward variation in exposure is due to the fact that concrete crushes before the BFRP failure threshold is reached. Therefore, any reduction of strength in BFRP bars did not translate onto the behavior of the beam. On the other hand, the impact of exposure was slightly observed in beams with the smaller Φ 10 BFRP bars. The beam reinforced with the unexposed Φ 10 BFRP yielded an ultimate moment equal to 24.76 kN.mm whereas the beam reinforced with the exposed Φ 10 BFRP showed a maximum moment of 22.90 kN.mm, a reduction of almost eight percent. Although the predicted mode of failure for the 2B10UC and 2B10EC beams was concrete crushing, the Φ 10 BFRP bars were closer to threshold of failure when compared to the Φ 12 BFRP bars. Thus, the behavior of the exposed BFRP bars slightly influenced the moment capacity of beams.

4.1.4. Cracking moment. The effects of exposure on the cracking moments of the 14 beams discussed hereafter are presented in Table 10. The experimental cracking moments are compared with the predicted cracking moment values. The cracking moments are calculated using the concrete properties through equation (13) of this report as provided by the ACI 440.1R [1] and ACI 318 [12]. The ratios of the cracking moment over the ultimate moment are also presented in this section. The findings are tabulated in the following subsections. It should be stated that, in general, the experimental cracking moments fall in the range from 0.48 to 1.44 of the predicted cracking moments [62]. In fact, by synthesizing many related studies, it is found that the average ratio of experimental cracking moment to the predicted cracking moment

is almost 0.89 [62]. The relatively low values for the experimental cracking moment can be attributed to restraint stresses in the concrete.

The first set of beams presented includes the sand coated GFRP RC beams. The set contained a total of four beams reinforced with Φ 8 and Φ 10 sand coated GFRP bars. The second set of beams includes ribbed GFRP RC beams. The set contains six beams reinforced with Φ 10, Φ 20, and Φ 26 ribbed GFRP bars. The last set of beams studied in this section includes sand coated BFRP RC beams. The set includes four beams reinforced with Φ 10 and Φ 12 sand coated BFRP bars. In general, the average ratio of experimental to predicted cracking moments of the 14 beams in this section was 0.65. As for the ratio of the cracking to ultimate moments for the aforementioned beams, an average value of 0.15 was deduced.

Table 10: Cracking moment (Group 1).

Beam	Experimental M_{cr} (kN.mm)	Predicted M_{cr} (kN.mm)	Exp./Pred. ACI [1]	M_{cr}/M_n
2G8EC	3.00	6.32	0.54	0.20
2G8UC	3.78	6.32	0.60	0.22
2G10EC	4.24	6.32	0.67	0.20
2G10UC	4.88	6.32	0.77	0.19
2G10ER	4.38	6.32	0.69	0.17
2G10UR	4.56	6.32	0.72	0.17
2G20ER	3.42	6.32	0.54	0.08
2G20UR	3.96	6.32	0.63	0.09
2G26ER	4.68	6.32	0.74	0.09
2G26UR	4.76	6.32	0.75	0.11
2B10EC	3.63	6.32	0.57	0.16
2B10UC	4.40	6.32	0.70	0.18
2B12EC	3.42	6.32	0.54	0.13
2B12UC	4.15	6.32	0.66	0.15
Average			0.65	0.15
Standard Deviation			0.08	

The predicated cracking moments for all beams is found to be 6.32 kN.mm. The predicated cracking moment is constant for all beams due to the fact that the concrete properties and beam cross section are constant for all beams in this study. The experimental cracking moments are generally smaller than the predicted values as shown in Table 10. In sand coated GFRP RC beams, the ratios of experimental to predicted cracking moments ranges from 0.54 to 0.77. The beams reinforced with the exposed sand coated GFRP bars registered lower cracking moments than beams reinforced with unexposed bars possessing the same diameter. As for the ratio of

cracking moments to the ultimate moment, the average value is found to be around 0.2. By observing the results in Table 10, it is concluded that exposure did not have any systematic impact on the ratio of cracking moment to ultimate moment of sand coated GFRP RC beams.

For beams reinforced with ribbed GFRP bars, it is also observed that experimental cracking moments are lower the predicted ones. The ratio of the experimental to predicted cracking moments in ribbed GFRP RC beams range from 0.54 to 0.75. As previously observed in sand coated GFRP RC beams, the beams reinforced with the exposed ribbed GFRP bars show lower cracking moment values than beams reinforced with unexposed ribbed bars with the same diameter. As for the ratio of cracking to ultimate moment, it is observed that the ratios for beams reinforced with exposed ribbed GFRP bars are slightly lower than those reinforced with unexposed ribbed GFRP bars.

Beams reinforced with sand coated BFRP bars are no exception to the previously observed trends. The experimental cracking moments are also lower than the predicted ones. The ratios of experimental to predicted cracking moments in BFRP RC beams range from 0.54 to 0.70. Similar to their GFRP counterparts, beams reinforced with exposed BFRP bars yielded lower cracking moment than beams reinforced with unexposed BFRP bars. Furthermore, the ratios of cracking to ultimate moments in exposed BFRP RC beams are slightly lower than those of unexposed BFRP RC beams.

It is clearly observed that for the FRP RC beams in group 1 and the rest of the beams in this study, the experimental cracking moments are on average 35% lower than the predict cracking moments. To accurately predict the cracking moment, some studies proposed to calculate the cracking moment using the direct tensile strength of concrete ($f_{ct} = 0.4\sqrt{f'_c}$) rather than modulus of rupture ($f_r = 0.62\sqrt{f'_c}$) [63].

4.1.5. Cracking width and propagation. This section provides the tabulated values of crack propagation as well as graphs of moment vs. cracks width for the 14 FRP RC beams in group 1. The moment vs. cracks width includes the 0.7 crack width limiting boundary proposed by the CSA 806 [13] and the ACI 440.1R [1]. Table 11 shows the moment causing the first 7 cracks. The first two cracks are equipped with

crack transducers to measure the cracks width of the beams. No systematic conclusion about the impact of exposure on crack propagation is drawn as in Table 11. Crack propagation is not impacted by the variation of exposure for FRP RC beams in group 1. In some cases, beams reinforced with unexposed bars require higher moments to develop new cracks than beams reinforced with exposed bars (2G20UR vs. 2G20ER). In other cases, the opposite is observed (2G26UR vs. 2G26ER).

Table 11: Crack number vs. moment (Group 1).

Beam	Crack Number						
	1	2	3	4	5	6	7
	Moment (kN.mm)						
2G8EC	3.1	4.4	5.9	9.2	NA	NA	NA
2G8UC	3.6	3.8	4.1	5.0	5.3	6.0	7.5
2G10EC	3.1	2.4	4.8	5.6	7.9	12.7	13.2
2G10UC	3.6	4.0	3.1	5.1	6.5	6.8	7.0
2G10ER	4.3	4.3	5.8	6.4	7.1	10.9	13.4
2G10UR	3.5	3.6	4.5	5.6	6.3	6.3	8.6
2G20ER	3.4	3.7	4.4	5.0	9.6	10.6	13.4
2G20UR	3.96	6.3	6.4	7.6	10.1	15.5	15.9
2G26ER	4.5	4.6	6.9	10.4	12.0	16.8	17.4
2G26UR	4.76	6.7	7.5	8.6	9.2	10.4	12.8
2B10EC	3.6	3.8	3.9	4.9	6.4	9.5	15.3
2B10UC	4.4	4.8	6.7	7.6	7.5	7.5	7.8
2B12EC	3.4	3.3	4.3	6.0	6.3	7.2	8.7
2B12UC	4.1	4.5	5.0	5.8	6.0	7.0	10.3

Perhaps the most significant takeaway from Table 11 is the low number of cracks for beam 2G8EC as it was the only beam in group 1 that developed only 4 cracks. Figure 32 shows a compression of the cracks of beams 2G8EC and 2G8UC. Images of cracks propagation for the remaining beams are shown in Appendix B.

(a)   (b)

Figure 32: Crack propagation of: (a) 2G8EC; and (b) 2G10UC.

Beam 2G8EC, as shown in Figure 32 (a) only yielded few cracks when compared with beam 2G8UC shown in Figure 32 (b). This is an important observation because beams with lower number of cracks have higher crack spacing which, in turn, translates to higher crack width. The high crack width of beam 2G8EC would, subsequently, cause the beam to have the highest k_b factor in this study. The k_b factor analysis is conducted in the next section.

Figure 33 shows the cracks width relationship against moment. The moment vs. crack width curves attempt to visually show the impact of exposure on group 1 beams. Figure 33 (a) shows the moment vs. crack width curves for the 4 sand coated GFRP RC beams. As it was observed above, the crack width in beam 2G8EC was increasing rapidly with any small increase in the applied moment. Generally, Beams reinforced with unexposed sand coated GFRP bars are more resistant to the increase of cracks width than the beams reinforced with the exposed bars.

Figure 33 (b) shows the shows the moment vs. crack width curves for the 6 ribbed GFRP RC beam in group 1. It is observed that beam 2G20UR is more resistant to increasement in crack width than beam 2G20ER. The remaining 4 ribbed GRRP RC beams show similar moment vs. cracks width curves, regardless of the exposure conditions. Lastly, Figure 33 (c) shows the moment vs. crack width curves for the 4 BFRP RC beam in group 1. The moment vs. crack width curves are very similar for the 4 BFRP RC beams. Beams reinforced with exposed BFRP bars and beams reinforced with unexposed BFRP bars show similar trends (see Figure 33 (c)). The ACI 440.1R crack width limit is added to each of the curves to show the cut off for the cracks width values they will ultimately be used in the k_b factor calculations.

(a)   (b)

71
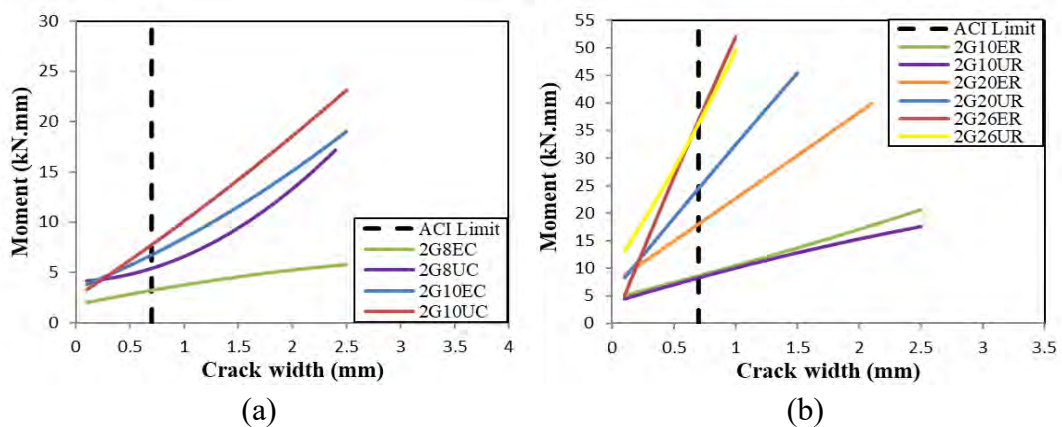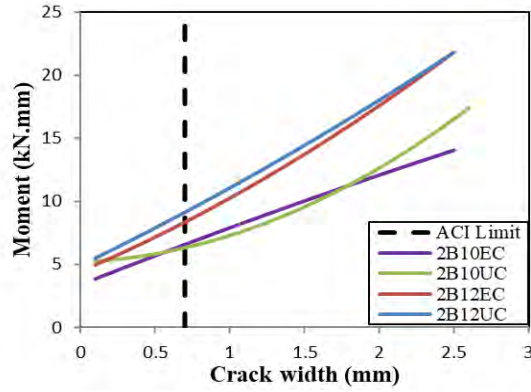
(c)

Figure 33: Moment vs. crack width (Group 1).

4.1.6. Bond-dependent coefficient. This section concludes the analysis in this study and provides observations on the final serviceability performance parameter dictated in the thesis objectives. The k_b factor is the culminating analysis of this study as it utilizes the data from the previous sections. Parameters including crack widths, reinforcement strain, reinforcement size, and reinforcement spacing are utilized to calculate k_b factor as per equation 13 of this report. The k_b factors are calculated at maximum permitted crack width of (0.7 mm) and at the service moment of 0.33 of the ultimate capacity of the RC beams. All calculations are conducted at crack widths not exceeding the 0.7 mm limit proposed by the CSA 802 [13, 64]. As previously stated, the k_b factor indicates a bond behavior superior to the bond between steel and concrete. In design codes, the k_b factor is taken as 1.4 according to the ACI 440.1R [57], 1.2 according to ISIS Manual No. 3 [15], and 0.8 according to CSA S16 [14].

The effects of exposure on the k_b factors of the 14 beams discussed hereafter are presented in Table 12. In general, the average k_b value of the 14 beams in this section is 0.81 which is close to the 0.8 k_b value proposed by the CSA S16 [14]. The k_b calculated herein is influenced by the strain in the FRP reinforcement and crack widths previously reported in in section 4.1.1 and section 4.1.5. Excluding the BFRP RC beams, the impact of exposure on the k_b values is noticeable for beams in group 1. Beams reinforced with exposed sand coated and ribbed GFRP bars show higher k_b values than the beams reinforced with unexposed bars. On the other hand, the k_b values of the BFRP RC beams are unaffected by exposure as can be seen in Table 12.

72

Table 12: bond-dependent coefficient, k_b factor (Group 1).

Beam	$0.3M_n$	w = 0.7 mm	Average
2G8EC	0.79	1.34	1.07
2G8UC	0.59	0.58	0.59
2G10EC	0.72	0.81	0.77
2G10UC	0.78	0.74	0.76
2G10ER	0.87	0.75	0.81
2G10UR	0.79	0.75	0.77
2G20ER	0.94	0.87	0.91
2G20UR	0.72	0.88	0.80
2G26ER	0.81	0.82	0.82
2G26UR	0.74	0.86	0.80
2B10EC	0.88	0.82	0.85
2B10UC	0.89	0.86	0.87
2B12EC	0.79	0.73	0.76
2B12UC	0.72	0.80	0.76

4.1.6.1. *Sand coated GFRP RC beams.* In sand coated GFRP RC beams, the values for k_b factor range from 0.59 for beam 2G8UC at the lowest to 1.07 for beam 2G8EC at the highest. It is noted that beam 2G8EC is the only beam in this study to yield bond behavior inferior to steel RC beams. The considerably large k_b factor of beam 2G8EC is attributed to the large crack widths at low loads values of said beam as shown in the previous section and as was seen in Figure 32. The k_b factors for beam 2G10EC and beam 2G10UC are calculated to be 0.77 and 0.76, respectively. It is observed that, similar to the beams reinforced with Φ 8 sand coated GFRP bars, the GFRP RC beam reinforced with Φ 10 unexposed bars shows a slightly better bond with concrete than their exposed counterparts.

On average, the k_b factor for beams reinforced with exposed sand coated GFRP bars (2G8EC and 2G10EC) is 0.92. The aforementioned average k_b factor is 36% higher than the 0.68 average k_b factor yielded by beams reinforced with unexposed sand coated GFRP (2G8UC and 2G10UC). Therefore, it is concluded that exposure does have a negative impact on the bond dependent coefficient of sand coated GFRP bars RC beams.

4.1.6.2. *Ribbed GFRP RC beams.* In ribbed GFRP RC beams, the values for k_b factor range from 0.77 for beam 2G10UR at the lowest to 0.91 for beam 2G20ER at the highest. As shown in Table 12, the k_b factors are: 0.81 and 0.77 for beams 2G10ER and 2G10UR, 0.91 and 0.80 for beams 2G20ER and 2G20UR, 0.82 and 0.80 for beams 2G26ER and 2G26UR, respectively. It is noted that ribbed GFRP RC

beams reinforced with exposed bars yielded a higher k_b factor than the beams reinforced with the unexposed bars. On average, the k_b factor for beams reinforced with exposed ribbed GFRP bars (2G10ER, 2G20ER, and 2G26ER) is 0.85. The aforementioned average k_b factor is 7% higher than the 0.79 average k_b factor yielded by beams reinforced with unexposed sand coated GFRP (2G10UR, 2G20UR, and 2G26UR). Therefore, it can be said that exposure has a negative impact on the bond strength of ribbed GFRP bars. It can also be concluded that, excluding the outlier Φ 8 reinforced beams, beams reinforced with ribbed GFRP bars are impacted by exposure to a higher extent than beams reinforced with sand coated GFRP bars. The difference in the post exposure performance between ribbed and sand coated GFRP bars is discussed more thoroughly in a later section.

4.1.6.3. *BFRP RC beams*. In BFRP RC beams, the values for k_b factor range from 0.76 for both 2B12EC and 2B12UC beams at the lowest to 0.87 for beam 2B10UC at the highest. Unlike their GFRP counterparts, the bond between the BFRP bars and concrete is not impacted by exposure of BFRP bars. There is almost no difference in the k_b factors of beams reinforced with exposed BFRP bars and beams reinforced with unexposed BFRP bars. The findings solidify a previous study [52] conducted by the author which concluded that the exposure to UAE climate conditions such as humidity, ultraviolet rays, rain, and temperature had no systematic impact on the k_b factors of BFRP RC beams.

4.2. Impact of Reinforcement Ratio

This section highlights the impact of reinforcement ratio on the strain values, flexural capacity, moment-deflection behavior, cracking moment, cracks width propagation, and bond-dependent coefficient.

4.2.1. Reinforcement and concrete strain. The effects of reinforcement ratio on the longitudinal reinforcement and concrete strains of the 11 beams analyzed in this section are presented in Table 13, Figure 34, Figure 35, and Figure 36. The first set of beams includes three beams reinforced with Φ 8, Φ 10, and Φ 20 sand coated exposed GFRP bars as shown in Figure 34. The second set of beams includes three beams reinforced with Φ 10, Φ 20, and Φ 26 ribbed exposed GFRP bars as shown in Figure 35. The last set of beams in this section includes five beams reinforced with Φ 8, Φ 10, Φ 12, Φ 16, and Φ 20 sand coated exposed BFRP bars as shown in Figure 36.

Table 13: Reinforcement and concrete strain values (Group 2).

Beam	Moment (kN·m)	Longitudinal Reinforcement Strain	Concrete Strain
2G8EC	15.33	0.020	0.0011
2G10EC	21.04	0.014	0.0030
2G20EC	41.27	0.011	0.0025
2G10ER	26.05	0.015	0.0016
2G20ER	42.00	0.008	0.0026
2G26ER	49.56	0.007	0.0033
2B8EC	18.16	0.012	0.0030
2B10EC	22.90	0.017	0.0022
2B12EC	27.09	0.018	0.0028
2B16EC	32.49	0.010	0.0030
2B20EC	42.14	0.009	0.0030

The sand coated GFRP reinforcement strain values are indirectly related to size of the bar as shown in Figure 34 (b). By observing the strain values in the table above, it is seen that beam 2G8EC fails due to FRP rupture when the exposed Φ 8 reinforcing bars reach their maximum rupture strain of 0.02. On the other hand, the beams reinforced Φ 10 and Φ 20 exposed sand coated GFRP bars fail in concrete crushing. Beams 2G10EC and 2G20EC reported maximum FRP strain values of 0.014 and 0.011, respectively. It is observed that increasing the reinforcement ratio by 310%, from 0.0047 (2G10EC) to 0.0194 (2G20EC), only decreased the maximum strain values in the reinforcement by 21%. The concrete strain values showed in Figure 34 (a) support the previously determined conclusions of the failure modes. Concrete strain in beam 2G20EC is not shown to reach the maximum concrete strain of 0.003 which can be attributed to disturbance in the concrete cover supporting the concrete strain gauges. In other words, the concrete cover supporting the strain gauge crushes before the full failure of the beam.

(a)   (b)
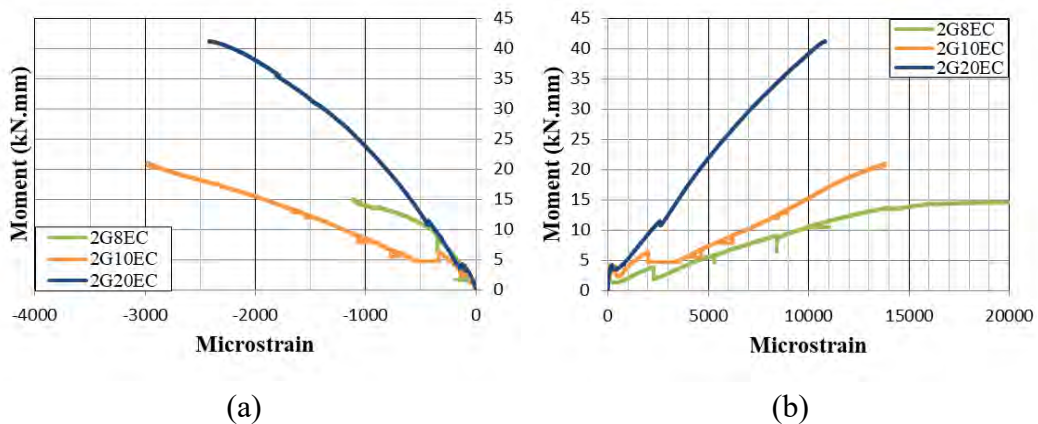
Figure 34: Moment vs. strain of sand coated GFRP RC beams (Group 2).

The strain values of the ribbed GFRP reinforcement in the under reinforced and over reinforced beams are reported in the section 4.2.3. The analysis which is presented in this section discusses the general relationship between the reinforcement ratio and reinforcement strains. For the over reinforced 2G20ER and 2G26ER, the reinforcement ratios were 0.0194 and 0.0308, respectively. The 59% increase in the reinforcement ratio in the previous two beams only decreased the FRP strain values by 13%, as shown in Figure 35 (b). The increase in reinforcement ratio for over reinforced beams (2G20ER and 2G26 ER) yielded a disproportional decrease in the strain of the exposed FRP reinforcement. Beam 2G10ER was not compared with the two other beams since it shows a different failure mode.

(a)   (b)
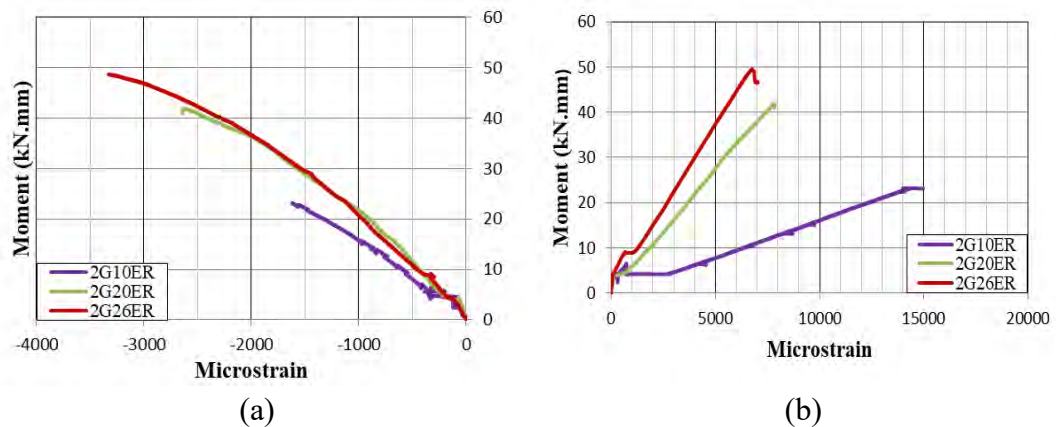
Figure 35: Moment vs. strain of ribbed GFRP RC beams (Group 2).

The sand coated BFRP beams are expected to fail in concrete crushing. Excluding beam 2B8EC, all beams had pf/pfb values much higher than 1.4. Beam 2B8EC had pf/pfb equal to 1.4 exactly which barley edges it out of the transition zone of failure and into the concrete crushing zone. To check the failure mode of beam 2B8EC, its strain values as shown in Figure 36 are utilized. An indication that 2B8EC do not fail in reinforcement rupture is that fact that maximum FRP strain value of the Φ 8 is reported to be 0.012 which is less than the rupture strain, as shown in Table 13 and Figure 36 (b). In addition, the concrete strain generated in the 2B8EC beams is higher than the maximum 0.003 limit which indicates that the beams did in fact, fail in concrete crushing. Similar to the GFRP RC beams, reinforcement ratio had an indirect disproportional relationship with the strain values of reinforcement in the BFRP RC beams. For example, increasing the reinforcement ratio by 310%

(2B10EC vs. 2B20EC) only decreases the maximum FRP reinforcement strain value by 47%.

(a)   (b)
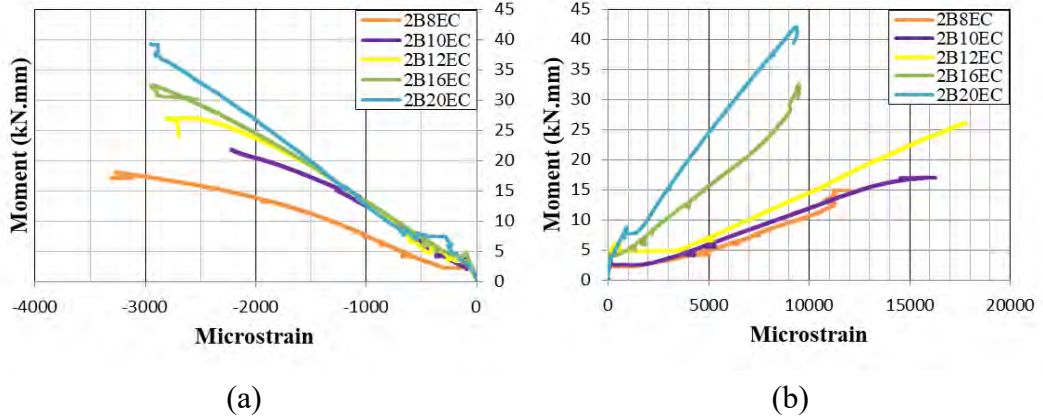
Figure 36: Moment vs. strain of sand coated BFRP RC beams (Group 2).

4.2.2. Flexural capacity and mode of failure. This section presents the failure modes for the 11 beams used to study the impact of reinforcement ratios. Out of the 11 beams of this group, only 2 beams fail due to FRP rupture with the rest failing due to concrete crushing. The two beams that fail due to FRP rupture were 2G8EC and 2G8ER, as discussed in the previous section. The ratios of the experimental to predicted moment capacities are shown in Table 14. Generally, it is observed that the higher the reinforcement ratio the more conservative the moment capacities predictions are. For instance, the ratio of experimental to predicted moment capacity for beam 2G20ER is 1.13 while the ratio for beam 2G26ER is calculated to be 1.16.

Table 14: Experimental vs. analytical moment capacities (Group 2).

| Beam | Experimental | | Predicted | Exp./Pred. ACI [1] | Failure |
	M_n (kN.mm)	δ (mm)	M_n (kN.mm)	M_n (kN.mm)	Mode
2G8EC	15.33	53.66	17.28	0.89	TC
2G10EC	21.04	36.54	22.11	0.95	CC
2G20EC	41.27	29.74	37.24	1.11	CC
2G10ER	26.05	36.83	25.86	1.01	TC
2G20ER	42.00	28.81	37.24	1.13	CC
2G26ER	49.56	23.14	42.57	1.16	CC
2B8EC	18.16	54.14	19.09	0.95	CC
2B10EC	22.90	41.22	23.02	0.99	CC
2B12EC	27.09	36.60	26.65	1.02	CC
2B16EC	32.49	28.03	33.11	0.98	CC
2B20EC	42.14	26.76	38.56	1.09	CC

4.2.3. Moment-deflection behavior. The impact of reinforcement ratio on flexural response of FRP RC beams is shown in Figure 37. A total of 11 beams are studied to evaluate the effect of reinforcement ratio on the moment vs. deflection behavior. All 11 beams are reinforced with exposed FRP bars. Figure 37 (a) and Figure 37 (b) show the moment vs. deflection curves of different reinforcement ratios for beams reinforced with sand coated and ribbed GFRP bars, respectively. Lastly, Figure 37 (c) shows the moment vs. deflection curves of BFRP reinforced beams that differ in reinforcement ratios.

(a)   (b)

(c)
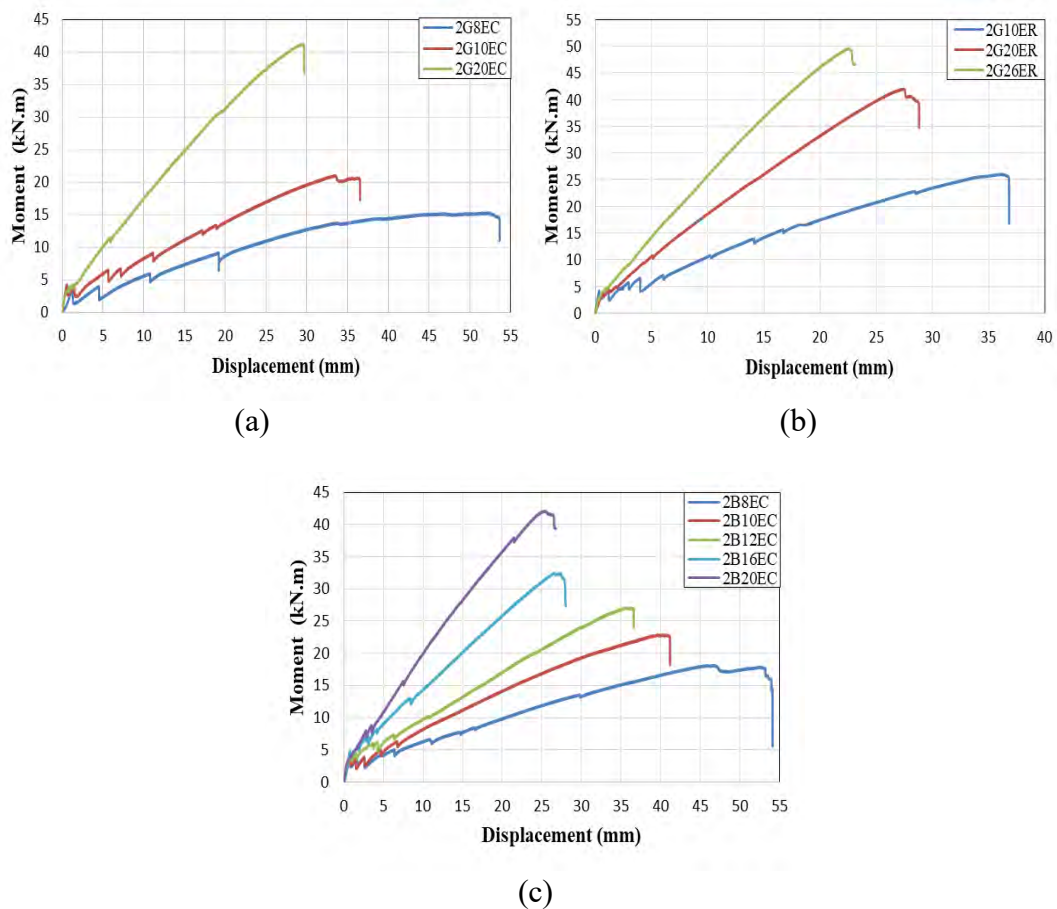
Figure 37: Moment vs. deflection (Group 2).

Evidently, beams with higher reinforcement ratio produced higher ultimate moments and lower deflection values. However, the amount of increase in ultimate moment is disproportional to the amount of increase in reinforcement ratio. For example, the reinforcement ratio of beam 2G20EC is 300 % higher than that of beam 2G10EC but the resulting increase in ultimate moment was only 96% as shown in

Figure 37 (a). The same increase of reinforcement ratio only yielded an increase of 61% in the ultimate moment between beams 2G10ER and 2G20ER as seen in Figure 37 (b). The BFRP reinforced beams, shown in Figure 37 (c), are no expectation to the aforementioned observation. The same increase in reinforcement ratio between beams 2B10EC and 2B20EC only warranted 84% increase in the ultimate moment. The same disproportional response is observed when looking at deflection. The increase in reinforcement ratio did not yield a proportional reduction in the deflection values.

      4.2.4. Cracking moment. The effects of reinforcement ratio on the cracking moments of the 11 beams analyzed in this section are presented in Table 15. The first set of beams presented comprises of the sand coated GFRP RC beams. The set contains a total of three beams reinforced with Φ 8, Φ 10, and Φ 20 sand coated exposed GFRP bars. The second set of beams comprises of ribbed GFRP RC beams. The set contained three beams reinforced with Φ 10, Φ 20, and Φ 26 ribbed exposed GFRP bars. The last set of beams studied in this section comprises of sand coated BFRP RC beams. The set includes four beams reinforced with Φ 8, Φ 10, Φ 12, Φ 16, and Φ 20 sand coated exposed BFRP bars. As previously mentioned all beams possess the same predicted cracking moment of 6.32. The average ratio of experimental to predicted cracking moments of the 11 beams in this section is 0.62 with a standard deviation of 0.08. As for the ratio of the cracking to ultimate moments for the aforementioned beams, an average value of 0.14 is deduced.

Table 15: Cracking moment (Group 2).

Beam	Experimental M_{cr} (kN.mm)	Predicted M_{cr} (kN.mm)	Exp./Pred. ACI [1]	M_{cr}/M_n
2G8EC	3.42	6.32	0.54	0.22
2G10EC	4.24	6.32	0.67	0.20
2G20EC	3.91	6.32	0.62	0.09
2G10ER	4.38	6.32	0.69	0.17
2G20ER	3.42	6.32	0.54	0.08
2G26ER	4.68	6.32	0.74	0.09
2B8EC	3.45	6.32	0.55	0.19
2B10EC	3.63	6.32	0.57	0.16
2B12EC	3.42	6.32	0.54	0.13
2B16EC	4.84	6.32	0.77	0.15
2B20EC	3.80	6.32	0.60	0.09
Average			0.62	0.14
Standard Deviation			0.08	0.05

Sand coated GFRP RC beams yielded experimental to predicted cracking moment ratios ranging from 0.54 to 0.67. No clear systematic impact of reinforcement ratio on the cracking moments could be observed which can be attributed to the fact that the cracking moment is a function of concrete properties rather than reinforcement properties. As for the ratio of cracking to ultimate moment, it is observed that beams with higher reinforcement ratios yielded lower cracking to ultimate moment ratios. The aforementioned observation is expected due to the fact that higher reinforcement ratios, by design, yield higher ultimate moment capacities of the beams.

Ribbed GFRP RC beams yielded experimental to predicted cracking moment ratios ranging from 0.54 to 0.74. Similar to the sand coated GFRP RC beams, no clear systematic impact of reinforcement ratio on the cracking moments could be observed. On the other hand, a conclusion could be draw about the impact of reinforcement ratio on the cracking to ultimate moment ratios. Generally, beams with higher reinforcement ratios yielded lower ratios of cracking to ultimate moment for the same reason discussed in the paragraph above.

Ribbed BFRP RC beams yielded experimental to predicted cracking moment ratios ranging from 0.54 to 0.74. The variations in reinforcement ratio do not produce a systematic impact on the cracking moment values. For the cracking to ultimate moment, BFRP RC beams show the same trend as their GFRP counterparts. With the exception of one outlier, the increase in reinforcement ratio yielded a decrease in the ratio of cracking to ultimate moments.

4.2.5. Cracking width and propagation. This section provides the tabulated values of crack propagation for the 11 FRP RC beams in group 2. Table 16 shows the moment causing the first 7 cracks in the 11 beams of group 2. No systematic conclusion about the impact of exposure on crack propagation is drawn as seen Table 16. The crack propagation is not impacted by the variation of reinforcement ratio for FRP RC beams in group 2. In some cases, beams with higher reinforcement ratio require higher moments for the developments of new cracks than beams with lower reinforcement ratio (2G20EC vs. 2G210EC). In other cases, the opposite relationship was observed where beams with higher reinforcement ratio require higher moments for the developments of new cracks (2B20EC vs. 2B10EC).

Table 16: Crack number vs. moment (Group 2).

Beam	Crack Number						
	1	2	3	4	5	6	7
	Moment (kN.mm)						
2G8EC	3.1	4.4	5.9	9.2	13.7	NA	NA
2G10EC	3.1	2.4	4.8	5.6	7.9	12.7	13.2
2G20EC	4.0	3.9	6.3	6.4	9.5	13.4	15.5
2G10ER	4.3	4.3	5.8	6.4	7.1	10.9	13.4
2G20ER	3.4	3.7	4.4	5.0	9.6	10.6	13.4
2G26ER	4.5	4.6	6.9	10.4	12.0	16.8	17.4
2B8EC	2.7	2.9	2.4	4.4	4.4	4.8	6.4
2B10EC	3.6	3.8	3.9	4.9	6.4	9.5	15.3
2B12EC	3.4	3.3	4.3	6.0	6.3	7.2	8.7
2B16EC	4.9	4.5	5.8	7.2	8.2	9.8	12.9
2B20EC	3.8	4.8	6.0	7.9	7.8	9.5	11.0

Figure 38 shows the moment vs. crack width curves of the 11 beams in group 2. It is concluded that the higher the reinforcement ratio the steeper the moment vs. crack width becomes. The increase in steepness seems to be proportional to the reinforcement ratio.

(a)

(b)

(c)
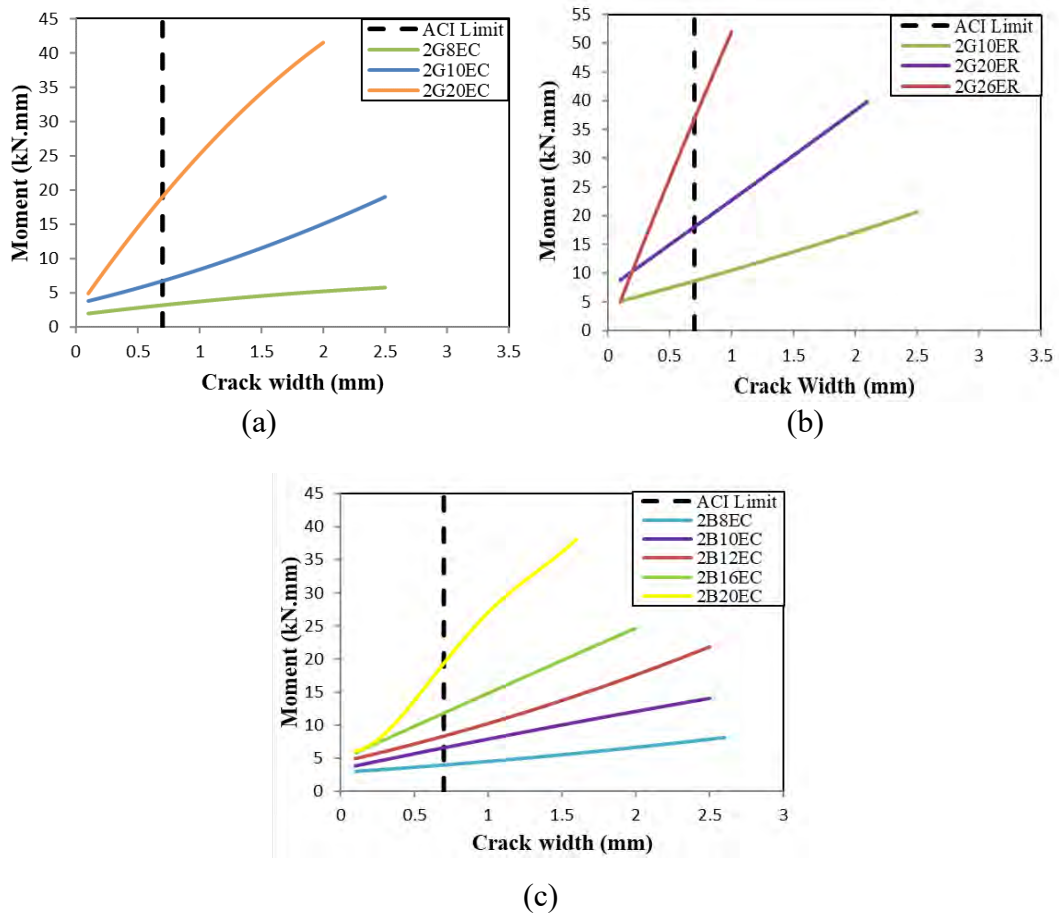
Figure 38:Moment vs. crack width (Group 2).

4.2.6. Bond-dependent coefficient. The effects of reinforcement ratio on the k_b factors of the 11 beams discussed hereafter are presented in Table 17. In general, the average k_b value of the 14 beams in this section is 0.86 which is slightly higher than the 0.8 k_b value proposed by the CSA S16 [14] but much lower than the 1.4 value proposed by ACI 440.1R [1].

Table 17: bond-dependent coefficient, k_b factor (Group 2).

Beam	0.3M_n	w = 0.7 mm	Average
2G8EC	0.79	1.34	1.07
2G10EC	0.72	0.81	0.77
2G20EC	0.75	0.95	0.85
2G10ER	0.87	0.75	0.81
2G20ER	0.94	0.87	0.91
2G26ER	0.81	0.82	0.82
2B8EC	0.74	0.93	0.84
2B10EC	0.88	0.82	0.85
2B12EC	0.79	0.73	0.76
2B16EC	0.79	0.83	0.81
2B20EC	0.94	0.97	0.95

The four sand coated GFRP RC beams have an average k_b factor equal to 0.90 which is the highest average in group 2. As for the three ribbed GFRP RC beams in this group, the average k_b factor is calculated to be 0.85. Lastly, BFRP RC beams in this group yielded an average k_b factor equal to 0.84. No relationship could be drawn to describe the impact of the reinforcement ratio on the k_b value of beams in group 2. In other words, there is no systematic increase or decrease in the k_b value when the FRP RC beams reinforcement ratios are varied.

4.3. Impact of Surface Texture

This section highlights the impact of surface texture on the strain values, flexural capacity, moment-deflection behavior, cracking moment, cracks width propagation, and bond-dependent coefficient.

4.3.1. Reinforcement and concrete strain. The effects of surface texture on the longitudinal reinforcement and concrete strain values of the four beams studied in this section are presented in Table 18, Figure 39, and Figure 40. The first set of beams includes the Φ 10 sand coated and ribbed GFRP RC beams. Subsequently, the second set of beams are used to analyze the strain values of the Φ 20 sand coated and ribbed GFRP RC beams. Table 18 shows that all beams of this group, except for 2G10ER,

fail in concrete crushing which becomes evident when observing the concrete and reinforcement strain values shown in Table 18.

Table 18: Reinforcement and concrete strain values (Group 3).

Beam	Moment (kN·m)	Longitudinal Reinforcement Strain	Concrete Strain
2G10EC	21.04	0.014	0.0030
2G10ER	26.05	0.015	0.0016
2G20EC	41.27	0.011	0.0025
2G20ER	42.00	0.008	0.0026

Beams reinforced with Φ 10 ribbed and sand coated GFRP bars had different mode of failure. It is observed in Figure 39 that the FRP reinforcement ruptures at a strain of 0.015 in Φ 10 reinforced with the ribbed GFRP bars. The rupture of the bars caused the beam to fail due to reinforcement rupture. The reinforcement strain in the beam reinforced with the sand coated GFRP bars reaches 0.014 without rupturing as shown in Figure 39 (b). Furthermore, Figure 39 (a) shows that the concrete section reaches its failure strain of 0.003 in beam 2G10EC but not in beam 2G10ER. The variation in surface texture did not have a significant impact on the reinforcement strain as both sand coated and ribbed bars show similar reinforcement strain curves.

(a)   (b)
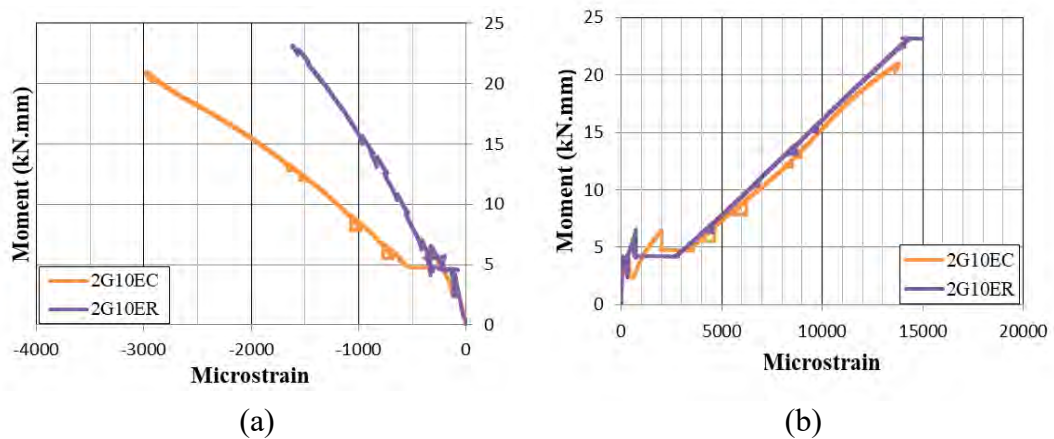
Figure 39: Moment vs. strain of Φ 10 GFRP RC beams (Group 3).

As for the beams reinforced with the Φ 20 sand coated GFRP bars, the strain of the reinforcement differs based on the variation in surface texture. The ribbed exposed GFRP bars show a maximum strain 27% lower than their sand coated counterparts as shown in Figure 40 (b). Strain curves of both types of bars were similar at the stage of service loads. However, the ribbed bars show a steeper curve

when moving towards the ultimate capacity. The concrete strain, on the other hand, is similar in both beams as shown in Figure 40 (a).

(a)   (b)
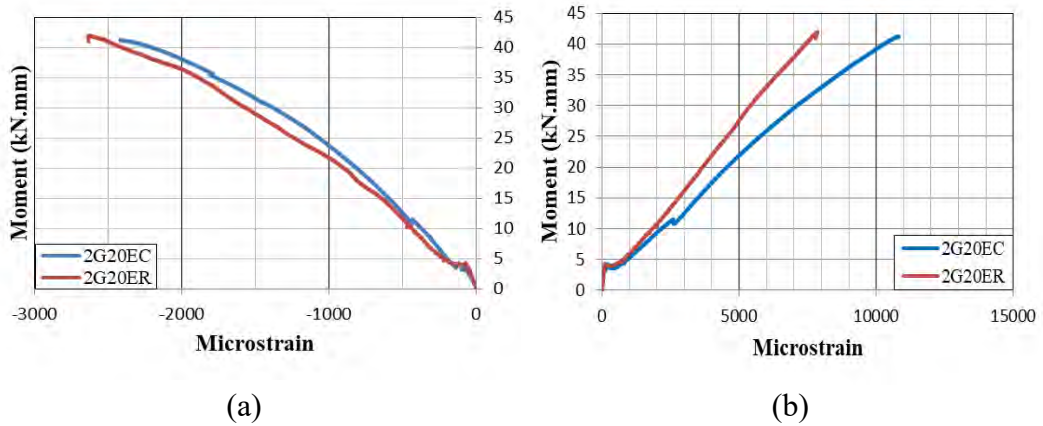
Figure 40: Moment vs. strain of Φ 20 GFRP RC beams (Group 3).

4.3.2. Flexural capacity and mode of failure. The 4 beams studied under the surface texture variation fail in both FRP rupture and concrete crushing. Beam 2G10ER is the only beam in group 3 to fail due to FRP rupture. The 2 remaining beams fail due to concrete crushing. The accuracy of the analytical predicted for beams in this group has already been discussed in the previous sections. The code is slightly more conservative when predicting the capacities of the beams reinforced with ribbed GFRP bars than beams reinforced with sand coated GFRP bars (see Table 19). Overall, however, the predicted capacities are close to the experimental ones.

Table 19: Experimental vs. analytical moment capacities (Group 3).

Beam	Experimental		Predicted	Exp./Pred. ACI [1]	Failure
	M_n (kN.mm)	δ (mm)	M_n (kN.mm)	M_n (kN.mm)	Mode
2G10EC	21.04	36.54	22.11	0.95	CC
2G10ER	26.05	36.83	25.86	1.01	TC
2G20EC	41.27	29.74	37.24	1.11	CC
2G20ER	42.00	28.81	37.24	1.13	CC

4.3.3. Moment-deflection behavior. The tested GFRP bars do not only differ in reinforcement ratio and exposure; they also differed in surface texture. Two ribbed and two sand coated exposed GFRP bars are used as the main reinforcement for beams included in this section's analysis. The beams reinforced with Φ 10 sand coated and ribbed GFRP bars fall in the transition zone of failure (mixed concrete

crushing plus reinforcement rupture failure mode), as previously mentioned. On the other hand, the beams reinforced with the Φ 20 GFRP bars fail purely by concrete crushing. Figure 41 shows the moment vs. deflection curves of the four above stated beams. The curves for beams reinforced with Φ 10 GFRP bars and beams reinforced Φ 20 exposed GFRP bars are shown in Figure 41 (a) and Figure 41 (b), respectively.

| (a) | (b) |
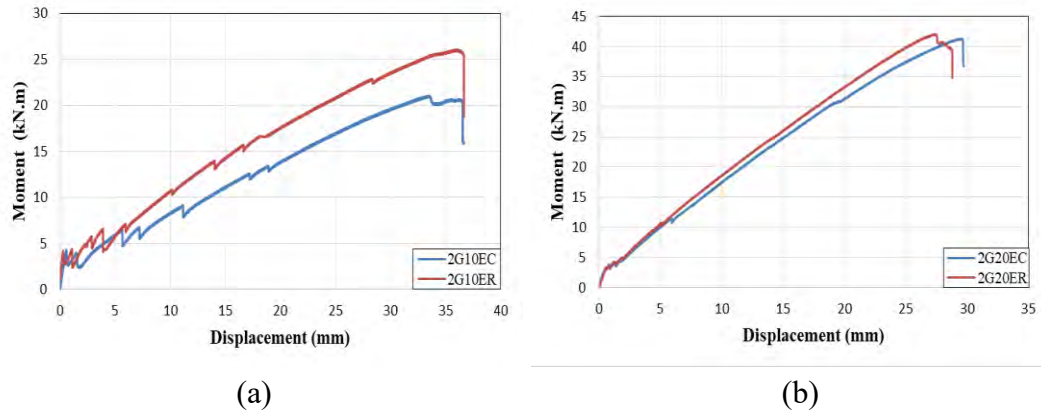
Figure 41: Moment vs. deflection (Group 3).

For the under reinforced GFRP beams (2G20EC and 2G20ER), the observed flexural behavior does not vary. The failure of the under reinforced beams is governed by the properties of the concrete. Therefore, the variations in surface texture do not impact the flexural behavior of the 2G20EC and 2G20ER beams. Both of the aforementioned beams reached an ultimate moment of approximately 43 kN.mm and yielded a deflection value just short of 30mm as seen in Figure 41 (b).

On the contrary, over reinforced beam in group 3 (2G10EC and 2G10ER) show clear variation of flexural behavior in response to variations in reinforcement surface texture. As observed in Figure 41 (a), the beam reinforced the exposed sand coated GFRP bars shows lower ultimate moment than the beam reinforced with the exposed ribbed GFRP bars. Both beams show similar deflection values; however, beam 2G10EC yielded a maximum moment equal to 21.04 kN.mm while beam 2G10ER yielded a maximum moment equal to 26.05 kN.mm. This variation is not due to the variation in surface texture; rather, it is due to the fact that both beams fall in the transition zone of failure. The fact that the two aforementioned beams fall in the transition zone means that failure could possibly occur due to FRP rupture or due to concrete crushing. By observing the maximum strain in concrete and FRP bars in both

beams, we deduce that the two beams differed in their failure mode. Strain behavior was discussed more thoroughly in section 4.3.1 of this chapter. However, for the sake of explaining the odd behavior of the two antecedent beams, it is crucial to provide an excerpt of the strain data. Figure 42 (a) and Figure 42 (b) show the moment vs. strain curves for the concrete and for the GFRP bars for 2G10EC and 2G10ER, respectively.

In Figure 42 (a), it is clear that the 2G10EC beam fails due concrete crushing. The figure shows that the GFRP bars do not reach their rupture strain since the max microstrain is shown to only be near 12000 microstrain. The concrete section of beam 2G10EC, as shown in the same figure, reached its maximum strain of 3000 microstrain. The predicted maximum moment for the 2G10EC beam is consistent with the experimental failure moment for beams failing in concrete crushing. On the other hand, it is distinctly shown in Figure 42 (a) that the 2G10ER beam failed due to FRP rupture. The FRP bar reached its maximum strain prior to the concrete section. The predicted maximum moment for the FRP rupture mode of failure of the 2G10ER beam is consistent with experimental moment capacity. In principle, the fact that beam 2G10ER beam failed in FRP rupture rather than concrete crushing is the cause of the higher moment capacity of the beam when compared with the 2G10EC beam. Thus, we conclude that surface texture of the FRP reinforcement does not impact the flexural behavior of the FRP reinforced beams.
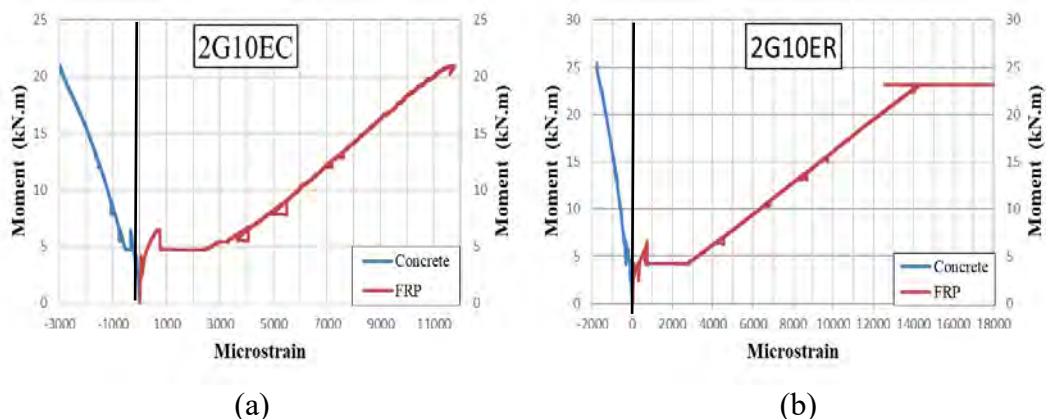

Figure 42: Moment vs. microstrain of: (a) 2G10EC; and (b) 2G10ER.

4.3.4. Cracking moment. The effects of surface texture on the cracking moments of the four beams studied in this section are presented in Table 20. The first set of beams includes the Φ 10 sand coated and ribbed GFRP RC beams.

Subsequently, the second set of beams presents cracking moments of the Φ 20 sand coated and ribbed GFRP RC beams. The average ratio of experimental to predicted cracking moments of the four beams in this section is 0.63 with a standard deviation of 0.06. As for the ratio of the cracking to ultimate moments for the aforementioned beams, an average value of 0.14 is deduced.

Table 20: Cracking moment (Group 3).

Beam	Experimental M_{cr} (kN.mm)	Predicted M_{cr} (kN.mm)	Exp./Pred. ACI [1]	M_{cr}/M_n
2G10EC	4.24	6.32	0.67	0.20
2G10ER	4.38	6.32	0.69	0.17
2G20EC	3.91	6.32	0.62	0.09
2G20ER	3.42	6.32	0.54	0.08
Average			0.63	0.14
Standard Deviation			0.06	

For the beams reinforced with the Φ 10 bars, the experimental to predicted ratios are 0.67 and 0.69 for beams 2G10EC and 2G10ER, respectively. The beam reinforced with ribbed Φ 10 GFRP bars showed higher experimental to predicted cracking moment ratio than the beam reinforced with the sand coated Φ 10 GFRP bars. The opposite is observed in beams reinforced with Φ 20 bars. The beam reinforced with ribbed GFRP bars yielded an experimental to predicted cracking moment ratio equal to 0.54 which is lower than the 0.62 ratio yielded by the beam reinforced with the sand coated Φ 20 bars. As for the ratio of cracking to ultimate moment ratio, it is observed that beams reinforced with sand coated GFRP bars have a higher ratio than beams reinforced with ribbed GFRP bars.

4.3.5. Cracking width and propagation. This section provides the tabulated values of crack propagation for the 4 FRP RC beams in group 3. Table 21 shows the moment causing the first 7 cracks in the 4 beams of group 3. No systematic conclusion about the impact of exposure on crack propagation is drawn as seen in Table 21. The crack propagation is not impacted by the variation of reinforcement surface texture of the FRP RC beams in group 3. For beams reinforced with Φ 10 FRP bars, the beams reinforced with the ribbed bars are slightly more resistant to developments of new cracks than the beams reinforced with the sand coated bars. On the other hand, beam 2G20EC (sand coated bars) are more resistant to the developments of new cracks than beam 2G20ER (ribbed bars).

Table 21: Crack number vs. moment (Group 3).

Beam	Crack Number						
	1	2	3	4	5	6	7
	Moment (kN.mm)						
2G10EC	3.1	2.4	4.8	5.6	7.9	12.7	13.2
2G10ER	4.3	4.3	5.8	6.4	7.1	10.9	13.4
2G20EC	4.0	3.9	6.3	6.4	9.5	13.4	15.5
2G20ER	3.4	3.7	4.4	5.0	9.6	10.6	13.4

Figure 43 shows the moment vs. crack width curves of the 4 beams in group 3. The steepness of the curves is almost the same, especially in the beams reinforced with the Φ 10 bars as shown in Figure 43 (a). For beams reinforced with Φ 20 bars, beam 2G20EC had a slightly higher steepness of curve than beam 2G20ER. The steepness of the curve is related to resistance of increase in cracks width. The steeper the moment vs. crack width the more the beam resist increase in cracks width.
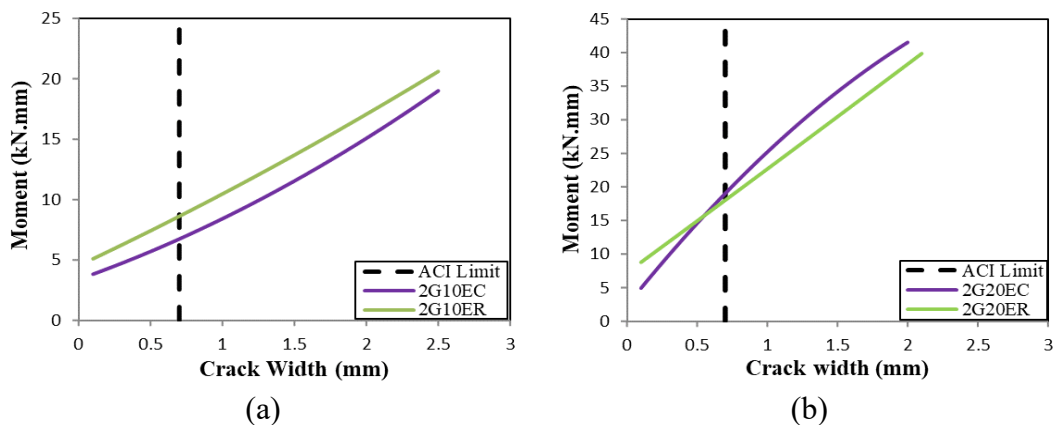
Figure 43: Moment vs. crack width (Group 3).

4.3.6. Bond-dependent coefficient. The effects of surface texture on the k_b factors of the 4 beams discussed hereafter are presented in Table 22. In general, the average k_b value of the 4 beams in this section is 0.84 which is close to the 0.8 k_b value proposed by the CSA S16 [14]. The k_b values range from 0.77 for beam 2G10EC at the lowest to 0.91 for beam 2G20ER at the highest. The beams reinforced with the ribbed GFRP bars yield an average k_b factor of 0.86 which is 6% higher than the 0.81 average k_b factor for beams reinforced with sand coated GFRP bars. In other words, sand coated GFRP bars show superior bond with concrete when compared with the ribbed GFRP bars. The previous observation is well established in the literature.

88

Table 22: bond-dependent coefficient, k_b factor (Group 3).

Beam	$0.3M_n$	w = 0.7 mm	Average
2G10EC	0.72	0.81	0.77
2G10ER	0.87	0.75	0.81
2G20EC	0.75	0.95	0.85
2G20ER	0.94	0.87	0.91

4.4. Impact of Number of Bars

This section highlights the impact of number of bars on the strain values, flexural capacity, moment-deflection behavior, cracking moment, cracks width propagation, and bond-dependent coefficient.

4.4.1. Reinforcement and concrete strain. The effects of the number of bars on the longitudinal reinforcement and concrete strains of the six beams studied in this section are presented in Table 23, Figure 44, and Figure 45. The first set of beams includes beams reinforced with 3 Φ 16 and 2 Φ 20 exposed sand coated GFRP bars as shown in Figure 44. The second set of analyzed beams focuses on beams reinforced with 3 Φ 10, 2 Φ 12, 3 Φ 16, and 2 Φ 20 exposed sand coated BFRP bars as shown of Figure 45.

Table 23: Reinforcement and concrete strain values (Group 4).

Beam	Moment (kN·m)	Longitudinal Reinforcement Strain	Concrete Strain
3G16EC	40.56	0.010	0.0023
2G20EC	41.27	0.011	0.0025
3B10EC	28.09	0.016	0.0021
2B12EC	27.09	0.018	0.0028
3B16EC	41.83	0.010	0.0021
2B20EC	42.14	0.009	0.0030

To analyze the impact of variation of number of bars in GFRP RC beams, beam 3G16EC is compared with beam 2G16EC. Beams 3G16EC and 2G20EC possess axial stiffness values that are in close proximity. Beam 3G16EC possesses an axial stiffness value equal to 27.07 MN while beam 3G16EC possesses an axial stiffness value equal to 28.20 MN. While both beams show similar flexural behavior (shown in section 4.4.3), there is a noticeable difference in their strain values. By observing the curves shown in Figure 44, it can be concluded that FRP reinforcement and concrete strains in beam 2G20EC were slightly higher than those of beam 3G16EC.

(a)   (b)
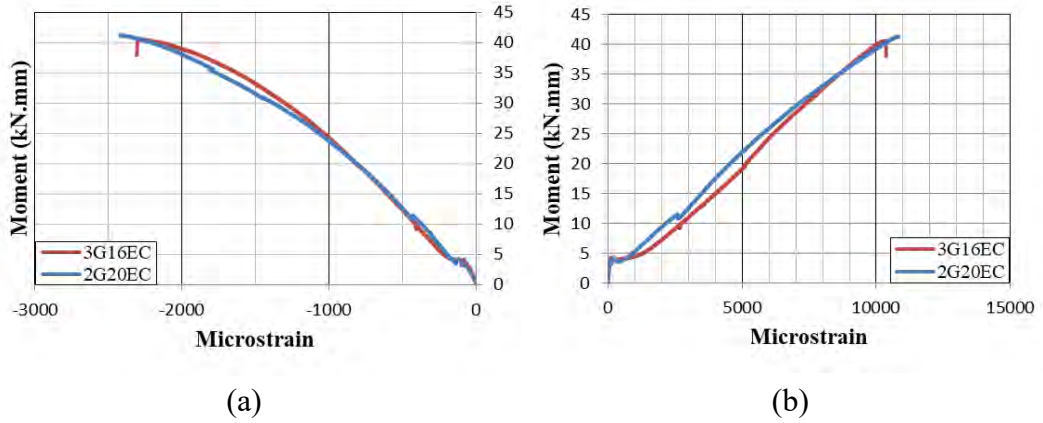
Figure 44: Moment vs. strain curves of GFRP RC beams (Group 4).

To analyze the impact of variation of number of bars in BFRP RC beams, beam 3B10EC is compared with beam 2B12EC and beam 3B16EC is compared with beam 2B20EC as shown in Figure 45. Figure 45(b) shows that the reinforcement strain curve of beam of beam 3B10EC possess steeper trend and lower maximum strain value when compared with beam 2B12EC. The concrete strain behavior of both aforementioned beams follows a similar trend as shown in Figure 45(a). On the contrary, concrete strain is steeper in beam 3B16EC than in beam 2B20EC with their reinforcement strain values and curves trend being almost similar.

(a)   (b)
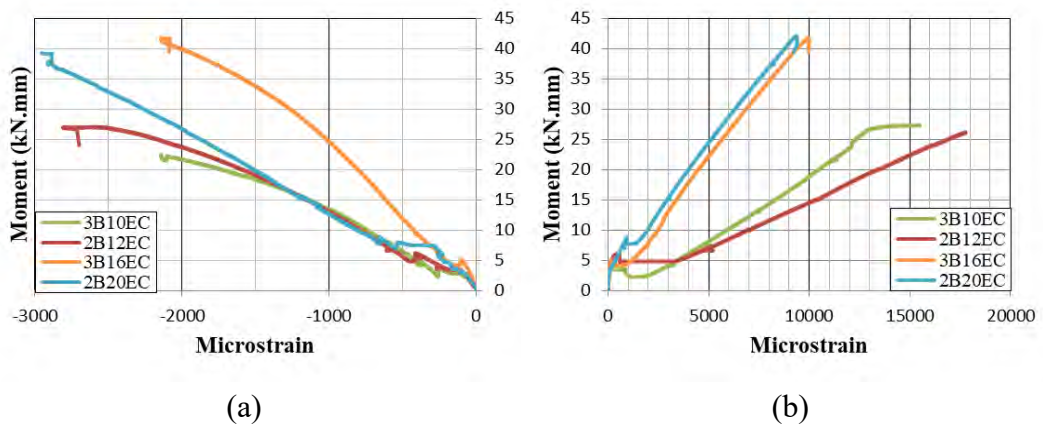
Figure 45: Moment vs. strain curves of BFRP RC beams (Group 4).

4.4.2. Flexural capacity and mode of failure. All 6 beams in group 4 fail due to concrete crushing. The predictions in this group are more conservative than in any other group. All beams have an experimental moment capacity higher than predicted moment capacities. The beams reinforced with the smaller diameters (Φ 10

90

and Φ 12) yield the least conservative predictions (see Table 24). This observation was already established while analyzing group 2 beams. As it was observed before, higher reinforcement ratios yielded more conservative predictions for the capacities.

.

Table 24: Experimental vs. analytical moment capacities (Group 4).

Beam	Experimental		Predicted	Exp./Pred. ACI [1]	Failure
	M_n (kN.mm)	δ (mm)	M_n (kN.mm)	M_n (kN.mm)	Mode
3G16EC	40.56	29.79	40.56	1.09	CC
2G20EC	41.27	29.74	41.27	1.11	CC
3B10EC	28.09	35.01	28.09	1.03	CC
2B12EC	27.09	36.60	27.09	1.02	CC
3B16EC	41.83	25.35	41.83	1.08	CC
2B20EC	42.14	26.76	42.14	1.09	CC

4.4.3. Moment-deflection behavior. Another area that is studied in this report is the impact of number of reinforcing FRP bars on the flexural response of the beams. The FRP bars used for the above-mentioned analysis are exposed sand coated GFRP and BFRP bars as shown in Figure 46. Figure 46 (a) shows the moment vs. deflection curves for two GFRP reinforced beams with almost similar axial stiffness (EA) values and different number of reinforcing bars (beam detailing). Figure 46 (b), subsequently, shows the same analysis on four BFRP beams.

(a)   (b)
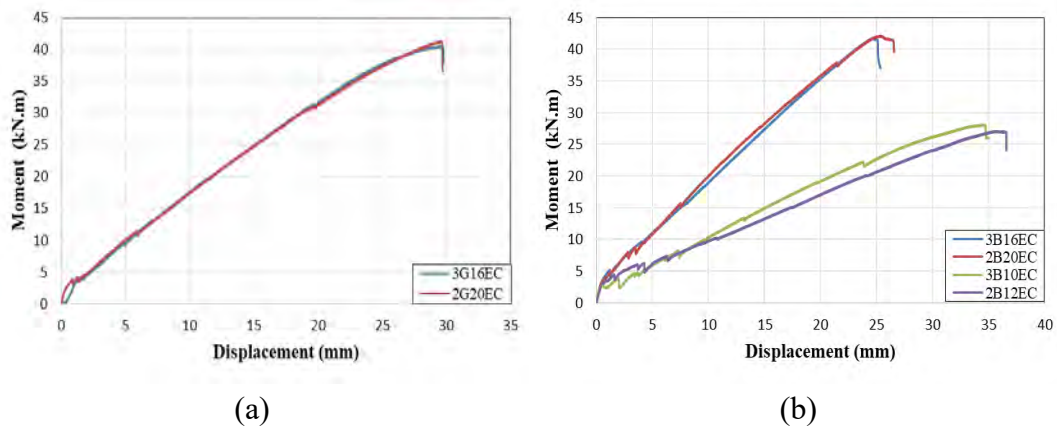
Figure 46: Moment vs. deflection (Group 4).

While keeping the axial stiffness constant, changes in beam detailing did not impact the flexural behavior of beams. GFRP reinforced beams 3G16EC and 2G20EC which had axial stiffness values equal to 27.07 MN and 28.2 MN, respectively. The proximity of the axial stiffness for the previous two beams yielded almost similar flexural response, as seen in Figure 46 (a). The same can be observed for the BFRP

reinforced beams shown in Figure 46 (b). Therefore, we conclude that, when keeping axial stiffness constant, beam detailing does not influence the flexural behavior of beams reinforced with exposed FRP bars.

4.4.4. Cracking moment. The effects of number of bars on the cracking moments of the six beams studied in this section are presented in Table 25. The first set of beams presented comprises of the beams reinforced with 3 Φ 16 and 2 Φ 20 sand coated GFRP bars. The second sets of beams analyzed comprises of beams reinforced with 3 Φ 10, 2 Φ 12, 3 Φ 16, and 2 Φ 20 sand coated BFRP bars. The average ratio of experimental to predicted cracking moments of the six beams in this section is 0.62 with a standard deviation of 0.11. As for the ratio of the cracking to ultimate moments for the aforementioned beams, an average value of 0.11 is deduced.

Table 25: Cracking moment (Group 4).

Beam	Experimental	Predicted	Exp./Pred. ACI [1]	Mcr/Mn
	M_{cr} (kN.mm)	M_{cr} (kN.mm)		
3G16EC	4.24	6.32	0.67	0.10
2G20EC	3.91	6.32	0.62	0.09
3B10EC	3.00	6.32	0.48	0.11
2B12EC	3.42	6.32	0.54	0.13
3B16EC	5.17	6.32	0.82	0.12
2B20EC	3.80	6.32	0.60	0.09
Average			0.62	0.11
Standard Deviation			0.11	

Beams reinforced sand coated GFRP bars reported experimental to predicted cracking moment ratios equal to 0.67 and 0.62 for beams 3G16EC and 2G20EC beams, respectively. The GFRP beam reinforced with the three bars shows higher experimental to predicted cracking moment ratio and cracking to ultimate moment ratio than the beam reinforced with the two bars. As for the BFRP RC beams, the results vary based on the size of the bar. In the set containing the smaller diameter bars, beam 3B10EC shows a lower experimental to predicted cracking moment ratio and cracking to ultimate moment ratio than beam 2B12EC. On the contrary, the beam reinforced with the 3 Φ 16 BFRP bars shows higher experimental to predicted cracking moment and cracking to ultimate moment ratios than the beam reinforced with the 2 Φ 20 BFRP bars. The observations of the ratios of the BFRP RC beams are similar to the observations about the ratios of the GFRP RC beams.

4.4.5. Cracking width and propagation. This section provides the tabulated values of crack propagation for the 6 FRP RC beams in group 4. Table 26 shows the moment causing the first 7 cracks in the 6 beams of group 4. No systematic conclusion about the impact of exposure on crack propagation is drawn as seen in Table 26. The crack propagation is not impacted by the variation of number of reinforcing bars in group 4 beams. For instance, beam 3B16EC shows higher moments required for the development of final cracks than beam 2B20EC does. On the other hand, beam 2G20EC shows higher resistance to the developments of cracks than beam 3G16EC does. For beams 3B10EC and 2B12EC, the beams resistance to the developments of cracks is very similar.

Table 26: Crack number vs. moment (Group 4).

Beam	Crack Number						
	1	2	3	4	5	6	7
	Moment (kN.mm)						
3G16EC	4.7	5.3	5.4	6.3	7.5	9.5	10.8
2G20EC	4.0	3.9	6.3	6.4	9.5	13.4	15.5
3B10EC	3.0	2.8	3.9	4.7	4.7	6.9	8.3
2B12EC	3.4	3.3	4.3	6.0	6.3	7.2	8.7
3B16EC	2.5	5.2	6.0	7.8	11.9	13.2	14.6
2B20EC	3.8	4.8	6.0	7.9	7.8	9.5	11.0

Figure 47 shows the moment vs. crack width curves of the 6 beams in group 4. The steepness of the BFRP curves is almost the same, as shown in Figure 47 (b). For the GFRP RC beams shown in Figure 47 (a), the beam containing the 2 longitudinal reinforcing bars (2G20EC) is more resistant to increase in cracks width than the beam containing the 3 longitudinal reinforcing bars (3G16EC).
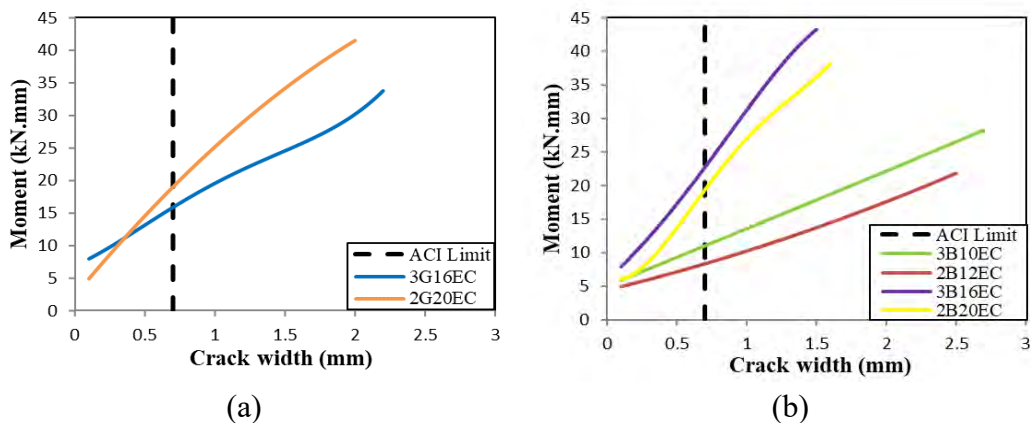

(a)   (b)

Figure 47: Moment vs. crack width (Group 4).

4.4.6. Bond-dependent coefficient. The effects of the number of longitudinal reinforcement bars on the k_b factors of the 6 beams discussed hereafter are presented in Table 27. In general, the average k_b value of the 6 beams in this section is 0.86 which is slightly higher than the 0.8 k_b value proposed by the CSA S16 [14] but much lower than the 1.4 value proposed by ACI 440.1R [1].

Table 27: bond-dependent coefficient, k_b factor (Group 4).

Beam	$0.3M_n$	w = 0.7 mm	Average
3G16EC	0.82	0.92	0.87
2G20EC	0.75	0.95	0.85
3B10EC	0.75	0.83	0.79
2B12EC	0.79	0.73	0.76
3B16EC	0.92	0.99	0.96
2B20EC	0.94	0.97	0.95

Bar spacing is indirectly related to the k_b value. Since the spacing between the bars plays a major role in determining the k_b value, it is expected that a clear conclusion would be drawn from this section. It should be noted that the spacing between bars in the beams reinforced with 3 Φ 16 bars is 39 mm compared with the 70 mm bar spacing in beams reinforced with 2 Φ 20 bars. Furthermore, the spacing between bars in the BFRP beams reinforced with 3 Φ 10 is 45 mm which is lower than the 85 mm bar spacing of beams reinforced with 2 Φ 12 bars.

Although the beams in this section have similar axial stiffness values, their k_b value differ. It is clear that beams with higher bar spacing yielded lower k_b value. In GFRP RC beams, for example, the beam reinforced with 3 Φ 16 bars had a k_b factor equal to 0.87 which is 2.5% higher than the k_b factor of the beam reinforced with 2 Φ 20 bars. Similarly, beams reinforced with 3 BFRP bars (3B10EC and 3B16EC) yielded an average k_b factor equal to 0.88 which is also 2.5% higher than the 0.86 average k_b factor for beams reinforced with 2 BFRP bars (2B12EC and 2B20EC).

4.5.   Impact of Bar Type

This section highlights the impact of bar type on the strain values, flexural capacity, moment-deflection behavior, cracking moment, cracks width propagation, and bond-dependent coefficient.

4.5.1. Reinforcement and concrete strain. The effects of reinforcement type on the longitudinal reinforcement and concrete strains of the three beams studied in

this section are presented in Table 28 and Figure 48. The beams in this section are reinforced with 2 Φ 12 BFRP, CFRP, and steel bars. The FRP bars were subjected to exposure.

Table 28: Reinforcement and concrete strain values (Group 5).

Beam	Moment (kN·m)	Longitudinal Reinforcement Strain	Concrete Strain
2B12EC	27.09	0.016	0.0028
2C12EC	41.27	0.013	0.0029
2S12	28.09	0.040	0.0013

Both FRP RC beams fail in concrete crushing as evident from the strain values shown in Table 28 and Figure 48. Both 2B12EC beam and 2C12EC beam show concrete strain values reaching near the ultimate concrete stain of 0.003. Beam 2C12EC showed lower FRP strain than beam 2B12EC (0.013 vs. 0.016). The lower FRP strain in beam 2C12EC is due to the relatively high modulus of elasticity of the CFRP bars. The steel RC beam fails due to reinforcement yielding. The concrete strain in the steel RC beam is much lower than the ultimate concrete strain while strain in the steel bars reaches 0.040 which is well beyond the yield strain of steel.
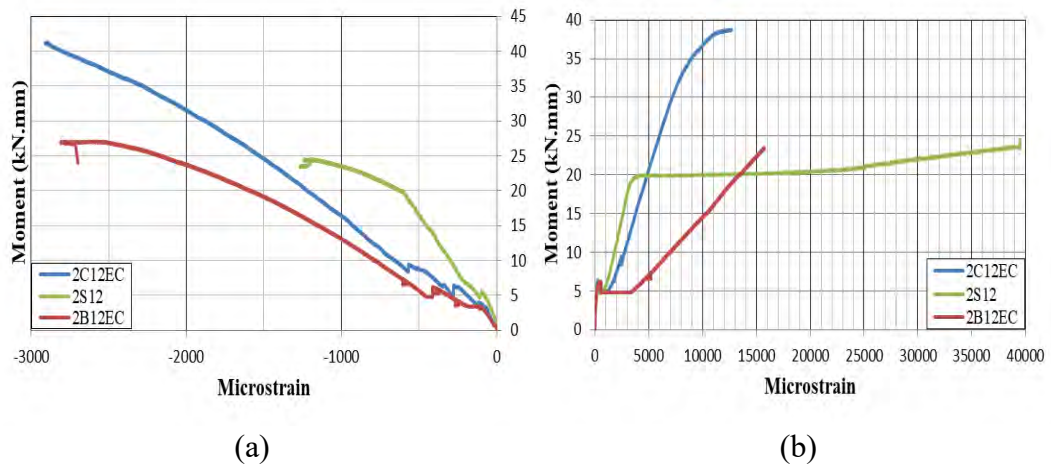

Figure 48: Moment vs. strain curves of BFRP RC beams (Group 5).

4.5.2. Flexural capacity and mode of failure. The two FRP RC beams in group 5 fail in concrete crushing as predicted using the ACI 440.1R [1]. The steel RC beam, on the other hand, fail due to steel yielding as predicted using the ACI 318 [12]. It is observed that the ACI 318 is more conservative than the ACI 440.1R when predicting the ultimate capacities seen in Table 29.

Table 29: Experimental vs. Analytical moment capacities (Group 5).

Beam	Experimental		Predicted	Exp./Pred. ACI [1,12]	Failure Mode
	M_n (kN.mm)	δ (mm)	M_n (kN.mm)	M_n (kN.mm)	
2B12EC	27.09	36.60	26.65	1.02	CC
2C12EC	41.36	24.75	37.17	1.11	CC
2S12	24.56	33.63	19.15	1.23	TC

4.5.3. Moment-deflection behavior. The last studied area of comparison is the type of reinforcement. To study the impact of variation in reinforcement type on the flexural response of the beam, exposed Φ 12 CFRP and BFRP bars were used. Furthermore, a Φ 12 steel reinforced beam is also used for control purposes. Figure 49 shows the moment deflection curves for the three beams reinforced with exposed CFRP and BFRP bars as well as steel bars. As observed in Figure 49, the beam reinforced with the exposed CFRP bars shows the highest moment capacity. Beam 2C12EC yielded a maximum moment equal to 41.4 kN.mm; 53% higher than the maximum moment produced by beam 2B12EC. The steel reinforced beam (2S12) shows the highest stiffness and the lowest moment capacity when compared with the FRP reinforced beams. The higher stiffness of the 2S12 beam is due to the higher modulus of the steel reinforcement. After the initial steepness, the moment deflection curve of the steel RC beam flattens after reaching the yield strain of the steel reinforcement. The curve remains, somewhat, flat until failure. The behavior of the steel RC beam was expected to differ from the behavior of the FRP. Steel, unlike, FRP does not exhibit linear elastic behavior until failure. Therefore, the moment values in FRP RC beams are proportional to the displacement values which is not the case for the steel RC beam.
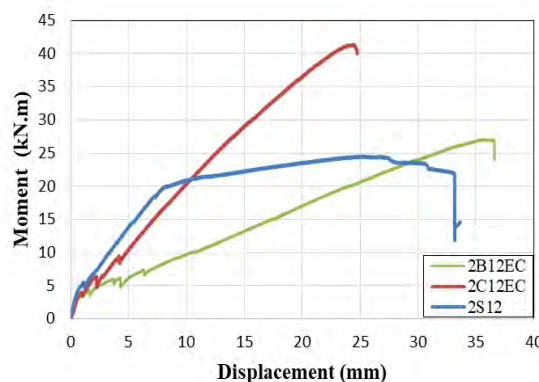

Figure 49: Moment vs. deflection (Group 5).

In addition to the evident difference in the shape of moment deflection curves between steel RC beams and FRP RC beams, it is clear that the curve of the steel RC beam is much smoother than that of FRP RC beams. While the relatively low modulus of elasticity of FRP reinforcement allows for load drops due to cracking, the high modulus of elasticity of steel prevents such drops [65]. The drops in moment values in FRP RC beams can be attributed to local decrease of stiffness in the FRP beams' cracked section.

4.5.4. Cracking moment. The effects of the type of the reinforcement bars on the cracking moments of the three beams studied in this section are presented in Table 30. Similar to the other FRP RC beams discussed before, the experimental cracking moment of CFRP RC beam is much lower than the predicted one. The experimental to predicted cracking moment of the CFRP RC beam is calculated to be 0.64 which falls in the range of the ratios calculated by the other FRP RC in this study. For the steel RC beam, the ratio of experimental to predicted cracking moment is 0.88 which is closer to the predicted cracking moment than any FRP RC beam.

Table 30: Cracking moment (Group 5).

Beam	Experimental M_{cr} (kN.mm)	Predicted M_{cr} (kN.mm)	Exp./Pred. ACI [1], [12]	M_{cr}/M_n
2B12EC	3.42	6.32	0.54	0.13
2C12EC	4.02	6.32	0.64	0.10
2S12	5.57	6.32	0.88	0.23
Average			0.69	0.15
Standard Deviation			0.10	

4.5.5. Cracking width and propagation. This section provides the values of tabulated crack propagation for the 2 FRP RC beams and 1 steel RC beam in group 5. The moment causing the first 7 cracks for the beams in this group is shown in Table 31.

Table 31: Crack number vs. moment (Group 5).

Beam	Crack Number						
	1	2	3	4	5	6	7
	Moment (kN.mm)						
2B12EC	3.4	3.3	4.3	6.0	6.3	7.2	8.7
2C12EC	3.3	3.9	6.3	6.4	6.6	9.4	11.7
2S12	5.0	5.6	5.7	8.2	10.5	14.3	15.8

It was observed in Table 31, that the steel RC beam shows the most resistance to the developments of the last final few cracks. The BFRP RC beam, on the contrary showed the least resistance to the developments of the last few cracks. The CFRP RC beam was in between the steel RC beam and the BFRP RC beam. The resistance behavior observed in group 5 beams can be attributed back to the elastic modulus of the reinforcement. Higher elastic modulus means lower deflection which, in turn, means fewer cracks.

Figure 50 shows the moment vs. crack width curves of the 2 FRP beams in group 3. The CFRP RC beam shows a slightly steeper curve than the BFRP RC beam. However, the biggest difference between the two curves is observed to be the magnitude of moments against similar crack width values. The aforementioned observation can be explained by the fact that CFRP bars have a higher modulus of elasticity which reduces the deflection and by default slows down the increase in crack width values.
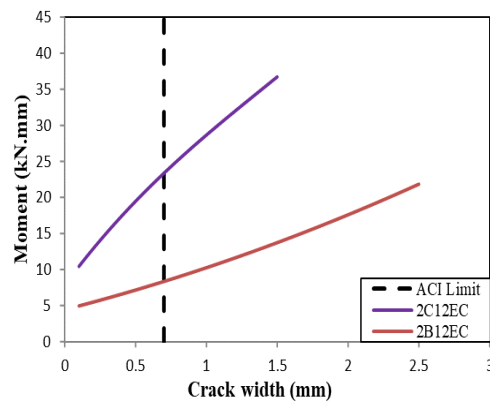

Figure 50: Moment vs. crack width (Group 5).

4.5.6. Bond-dependent coefficient. This section examines the impact of variation in the reinforcement type on the k_b value. One beam reinforced with CFRP bars subjected to exposure is compared to a beam reinforced with exposed BFRP bars and to another beam reinforced with steel bars that are not subjected to exposure. The steel RC beams serves as a reference. The k_b value for the beams in group 5 is shown in Table 32. It is observed that the CFRP RC beam yielded a k_b value equal to 0.67 which is 12% lower than the 0.76 k_b value of the BFRP RC beam. The k_b value of the steel RC beams is assumed to be one as per the ACI 440.1R design code [1].

98

Table 32: bond-dependent coefficient, k_b factor (Group 5).

Beam	$0.3M_n$	w = 0.7 mm	Average
2B12EC	0.79	0.73	0.76
2C12EC	0.54	0.80	0.67
2S12*	1	1	1

Chapter 5. Conclusion

In this study, the impact of a 28 month exposure to ultraviolet rays, humidity, and rain on the flexural behavior and serviceability performance of FRP RC beams was investigated. More specifically, the study analyzed the impact of such exposure on parameters such as: strain values, flexural capacity, moment vs. deflection, cracking moments, cracks width, and bond-dependent coefficient (k_b). In addition to exposure, the impact of factors such as reinforcement ratio, reinforcement surface texture, number of reinforcement bars, and reinforcement type on the flexural behavior and serviceability performance of FRP beams was studied. The report attempted to assess the provisions for FRP design as provided by the ACI 440.1R and other codes. A total of 23 beams divided into 5 groups were analyzed to achieve the goals of this study. After analyzing the results of the study conducted herein, the following was concluded:

- Exposure had more impact on the serviceability limit state than it had on the flexural behavior of FRP RC beams. Exposure only impacted the flexural capacity of the under-reinforced FRP beams but impacted the serviceability of almost all under-reinforced and over-reinforced FRP beams.

- The flexural capacity was impacted by the utilization of exposed bars in under-reinforced FRP RC beams but was not influenced by utilization of exposed in over-reinforced FRP RC beams. Under-reinforced beams such as the beam reinforced with Φ 8 sand coated GFRP bars subjected to exposure showed 11% reduction in the moment capacity as well as higher maximum deflection when compared with the reference beams reinforced with unexposed bars. However, there was no systematic impact caused by exposure on the flexural behavior of over-reinforced FRP RC beams.

- The flexural capacity was indirectly proportional to the reinforcement ratio. Furthermore, surface texture of reinforcement did not influence the flexural behavior of the FRP RC beams. Also, beams with similar stiffness showed similar flexural behavior regardless of the number of reinforcement bar.

- For the most part, the strain values were higher in the unexposed FRP bars than in the exposed FRP bars. The higher strain value indicates a better bond

behavior between the unexposed FRP bars and the concrete. In other words, higher strain values yield lower k_b values which is observed clearly in the GFRP RC beams.

- The ACI code underestimated the values for the cracking moment by an average of 35%. Furthermore, the ratios of cracking moment to ultimate moment for beams reinforced with exposed ribbed GFRP bars were slightly lower than the ratios for beams reinforced with unexposed ribbed GFRP bars.

- Ribbed FRP bars were more impacted by exposure than their sand coated counterparts.

- The k_b values for beams reinforced with exposed GFRP bars were higher than those for beams reinforced with unexposed GFRP bars. The average k_b value of beams reinforced with exposed sand coated GFRP bars was 36% more than the k_b value of beams reinforced with unexposed sand coated GFRP bars. As for beams reinforced with exposed ribbed GFRP bars, the average k_b value was 7% higher than it was for the beams reinforced with the unexposed bars. The k_b values of BFRP RC beams were unaffected by exposure.

- Even with harsh exposure to the UAE climate, FRP bars are still resilient enough to be used in construction. Although FRP bars subjected to exposure showed inferior performance to their unexposed counterparts, they still showed superior performance when compared with steel reinforcement.

References

]1[American Concrete Institute, "Guide for the design and construction of structural concrete reinforced with fiber-reinforced polymer (FRP) bars," ACI 440.1R-15, ACI Committee 440, Farmington Hills, MI, USA, 2015.

]2[L. C. Bank, *Composites for construction : structural design with FRP materials*. Hoboken, N.J.: John Wiley & Sons (in English), 2006.

]3[L. Hollaway, "The evolution of and the way forward for advanced polymer composites in the civil infrastructure," *Construction and Building Materials,* vol. 17, no. 6, pp. 365-378, 2003.

]4[H. Zhang, L. Liao, R. Zhao, J. Zhou, M. Yang, and R. Xia, "The Non-Destructive Test of Steel Corrosion in Reinforced Concrete Bridges Using a Micro-Magnetic Sensor," *Sensors (Basel, Switzerland),* vol. 16, no. 9, 2016.

]5[M. El-Mogy, A. El-Ragaby, and E. El-Salakawy, "Flexural Behavior of Continuous FRP-Reinforced Concrete Beams," *Journal of Composites for Construction,* vol. 14, pp. 669-680, 2010.

]6[C. Li, D. Gao, Y. Wang, and J. Tang, "Effect of high temperature on the bond performance between basalt fibre reinforced polymer (BFRP) bars and concrete," *Construction and Building Materials,* vol. 141, pp. 44-51, 2017.

]7[T. D'Antino and M. A. Pisani, "Long-term behavior of GFRP reinforcing bars," *Composite Structures,* vol. 227, 2019.

]8[S. Misra, H. Mutsuyoshi, T. Uomoto, and F. Katsuki, "Use of Fiber Reinforced Polymer Composites as Reinforcing Material for Concrete," *Journal of Materials in Civil Engineering,* vol. 14, pp. 191-209, 2002.

]9[M. N. Habeeb, "Flexural Behavior of Continuous GFRP Reinforced Concrete Beams," *Journal of Composites for Construction,* vol. 12, pp. 115-124, 2008.

]10[M. Robert, P. Cousin, B. Benmokrane, and N. C. Canadian Society for Civil Engineering Annual Conference St. Johns, "Behaviour of GFRP reinforcing bars subjected to extreme temperatures," *Proceedings, Annual Conference - Canadian Society for Civil Engineering,* vol. 3, pp. 1587-1596, 2009.

]11[D .Tomlinson and A. Fam, "Performance of concrete beams reinforced with basalt FRP for flexure and shear," *Journal of composites for construction,* vol. 19, no. 2, p. 04014036, 2015.

]12[American Concrete Institute, "Building code requirements for structural concrete and commentary," ACI 318-19, Farmington Hills, MI, USA, 2019.

]13[Canadian Standard Association, "Design and construction of building structures with fibre-reinforced polymers," CSA-S806-12, Mississauga, Ontario, Canada, 2012.

]14[Canadian Standard Association, "Canadian Highway Bridge Design Code," CSA-S6-14, Mississauga, Ontario, Canada, 2014.

]15[Intelligent Sensing for Innovative Structures, "Reinforcing Concrete Structures with Fibre Reinforced Polymers (FRPs)," Design Manual No. 3, ISIS Canada, Manitoba, Canada, 2012.

]16[F. Elgabbas, P. Vincent, E. A. Ahmed, and B. Benmokrane, "Experimental testing of basalt-fiber-reinforced polymer bars in concrete beams," *Composites Part B,* vol. 91, pp. 205-218, 2016.

]17[A. El Refai, F. Abed, and A. Al-Rahmani, "Structural performance and serviceability of concrete beams reinforced with hybrid (GFRP and steel) bars," *Construction and Building Materials,* vol. 96, pp. 518-529, 2015.

]18[L. C. Bank, "Properties of FRP Reinforcement for Concrete," *Developments in Civil Engineering,* vol. 42, p. 59, 1993.

]19[F. Elgabbas, E. A. Ahmed, and B. Benmokrane, "Physical and mechanical characteristics of new basalt-FRP bars for reinforcing concrete structures," *Construction and Building Materials,* vol. 95, pp. 623-635, 2015.

]20[M. Abedini, E. Akhlaghi, J. Mehrmashhadi, M. Mussa, M. Ansari, and T. Momeni, "Evaluation of Concrete Structures Reinforced with Fiber Reinforced Polymers Bars: A Review," *Journal of Asian Scientific Research,* vol. 7, pp. 165-175, 06/02 2017.

]21[American Concrete Institute, "Guide Test Methods for Fiber-Reinforced Polymers (FRPs) for Reinforcing or Strengthening Concrete Structures," ACI 440.4R-04, ACI Committee 440, Farmington Hills, MI, USA, 2004.

]22[ASTM International, "Standard Test Method for Tensile Properties of Fiber Reinforced Polymer Matrix Composite Bars," ASTM D7205/D7205M-06, West Conshohocken, PA, USA, 2016.

]23[C. Barris, L. Torres, M. Baena, K. Pilakoutas, and M. Guadagnini, "Serviceability limit state of FRP RC beams," *Advances in Structural Engineering,* vol. 15, pp. 653-664, 2012.

]24[M. Pearson, T. Donchev, and M. Limbachiya, "An investigation into the sustainability of FRP reinforcing bars," in Proc. Fourth International Conference on Durability & Sustainability of Fiber Reinforced Polymer (FRP) Composites for Construction and Rehabilitation, Quebec City, Canada, 2011, pp. 20-22.

]25[Z. Afifi Mohammad, M. Mohamed Hamdy, and B. Benmokrane, "Axial Capacity of Circular Concrete Columns Reinforced with GFRP Bars and Spirals," *Journal of Composites for Construction,* vol. 18, no. 1, p. 04013017, 2014.

]26[L. AlNajmi and F. Abed, "Evaluation of FRP bars under compression and their performance in RC columns," *Materials,* vol. 13, no. 20, p. 4541, 2020.

]27[N. Elmessalami, A. El Refai, and F. Abed, "Fiber-reinforced polymers bars for compression reinforcement: A promising alternative to steel bars," *Construction and Building Materials,* vol. 209, pp. 725-737, 2019.

]28[F. Abed, C. Oucif, Y. Awera, H. H. Mhanna, and H. Alkhraisha, "FE modeling of concrete beams and columns reinforced with FRP composites," *Defence Technology,* v ol. 17, no. 1, pp. 1-14, 2020.

]29[K. Khorramian and P. Sadeghian, "Experimental and analytical behavior of short concrete columns reinforced with GFRP bars under eccentric loading," *Engineering Structures,* vol. 151, pp. 761-773, 2017.

]30[N. Elmesalami, F. Abed, and A. E. Refai, "Concrete Columns Reinforced with GFRP and BFRP Bars under Concentric and Eccentric Loads: Experimental Testing and Analytical Investigation," *Journal of Composites for Construction,* vol. 25, no. 2, p. 04021003, 2021.

]31[N. ElMessalami, F. Abed, and A. El Refai, "Response of concrete columns reinforced with longitudinal and transverse BFRP bars under concentric and eccentric loading," *Composite Structures,* vol ,255 .p. 113057, 2021.

]32[F. Abed, Z. Mehaini, C. Oucif, A. Abdul–Latif, and R. Baleh, "Quasi-static and dynamic response of GFRP and BFRP bars under compression," *Composites Part C: Open Access,* vol. 2, p. 100034, 2020.

]33[O. Chaallal and B. Benmokrane, "Pullout and bond of glass-fibre rods embedded in concrete and cement grout," *Materials and Structures,* vol. 26, no. 3, pp. 167-175, 1993.

]34[A. Altalmas, A. El Refai, and F. Abed, "Bond degradation of basalt fiber-reinforced polymer (BFRP) bars exposed to accelerated aging conditions," *Construction and Building Materials,* vol. 81, pp. 162-171, 2015.

]35[b. Ovitigala, M. Ibrahim, and M. Issa, "Serviceability and Ultimate Load Behavior of Concrete Beams Reinforced with Basalt Fiber-Reinforced Polymer Bars," *ACI Structural Journal,* vol. 113, pp.757-768, 2016.

]36[B. Saikia, P. Kumar, J. Thomas, K. S. N. Rao, and A. Ramaswamy, "Strength and serviceability performance of beams reinforced with GFRP bars in flexure," *Construction and Building Materials,* vol. 21, no. 8, pp. 1709-1719, 2007.

]37[F. Elgabbas, B. Benmokrane, and E. A. M. A. Ahmed, "Flexural Behavior of Concrete Beams Reinforced with Ribbed Basalt-FRP Bars under Static Loads," *Journal of Composites for Construction,* vol. 21, p. 04016098, 2017.

]38[F. Abed and A. R. Alhafiz, "Effect of basalt fibers on the flexural behavior of concrete beams reinforced with BFRP bars," *Composite Structures,* vol. 215, pp. 23-34, 2019.

]39[F. Abed, M. Al-Mimar, and S. Ahmed, "Performance of BFRP RC beams using high strength concrete," *Composites Part C: Open Access,* vol. 4, p. 100107, 2021.

]40[A. El Refai and F. Abed, "Concrete Contribution to Shear Strength of Beams Reinforced with Basalt Fiber-Reinforced Bars," *Journal of Composites for Construction,* vol. 20, no. 4, 2016.

]41[F. Abed, A. El Refai, and S. Abdalla, "Experimental and finite element investigation of the shear performance of BFRP-RC short beams," *Structures,* vol. 20, pp. 689-701, 2019.

]42[G .Wu, Z.-Q. Dong, X. Wang, Y. Zhu, and Z.-S. Wu, "Prediction of Long-Term Performance and Durability of BFRP Bars under the Combined Effect of Sustained Load and Corrosive Solutions," *Journal of Composites for Construction,* vol. 19, no. 3, p. 04014058, 2015.

]43[J. Sim, C. Park, and D. Y. Moon, "Characteristics of basalt fiber as a strengthening material for concrete structures," *Composites Part B,* vol. 36, no. 6, pp. 504-512, 2005.

]44[M. Wang, Z. Zhang, Y. Li, M. Li, and Z. Sun, "Chemical Durability and Mechanical Properties of Alkali-proof Basalt Fiber and its Reinforced Epoxy Composites," *Journal of Reinforced Plastics and Composites,* vol. 27, no. 4, pp. 393-407, 2008.

]45[V. Calvet, M. Valcuende, J. Benlloch, and J. Cánoves, "Influence of moderate temperatures on the bond between carbon fibre reinforced polymer bars (CFRP) and concrete," *Construction & building materials.,* vol. 94, pp. 589-604, 2015.

]46[T. D'Antino, M .A. Pisani, and C. Poggi, "Effect of the environment on the performance of GFRP reinforcing bars," *Composites Part B,* vol. 141, pp. 123-136, 2018.

]47[R. Masmoudi, A. Masmoudi, M. B. Ouezdou, and A. Daoud, "Long-term bond performance of GFRP bars in concrete under temperature ranging from

20 °C to 80 °C," *Construction and Building Materials,* vol. 25, no. 2, pp. 486-493, 2011.

[48] F. Yan and Z. Lin, "Bond durability assessment and long-term degradation prediction for GFRP bars to fiber-reinforced concrete under saline solutions," *Composite Structures,* vol. 161, pp. 393-406, 2017.

[49] M. Robert, "Behavior of GFRP Reinforcing Bars Subjected to Extreme Temperatures," *Journal of Composites for Construction,* vol. 14, pp. 353-360, 2010.

[50] A. Alvarez, A. Zaidi, and R. Masmoudi, *Bond-slip behaviour of FRP bars under low and high temperature - experimental and theoretical studies*, CDCC-2007, pp. 523-530, 2007.

[51] N. Galati, A. Nanni, L. R. Dharani, F. Focacci, and M. A. Aiello, "Thermal effects on bond between FRP rebars and concrete," *Composites Part A: Applied Science and Manufacturing,* vol. 37, no. 8, pp. 1223-1230, 2006.

[52] H. Alkhraisha, H. Mhanna, N. Tello, and F. Abed, "Serviceability and Flexural Behavior of Concrete Beams Reinforced with Basalt Fiber-Reinforced Polymer (BFRP) Bars Exposed to Harsh Conditions," *Polymers,* vol. 12, no. 9, p. 2110, 2020.

[53] World Weather Online. "Sharjah Monthly Climate Averages." Worldweatheronline.com. https://www.worldweatheronline.com/sharjah-weather -averages/sharjah/ae.aspx (accessed Mar. 1,2020).

[54] P. Gergely and L. A. Lutz, "Maximum crack width in reinforced concrete flexural members," *Special Publication,* vol. 20, pp. 87-117, 1968.

[55] American Concrete Institute, "Guide for the design and construction of structural concrete reinforced with fiber-reinforced polymer (FRP) bars," ACI 440.1R-01, ACI Committee 440, Farmington Hills, MI, USA, 2001.

[56] R. J. Frosch, "Another look at cracking and crack control in reinforced concrete," *Structural Journal,* vol. 96, no. 3, pp. 437-442, 1999.

[57] American Concrete Institute, "Guide for the design and construction of structural concrete reinforced with fiber-reinforced polymer (FRP) bars," ACI 440.1R-06, ACI Committee 440, Farmington Hills, MI, USA, 2006.

[58] C. E. Bakis *et al.*, "Evaluation of crack widths in concrete flexural members reinforced with FRP bars," in *3rd International Conference on Composites in Civil Engineering, CICE 2006*, 2020: International Institute for FRP in Construction (IIFC), pp. 307-310.

[59] D. J. Elwell, G. Fu, B. New York . Transportation Research and Development, and A. United States. Federal Highway, *Compression testing of concrete : cylinders vs. cubes* (Special report / Transportation Research and Development Bureau, New York State Department of Transportation ; 119). Albany: Transportation Research and Development Bureau, New York State Dept. of Transportation (in English), 1995.

[60] S. Abedi. "Evaluation of the bond and tensile strength of GFRP bars exposed to harsh environment." Master thesis, American University of Sharjah, Sharjah, UAE, 2014.

[61] M. A. Rifai, H. El-Hassan, T. El-Maaddawy, and F. Abed, "Durability of basalt FRP reinforcing bars in alkaline solution and moist concrete environments," *Construction and Building Materials,* vol. 243, p. 11825, 2020.

[62] P. H. Bischoff, "Equivalent Moment of Inertia Based on Integration of Curvature," *Journal of Composites for Construction*, vol. 15, no. 3*,* pp. 263-273, 2011.

[63] M. Noël and K. Soudki, "Estimation of the crack width and deformation of FRP-reinforced concrete flexural members with and without transverse shear reinforcement ",*Engineering Structures,* vol. 59, pp. 393-398, 2014.

[64] A. El-Nemr, E. A. Ahmed, C. Barris, and B. Benmokrane, "Bond-dependent coefficient of glass- and carbon-FRP bars in normal- and high-strength concretes," *Construction and Building Materials,* vol. 113, pp. 77-89, 2016.

[65] C. G. Karayannis, P.-M. K. Kosmidou, and C. E. Chalioris, "Reinforced Concrete Beams with Carbon-Fiber-Reinforced Polymer Bars—Experimental Study," *Fibers,* vol. 6, no. 4, p. 99, 2018.

Appendix A: Failure Modes

Figure 51: Failure mode of beam 2G8EC.

Figure 52: Failure mode of beam 2G10EC.

Figure 53: Failure mode of beam 3G16EC.

Figure 54: Failure mode of beam 2G20EC.

Figure 55: Failure mode of beam 2G8UC.
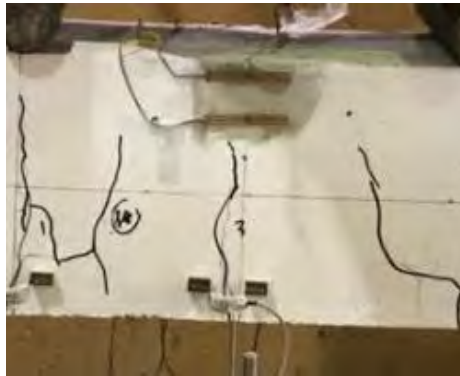
Figure 56: Failure mode of beam 2G10UC.

Figure 57: Failure mode of beam 2G10ER.

Figure 58: Failure mode of beam 2G20ER.

Figure 59 : Failure mode of beam 2G26ER.

Figure 60: Failure mode of beam 2G10UR.

Figure 61: Failure mode of beam 2G20UR.

Figure 62: Failure mode of beam 2G26UR.

Figure 63: Failure mode of beam 2B8EC.

Figure 64: Failure mode of beam 2B10EC.

Figure 65: Failure mode of beam 3B10EC.

Figure 66: Failure mode of beam 2B12EC.

Figure 67: Failure mode of beam 2B16EC.

Figure 68: Failure mode of beam 3B16EC.

Figure 69: Failure mode of beam 2B20EC.

Figure 70: Failure mode of beam 2B10UC.

Figure 71: Failure mode of beam 2B12UC.

Figure 72: Failure mode of beam 2C12EC.

Figure 73: Failure mode of beam 2S12.
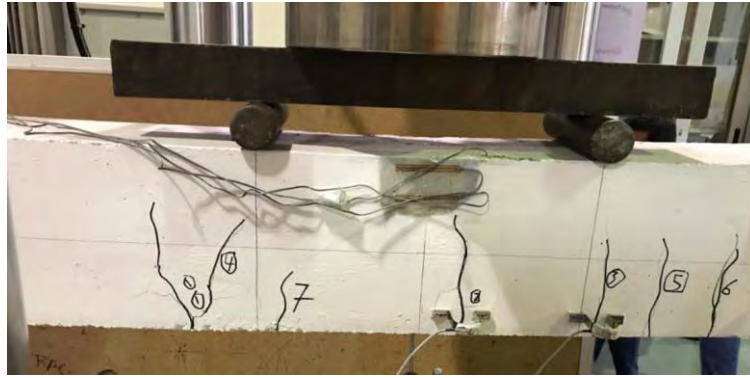
Appendix B: Cracks Propagation

Figure 74: Cracks propagation of beam 2G8EC.

Figure 75: Cracks propagation of beam 2G10EC.

Figure 76: Cracks propagation of beam 3G16EC.

Figure 77: Cracks propagation of beam 2G20EC.

Figure 78: Cracks propagation of beam 2G8UC.

Figure 79: Cracks propagation of beam 2G10UC.
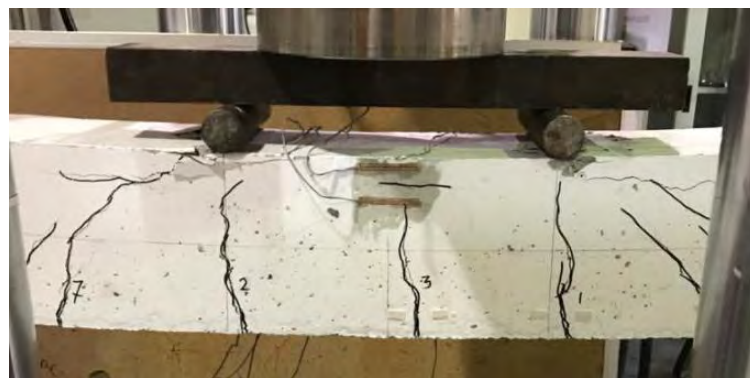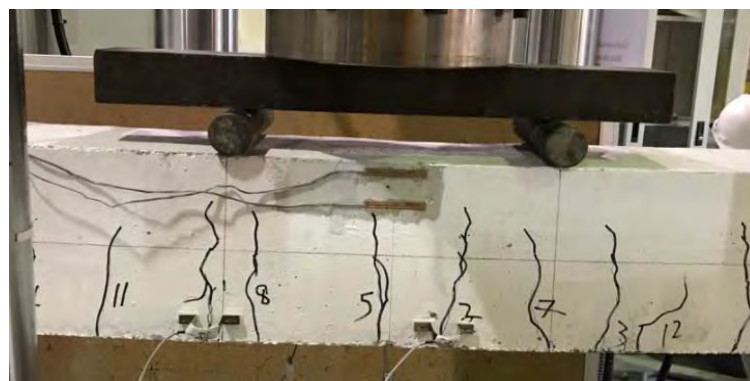

Figure 80: Cracks propagation of beam 2G10ER.

Figure 81: Cracks propagation of beam 2G20ER.

Figure 82 : Cracks propagation of beam 2G26ER.
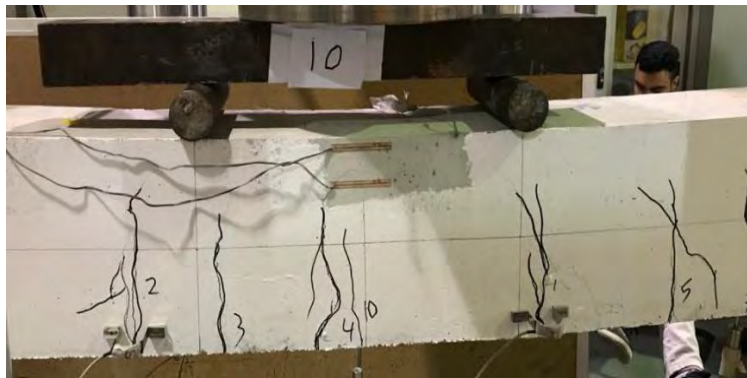
Figure 83: Cracks propagation of beam 2G10UR.
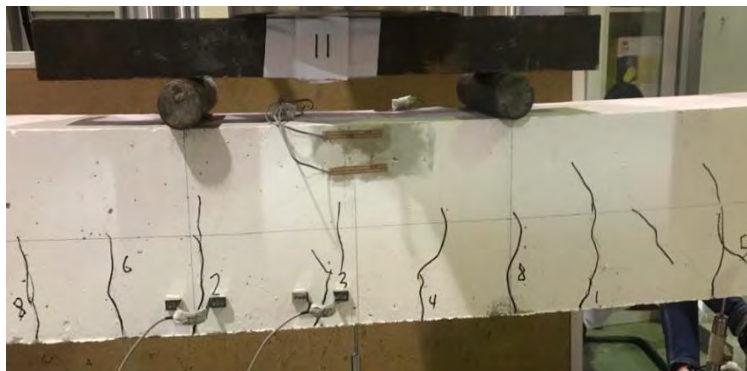
Figure 84: Cracks propagation of beam 2G20UR.
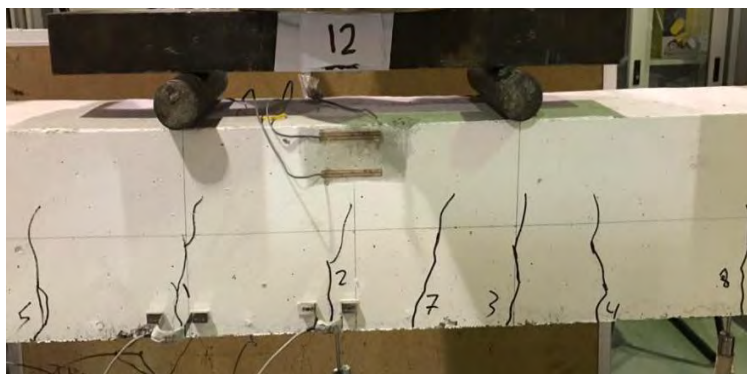
Figure 85: Cracks propagation of beam 2G26UR.

Figure 86: Cracks propagation of beam 2B8EC.

Figure 87: Cracks propagation of beam 2B10EC.

Figure 88: Cracks propagation of beam 3B10EC.

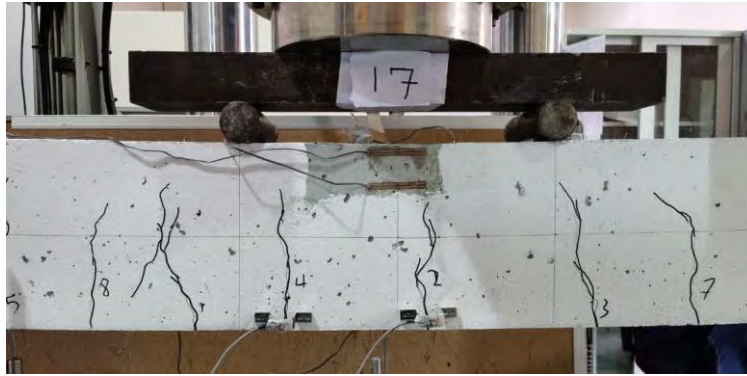Figure 89: Cracks propagation of beam 2B12EC.

Figure 90: Cracks propagation of beam 2B16EC.

Figure 91: Cracks propagation of beam 3B16EC.

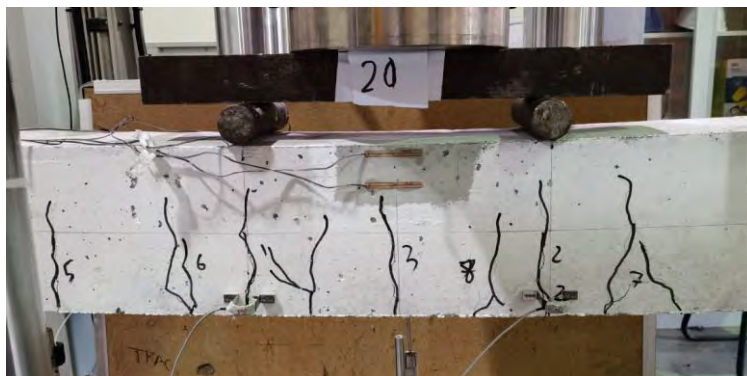Figure 92: Cracks propagation of beam 2B20EC.
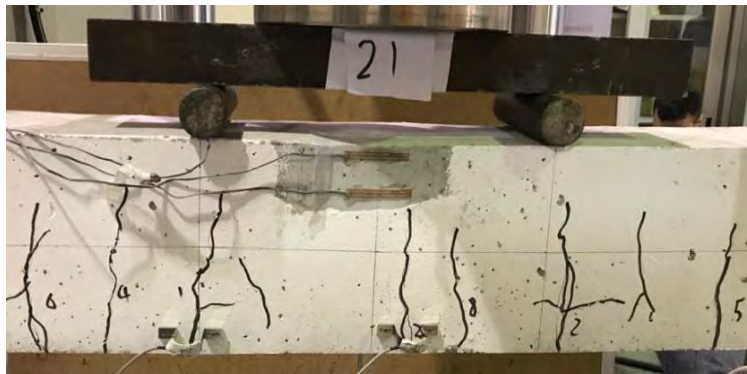

Figure 93: Cracks Propagation of beam 2B10UC.

Figure 94: Cracks propagation of beam 2B12UC.

Figure 95: Cracks propagation of beam 2C12EC.

Figure 96: Cracks propagation of beam 2S12.

Vita

Hakem Mohammad Alkhraisha was born in 1994, in Amman, Jordan. He obtained his high school diploma from Leavenworth high school, in Kansas, USA. He received his B.Sc. degree in Civil Engineering with Honors from the United States Military Academy at West Point in 2017. From 2017 to 2018, he worked as a Second Lieutenant at the Directorate of Housing and Military Works, in Jordan. In September 2018, he joined the Civil Engineering Master's program at the American University of Sharjah as a Graduate Teaching Assistant. During his master's studies, he authored and co-authored two journal papers and three conference papers.